WOOD AND FIBER SCIENCE

The Sustainable Natural Materials Journal

Volume 57, Number 2, 2025 (ISSN 0735-6161)

Open Access

JOURNAL OF THE

SWST – International Society of Wood Science and Technology

WOOD AND FIBER SCIENCE

Wood and Fiber Science is published quarterly in January, April, July, and October by the Society of Wood Science and Technology, P.O. Box 6155, Monona, WI 53716-6155

There are three classes of membership (electronic only) in the Society: Members – dues $150; Retired Members – dues $75; Student Members – dues $25. We also have a membership category for individuals from Emerging Countries where individual members pay $30, individual students pay $10; Emerging Groups of 10 pay $290, and Student Groups of 10 pay $90. Institutions and individuals who are not members pay $300 per volume (electronic only). Applications for membership and information about the Society may be obtained from the Executive Director, Society of Wood Science and Technology, P.O. Box 6155, Monona, WI 53716-6155 or found at the website https://www.swst.org.

Site licenses are also available with a charge of:

$300/yr for single online membership, access by password and email
$500/yr for institutional subscribers with 2–10 IP addresses
$750/yr for institutional subscribers with 11–50 IP addresses
$1000/yr for institutional subscribers with 51–100 IP addresses
$1500/yr for institution subscribers with 101–200 IP addresses
$2000/yr for institutions subscribers with over 200 IP addresses.

New subscriptions begin with the first issue of a new volume. All subscriptions are to be ordered through the Executive Director, Society of Wood Science and Technology. The Executive Director, at the Business Office shown below or by email to execdir@swst.org, should be notified 30 days in advance of a change of email address.

Business Office: Society of Wood Science and Technology, P.O. Box 6155, Monona, WI 53716-6155.
Editorial Office: Jeff Morrell, jeff.morrell@oregonstate.edu

EDITORIAL AND PUBLICATION POLICY

Wood and Fiber Science as the official publication of the Society of Wood Science and Technology publishes open access papers with both professional and technical content. Original papers of professional concern, or based on research of international interest dealing with the science, processing, and manufacture of wood and composite products of wood or wood fiber origin will be considered.

All manuscripts are to be written in US English, the text should be proofread by a native speaker of English prior to submission. Any manuscript submitted must be unpublished work not being offered for publication elsewhere.

Papers will be reviewed by referees selected by the editor and will be published in approximately the order in which the final version is received. Research papers will be judged on the basis of their contribution of original data, rigor of analysis, and interpretations of results; in the case of reviews, on their relevancy and completeness.

Color photos/graphics will be offered at no additional cost to authors. The Open Access fee will be $1800/article for SWST members and $2000/article for nonmembers. Reduced rates are available for authors based in developing countries.

Technical Notes

Authors are invited to submit Technical Notes to the Journal. A Technical Note is a concise description of a new research finding, development, procedure, or device. The length should be **no more than two printed pages in WFS**, which would be five pages or less of double-spaced text (TNR12) with normal margins on 8.5 x 11 paper, including space for figures and tables. In order to meet the limitation on space, figures and tables should be minimized, as should be the introduction, literature review and references. The Journal will attempt to expedite the review and publication process. As with research papers, Technical Notes must be original and go through a similar double-blind, peer review process.

On-line Access to *Wood and Fiber Science* Back Issues

SWST is providing readers with a means of searching all articles in *Wood and Fiber Science* from 1968 to present.

Visit the SWST website at https://www.swst.org and go to Wood & Fiber Science Online. Click on either SWST Member Publication access (SWST members) or Subscriber Publication access (Institution Access). All must login with their email and password on the https://www.swst.org site or use their ip authentication if they have a site license.

As an added benefit to our current subscribers, you can now access the electronic version of every printed article along with exciting enhancements that include:

- IP authentication for institutions (only with site license)
- Enhanced search capabilities
- Email alerting of new issues
- Custom links to your favorite titles

(ISSN 0735-6161)

WOOD AND FIBER SCIENCE

JOURNAL OF THE SOCIETY OF WOOD SCIENCE AND TECHNOLOGY

VOLUME 57 APRIL 2025 NUMBER 2

CONTENTS

Articles

Chemical constituents, physical, and mechanical properties of Indonesian sugar palm (*Arenga longipes* Mogea) trunk

*Luthfi Hakim**
Assoc. Professor
Lab. of Forest Product Technology, Faculty of Forestry, Universitas Sumatera Utara
Deli Serdang, 20353
E-mail: luthfi@usu.ac.id

Ganis Lukmandaru
Professor
Faculty of Forestry, Universitas Gadjah Mada
Yogyakarta, 55281
Email: glukmandaru@ugm.ac.id

Jajang Sutiawan
Senior researcher
Research Center for Biomass and Bioproduct, National Research and Innovation Agency
Cibinong, 16911
Email: Jajang.sutiawan@brin.go.id

Tito Sucipto
Assistant Professor
Lab. of Forest Product Technology, Faculty of Forestry, Universitas Sumatera Utara
Deli Serdang, 20353
Email: tito@usu.ac.id

Apri Heri Iswanto
Professor
Lab. of Forest Product Technology, Faculty of Forestry, Universitas Sumatera Utara
Deli Serdang, 20353
Email: apri@usu.ac.id

Yunida Syariani Lubis
Junior researcher
Research Center for Applied Botany, National Research and Innovation Agency
Cibinong, 16911
Email: yuni030@brin.go.id

Erlina Nurul Aini
Junior researcher
Research Center for Biomass and Bioproduct, National Research and Innovation Agency
Cibinong, 16911
Email: erli010@brin.go.id

(Received 24 October 2024)

Abstract. Wood density, chemical characteristics, and mechanical properties in the stem (vertical and horizontal) were studied for the Indonesian sugar palm (*Arenga longipes*) grown in Sumatera Island in Indonesia. This species is widely used industrially and is widely distributed on the island of North Sumatra. A 15-year-old palm tree was harvested (40 cm diameter at breast height) then sampled at seven heights above the ground (1, 2, 3, 4, 5, 6, and 7 m of trunk height) and at five horizontal positions (4, 8, 12, 16, and 20 cm of radius from the bark) at each height. The sections were evaluated for chemical constituents, density, modulus of rupture (MOR), modulus of elasticity (MOE), tensile strength, and compression strength using British Standard BS 373 (1957). The chemistry of the trunk was also evaluated by gas chromatography-mass spectroscopy (GC-MS), Fourier transform-infrared spectroscopy (FTIR), and thermogravimetric analysis (TGA). The distribution of chemical constituents of *A. longipes* stem was as follows: 24.97–39.23% α-cellulose, 68.03–78.04% holocellulose, 23.01–34.44% lignin, and 1.62–3.41% ash content. Density varied from 0.13 to 0.75 g/cm^3. Modulus of rupture varied from 10.42 to 143.49 MPa, modulus of elasticity varied from 0.35 to 24.92 GPa, tensile strength ranged from 0.55 to 16.03 GPa, and compressive strength ranged from 0.53 to 6.14 MPa. Hexadecenoic acid and octadecanoic acid were both detected, and the latter compound was most common (97.98% of peak area). The FTIR analysis indicated a hydrophilic tendency in the material, which was attributed to the presence of hydroxyl functional groups in cellulose and lignin. Thermal decomposition occurred at temperatures as high as 402°C, representing an 18% degradation. The horizontal variation within the trunk was highly significant for all traits, while the vertical variation was significant only for density and mechanical properties. A strong correlation was observed between density and mechanical properties. *A. longipes* has potential as an alternative raw material, capable of supplying the industry with valuable timber substitutes, particularly for material from the outer circumference of the stem.

Keywords: Chemical properties, Density, Modulus of rupture, Sugar palm, Horizontal variability, Vertical variability

* Corresponding author

Introduction

Arenga, a genus of palms native to Asia, is renowned for producing edible products from both its sap and fruit (Johnson 1992). The Indonesian sugar palm, *Arenga longipes*, was first identified on Sumatra Island by Mogea (2004), and it has since been recognized as a multi-purpose plant, classified as a non-timber forest product (NTFP). On Sumatra, particularly in North Sumatra, *A. longipes* has long been cultivated by local communities, primarily for tapping its sap to produce palm sugar and traditional wine (Azhar et al. 2019; Fadhilla et al. 2023). The fruit of *A. longipes* is also rich in carbohydrates and has been used as a traditional food source (Gunawan et al. 2018). Despite its extensive use in Indonesia, *A. longipes* has not been widely explored or utilized in India, particularly with regard to its stem (Pillai et al. 2020). In contrast, another species of sugar palm (*A. pinnata*) is an integral part of local economies in Malaysia, where it is utilized for producing palm sugar and the fruit known as "*kolang-kaling*" (Muda et al. 2024).

Historically, the sugar palm has been cultivated in Indonesia through agroforestry systems and is classified as a multi-purpose tree species (MPTS), providing various livelihood benefits to local communities (Haryoso et al. 2020; Mogea et al. 1991). In 2020, the area under sugar palm cultivation in North Sumatra was estimated at 7,063 hectares, yielding 6,619 tons of palm sugar (BPS 2021). These community-managed plantations are often subject to selective cutting for traditional building materials and flooring, and the trunks have considerable market value for the production of wood-based products (Nuryawan et al. 2017). However, despite its growing importance, little is known about the lignocellulosic properties of *A. longipes* trunks, with most studies focusing on plant morphology (Nirawati et al. 2020) and the diversity of its uses, tapping flow discharge, and conservation efforts (Fadhilla et al. 2023). Our previous research has examined the anatomical, fiber morphology, and mechanical properties of *A. longipes* fronds (Hakim et al. 2023); and properties for construction applications, such as density and mechanical strength (modulus of rupture – MOR; modulus of elasticity – MOE), are also of particular interest. These properties are often correlated with density, which influences the performance and quality of the final products (Hakim et al. 2022).

Previous studies on *A. pinnata* have suggested that its trunk could serve as a raw material for wood substitutes, suggesting the potential for similar applications with *A. longipes* due to the morphological similarities between the two species. The trunk of *A. longipes* is particularly notable for its fibrous, spongy texture, which is both strong and lightweight. Its structure consists of thick, interwoven fibers, providing high mechanical strength and flexibility, making it useful for applications such as construction, handicrafts, and furniture production.

The overall objective of this study was to assess the chemical, physical, and mechanical properties of Indonesian sugar palm (*A. longipes*) in Indonesia as a high-value wood substitute.

Materials and Methods

Sample preparations

A 15-year-old *A. longipes* trunk was harvested from Langkat district, North Sumatra Province, Indonesia (Figure 1) at the end of production for tapping sap. The trunk had a 40-cm over bark diameter at breast height. Diameter at 1.3 m height (diameter at breast height) was determined as the mean of two cross diameters, and the stem was trimmed to 7 m. Forty-centimeter-thick disks were cut at 1, 2, 3, 4, 5, 6, and 7 m of total trunk height. Specimens were cut at five distances from the bark to the pith / horizontal direction (4, 8, 12, 16, and 20 cm of the radius length). All vertical and horizontal treatments were repeated five times. The complete sampling and repetition techniques are shown in Table 1. The specimens were conditioned to constant mass at 25 ± 2 °C and 65% ± 5% relative humidity and maintained in this condition until required for testing. The average moisture content of the test pieces after this stage was 12%. Figure 2 is an illustration of sample pattern in both vertical and horizontal directions.

Chemical constituents, physical and mechanical testing

Holocellulose, α-cellulose, lignin content, and ash were evaluated on 25 specimens per radial stem position. Holocellulose content was analyzed based on ASTM D 1104 (1978), using 40-50 mesh extractive-free powder (pre-extracted using ethanol-toluene). As much as 0.7 ± 0.05 g (*W1*) of oven-dried powder was put into 50 mL acetic acid and 2% NaOH. One L

Table 1. Experimental plan used to assess the properties of *A. longipes* stems

Vertical direction	Horizontal direction				
	4 cm	8 cm	12 cm	16 cm	20 cm
1 m	V_1H_1	V_1H_2	V_1H_3	V_1H_4	V_1H_5
2 m	V_2H_1	V_2H_2	V_2H_3	V_2H_4	V_2H_5
3 m	V_3H_1	V_3H_2	V_3H_3	V_3H_4	V_3H_5
4 m	V_4H_1	V_4H_2	V_4H_3	V_4H_4	V_4H_5
5 m	V_5H_1	V_5H_2	V_5H_3	V_5H_4	V_5H_5
6 m	V_6H_1	V_6H_2	V_6H_3	V_6H_4	V_6H_5
7 m	V_7H_1	V_7H_2	V_7H_3	V_7H_4	V_7H_5

Note: each sample was repeated five times.

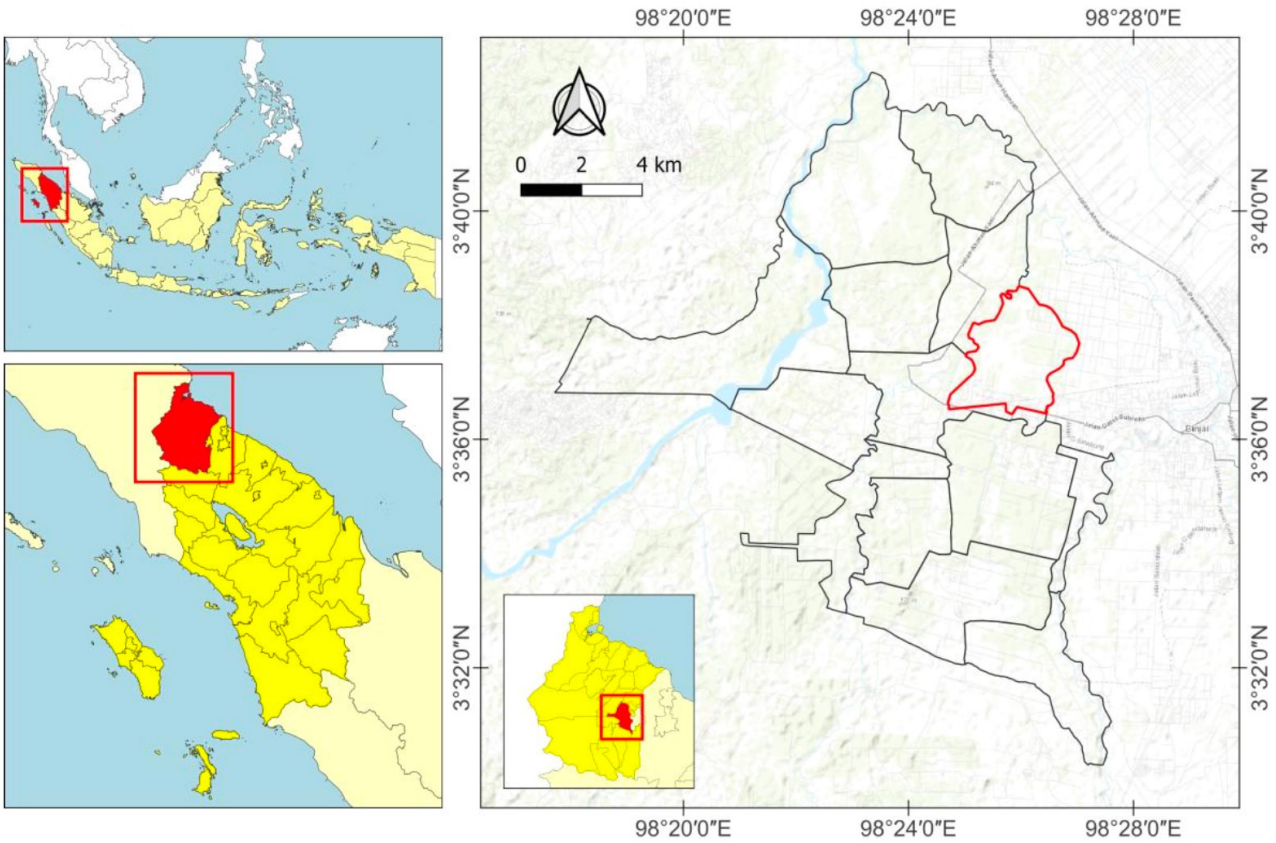

Figure 1. Location of *A. longipes* harvesting in Langkat district, North Sumatera, Indonesia.

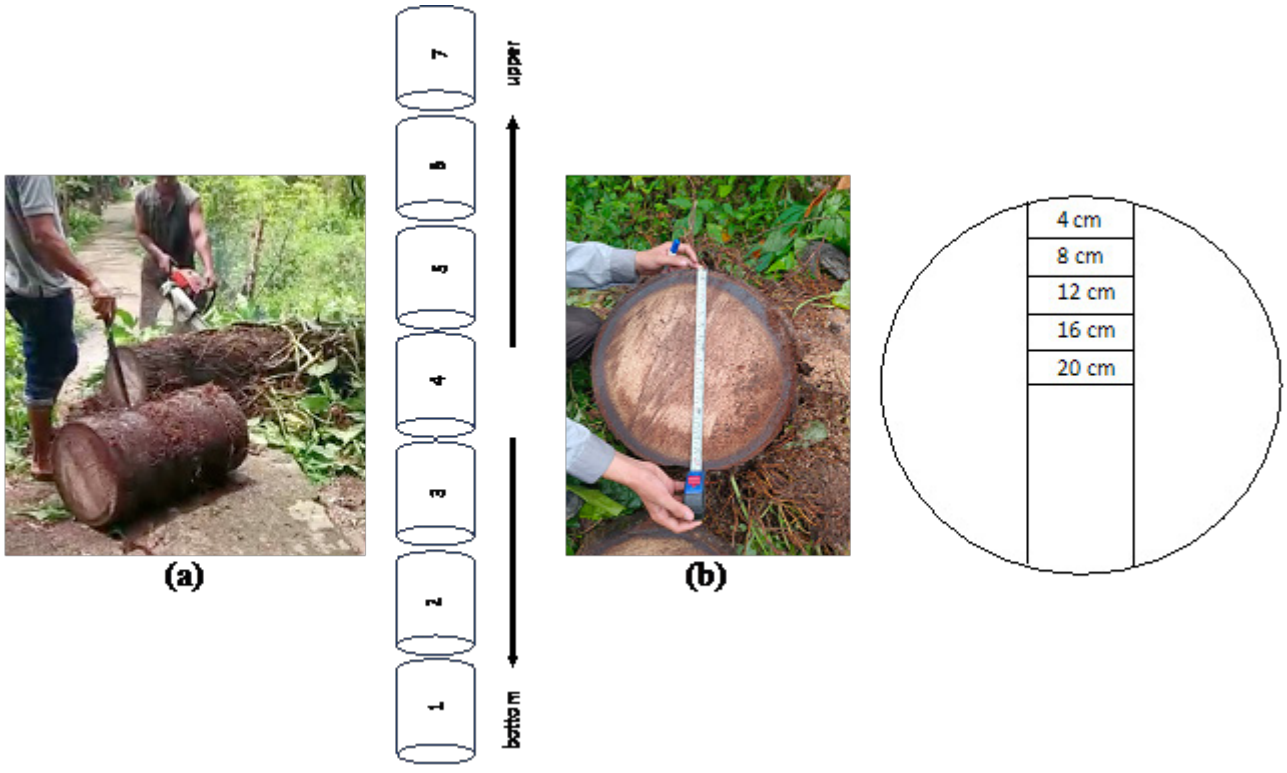

Figure 2. Photograph and schematic showing (a) vertical directions and (b) horizontal directions on the *A. longipes* stems.

of 20% $NaClO_2$ (w/v) solution was added and heated at 70°C while shaking every 30 minutes for 150 minutes. One ml of 20% $NaClO_2$ was added after 45, 90, and 150 minutes. The solution was heated for 4 hours, then cooled in ice water, and 15 mL of distilled water was added. The sample was filtered and washed successively with 100 ml of 1% acetic acid and 2–5 mL of acetone, then oven dried to constant mass at 103 ± 2 °C (*W2*) and weighed. Holocellulose content was calculated based on the equation below:

$$\text{Holocellulose (\%)} = \frac{W2}{W1} x100\% \quad (1)$$

Cellulose content was determined according to ASTM D 1103 (2001). The powder prepared for holocellulose analysis was used to determine α-cellulose content. The holocellulose was dissolved in 3 ml of 17.5% NaOH until completely submerged, and the mixture was stirred for 1 minute (*W1*). After soaking for 5 minutes, 3 ml of 17.5% NaOH was added and the mixture was stirred again for + 1 minute. The solution was left for 35 minutes, then 6 mL of distilled water was added before the mixture was filtered and washed with 60 mL of distilled water. Ten mL of 10% acetic acid was added with stirring. The mixture was filtered and washed with 60 mL of distilled water and 10 mL of acetone. The sample was oven dried to constant mass at 103 ± 2 °C and weighed (*W2*). The α-cellulose content was calculated based on the equation below:

$$\alpha\text{-cellulose (\%)} = \frac{W2}{W1} x100\% \quad (2)$$

Lignin content was determined based on ASTM D 1106 (2021). Up to 1 g (*W1*) of extractive-free powder was dissolved in 400 mL of boiling water and heated for 3 hours. The material was filtered and air-dried then dissolved in 15 mL of 72% sulfuric acid at 12–15°C for 1 minute. The mixture was left for 2 hours at 18–20°C with occasional stirring. The sample was heated in boiling water for 4 hours. Insoluble materials that precipitated were removed by filtration, and the filtrate was washed with hot water to remove residual acid. The samples were oven dried to constant mass at 103 ± 2 °C (*W2*). Lignin content was calculated based on the equation below:

$$\text{Lignin content (\%)} = \frac{W2}{W1} x100\% \quad (3)$$

Ash content was determined according to the ASTM D 1102 (2021). Around 2 g of sugar palm stem ground to 40-60 mesh (*W1*) was put into a furnace and heated at 600°C for 1 hour, cooled in a desiccator, and oven dried to constant mass at 103 ± 2 °C (*W2*). Ash content was calculated by the equation below:

$$\text{Ash content (\%)} = \frac{W2}{W1} x100\% \quad (4)$$

Mass and volume were measured after 2-cm cubes from each location were conditioned to 12% moisture content. Samples were measured before and after conditioning to determine shrinkage. The tests were performed on 25 specimens per radial stem position. Density was calculated by the equation below:

$$\text{Density (g/cm}^3\text{)} = \frac{Wood\ mass\ (g)}{Wood\ Volume\ (cm^3)} \quad (5)$$

The mechanical testing consisted of MOR, MOE, tensile strength, and compression tests. The mechanical tests were performed on 25 specimens per radial stem positions. The MOR and MOE were determined by a three-point bending test according to British Standard BS-373 (1957) on 2-cm by 2-cm by 30-cm-long beams with a 28-cm span. Load was applied at a rate of 6.5 mm/min. Load and displacement were continuously measured to failure, with a 1% deformation accuracy. A total of 25 specimens were tested per radial stem position.

Tension and compression parallel to grain strength were determined according to British Standard BS-373 (1957). For tensile tests, the form and dimensions of the test piece used in one method to determine tension parallel to grain strength must be as shown in the British Standard (1957). The test piece was positioned so that the direction of the annual rings in the cuboidal section was perpendicular to the bigger cross-sectional dimensions. The actual dimensions of the minimum cross-section must be measured. Load was applied at a constant head speed. Compression and tension load were applied to the test piece at a constant head speed of 1.25 mm per minute to failure. Tensile strength was calculated as the load/cross sectional area. Compression and tension tests were performed on a 50 kN universal testing machine (Tensilon RTF 1350, Japan) A total of 25 samples were tested for compression or tension at each position in the trunk.

Gas chromatography-mass spectroscopy analysis

Sugar palm trunk powder was extracted in an ethanol and benzene solution (1:0.4 v/v) for 8 hours. The extractive solution was analyzed using gas chromatography-mass spectrometry (GC-MS) on an Agilent Technologist, Mass Hunter 5977 (GC-MS 7890B, Santa Clara, CA USA) and a mass detector. The carrier gas utilized was helium with a flow rate of 1 mL per minute. One µL of the supernatant was injected into the GC-MS. Temperature was raised at a rate of 15°C per minute from 80°C to 200°C, then at 5°C per minute from 200°C to 280°C, and held at a constant temperature of 280°C for 5 minutes. The ion source was set at 230°C, and an ionization

potential of 70 eV was selected. The GC-MS interpretation relied on the National Institute of Standards and Technology (NIST) database (Lovestead and Urness 2019).

Fourier transform infrared (FT-IR) analysis

Sugar palm trunk powder samples were boiled for 2 hours to remove any extractives. After cooling the samples were stored for 1 hour at room temperature. The samples were filtered through a 100-mesh screen and the precipitate was dried for 12 hours at 35 ± 5 °C. The samples were mixed with KBr and compressed to a pellet that was analyzed on a Shimadzu FTIR-4200 spectrophotometer (Shimadzu, Tokyo, Japan) at a resolution of 12 cm^{-1}. Peaks were subjected to auto-correction and assigned to certain functional groups.

Thermogravinetry analysis (TGA)

Thermal stability and rate of mass change of the sugar palm trunk were measured by thermogravimetric analysis using an Ekstar SIII-Type 7300 Thermogravimetric Analyser (Hitachi, Tokyo, Japan). Approximately 10 mg were heated in an aluminum crucible from room temperature, gradually increasing to 600°C at a rate of 10°C per minute under a nitrogen at a flow rate of 30 mL/min.

Data analysis

The experimental design was a factorial complete randomized design with vertical and horizontal direction as factors. An analysis of variance (ANOVA) was performed according to the linear model. Variance components for the sources of variation were also estimated. Differences between means were examined using Duncan's multiple range test at $\alpha = 0.05$. Correlation coefficients between density and mechanical properties were calculated by considering the average values per sample by linear regression analysis using the least squares method. Statistical analysis was performed using R-studio version 4.2.2.

Results and discussion

Chemical content

Figure 3 shows the α-cellulose, holocellulose, lignin, and ash content of the *A. longipes* stem. Generally, α-cellulose content decreased from bark to the pith (horizontally) with a higher value of 39.23% at the bottom and outer position to a lower value of 24.97% at the upper and inner position. The α-cellulose content did not differ significantly from the bottom to the upper position, although there was a general decrease;

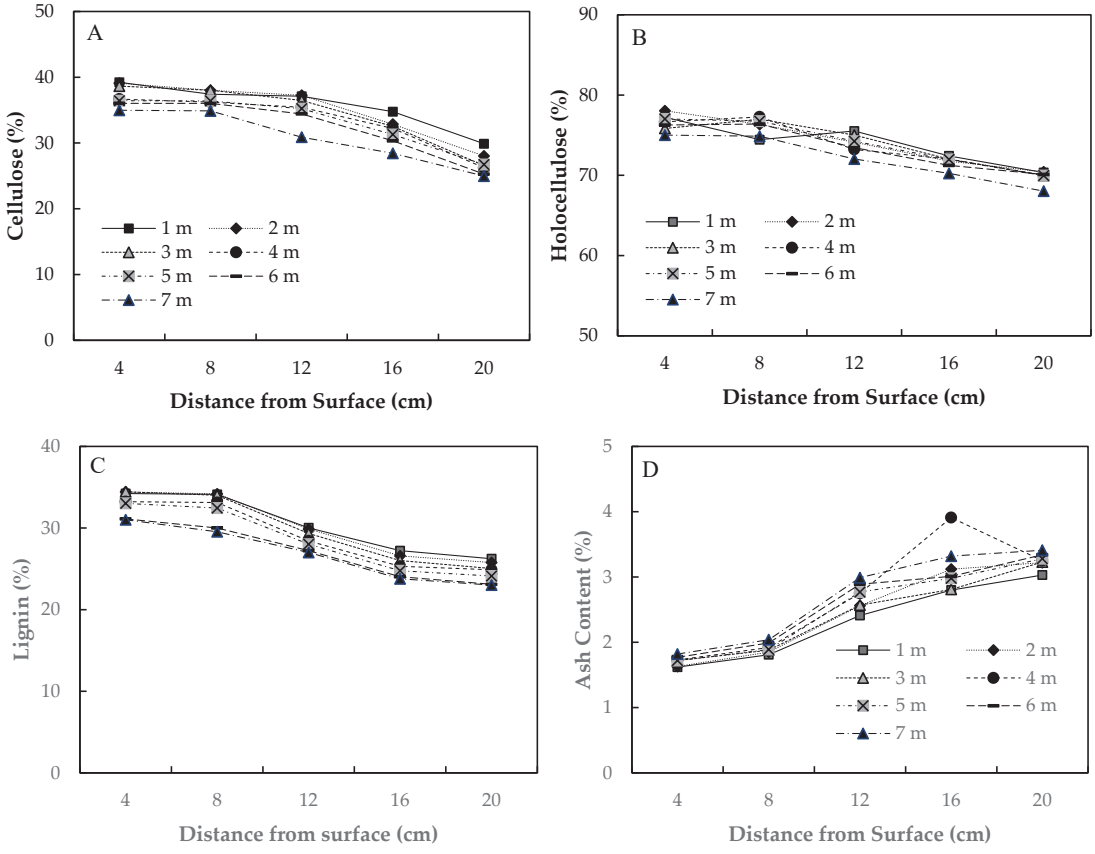

Figure 3. Concentrations (% m/m) of cellulose, holocellulose, lignin, and ash at selected distances above the ground and inward from the bark of an *A. longipes* stem.

α-cellulose content near the bark tended to be higher than towards the pith. This phenomenon likely reflects the higher density in that zone, reflecting the need to concentrate flexural properties around the circumference. Figure 1 (a) shows that the peripheral zone was only 2–3 cm thick, while the stem diameter was 40 cm. In addition, the density of palm wood is affected by the abundance of fibrovascular bundle (FVB) tissue. Conversely, increased parenchyma tissue towards the pith has less cellulose. Sahari et al. (2012) reported that *A. pinnata* contained 40.6% α-cellulose in the trunk which was slightly higher than that of *A. longipes*. Cellulose content of palm trees increases with increasing height; however, as the palm trees get older, the content decreases, which has been related to the maturity stage of the fiber (Imraan et al. 2023).

Trends with holocellulose content were similar to those for α-cellulose. Holocellulose content tended to decrease from the bark to the pith, reflecting the important of cellulose in the outer circumference supporting the stem. There was no significant difference in holocellulose content with distance from the ground, although levels were slightly higher near the base. Holocellulose content in *A. longipes* tended to decrease from the bottom to the upper position, as well as the outer (periphery) to the pith. The high carbohydrate content in *A. longipes* reflects the fact that this palm can produce a lot of sugar. A previous study of *A. pinnata* found holocellulose contents of 61.1%, 81.2%, 71.8%, and 65.6% for sugar palm trunk, frond, sugar palm bunch, and black fiber, respectively (Wulandari and Erwinsyah 2020).

Lignin distribution along the trunk also tended to decrease from the bottom to the top and from the periphery to the pith and ranged from 34.44% to 23.01%. Our previously research reported that the lignin content of the *A. longipes* bunch was 27.23%, which is lower than that of the trunk (Hakim et al. 2024). Sahari et al. (2012) reported that the lignin content of the *A. pinnata* trunk was higher at 46.4%,

Ash content tended to increase from the periphery to the pith (horizontal), but was similar with height. Ash content of *A. longipes* was slightly lower than *A. pinnata* actively (Sahari et al. 2012).

Wood density of *A. longipes trunk*

Air-dry density (at 12% moisture content) of the Indonesian sugar palm trunk ranged from 0.13 to 0.75 g/cm^3 (Table 2). Density was significantly higher at the bottom and outer section of the trunk. Density 1 m from the base had the largest range, with mean values from 0.73 to 0.75 g/cm^3. Density also decreased significantly from the bark (4 cm) to the pith (16 cm), then remained constant further inward. Density variations in palms reflect the presence of FVB tissue (fiber, xylem, and phloem) whose frequency tends to decrease from the skin towards the pith (Hakim et al. 2021; Srivaro et al. 2018a; Takoumbe et al. 2023; Wulandari and Erwinsyah 2020). Lower density in the middle zone of the stem is affected by the large amount of parenchyma tissue, which does not have a structural function in supporting the stem and tends to be less dense (Srivaro et al. 2020). These results were similar to those found for coconut palm wood and oil palm trunk zones (Rana et al. 2015; Srivaro et al. 2018b). Rana et al. (2015) also reported that coconut palm wood was denser in the core than the peripheral zone.

Hartono et al. (2019) found that *A. pinnata* had a significantly lower density (0.12–0.51 g/cm^3) at the same age (15 years) than *A longipes*. Another palm (*Elaeis guenensis*) had a density range of 2.22–4.04 g/cm^3, also lower than the density of *A. longipes* (Srivaro et al. 2018a). Likewise, the density of coconut (*Cocos nucifera*) trunk is also lower than that of *A. longipes* (Rana et al. 2015). Male and female varieties of *Borassus aethiopum* have densities between 0.26–0.86 g/cm^3 and 0.21–0.75 g/cm^3 from inner to outer position, respectively (Lego et al. 2018). Date palm stems (*Phoenix dactylifera* L.) were found to have wet and dry densities of 0.46 g/cm^3 and 0.69 g/cm^3, respectively (Rizanti et al. 2018). The density distribution of palm wood is contingent upon the number of FVB and parenchyma tissue (Ishiguri et al. 2007). The density distribution of Indonesian sugar palm wood is determined by the unique structure and content of the palm trunk, as well as its capacity to adjust to the tropical environment. While the core is typically not commercially used, the outer section is highly valued for its strength, durability, and versatility in industries such as construction and furniture manufacturing. Density variation can be linked to the quantity and arrangement of vascular bundles and the diameter and thickness of the cell walls within the bundles.

Vertical density also decreased from the bottom to the upper position, with a consistent pattern for each horizontal section, except at the bottom (Table 2). The variations may result from climate conditions during growth, geographical site, and tree age (Machado et al. 2014). Interestingly, the interaction between vertical and horizontal variations was highly significant, and the pattern was consistent for the same position.

Dimensional shrinkage

Generally, dimensional shrinkage increased from the bark to the pith, horizontally (Figure 4). Longui et al. (2014) reported the average value of volumetric shrinkage palm wood

Table 2. Average density from the top to bottom and surface to pith of an *A. longipes* stem.

Vertical direction	Density (g/cm^3)				
	Horizontal direction				
	4 cm	8 cm	12 cm	16 cm	20 cm
1 m	0.75 + 0.13 a	0.59 + 0.13 b	0.53 + 0.17 c	0.37 + 0.07 e	0.29 + 0.04 f
2 m	0.75 + 0.12 a	0.61 + 0.11 b	0.50 + 0.14 c	0.35 + 0.06 e	0.28 + 0.05 f
3 m	0.74 + 0.13 a	0.60 + 0.14 b	0.47 + 0.19 c	0.35 + 0.08 e	0.28 + 0.04 f
4 m	0.73 + 0.13 a	0.56 + 0.11 b	0.43 + 0.17 d	0.31 + 0.01 f	0.24+ 0.08 g
5 m	0.73 + 0.12 a	0.51 + 0.13 c	0.42 + 0.03 d	0.29 + 0.04 f	0.22 + 0.05 g
6 m	0.73 + 0.15 a	0.49 + 0.16 c	0.37 + 0.07 e	0.25 + 0.04 g	0.20 + 0.08 g
7 m	0.73 + 0.12 a	0.46 + 0.13 c	0.29 + 0.08 f	0.18 + 0.02 g	0.13 + 0.03 h

Note: Values represent means of five samples per location, while figures in parentheses represent one standard deviation. Values followed by same letters are not significantly different from each other by Duncan's multiple range test (α = 0.05).

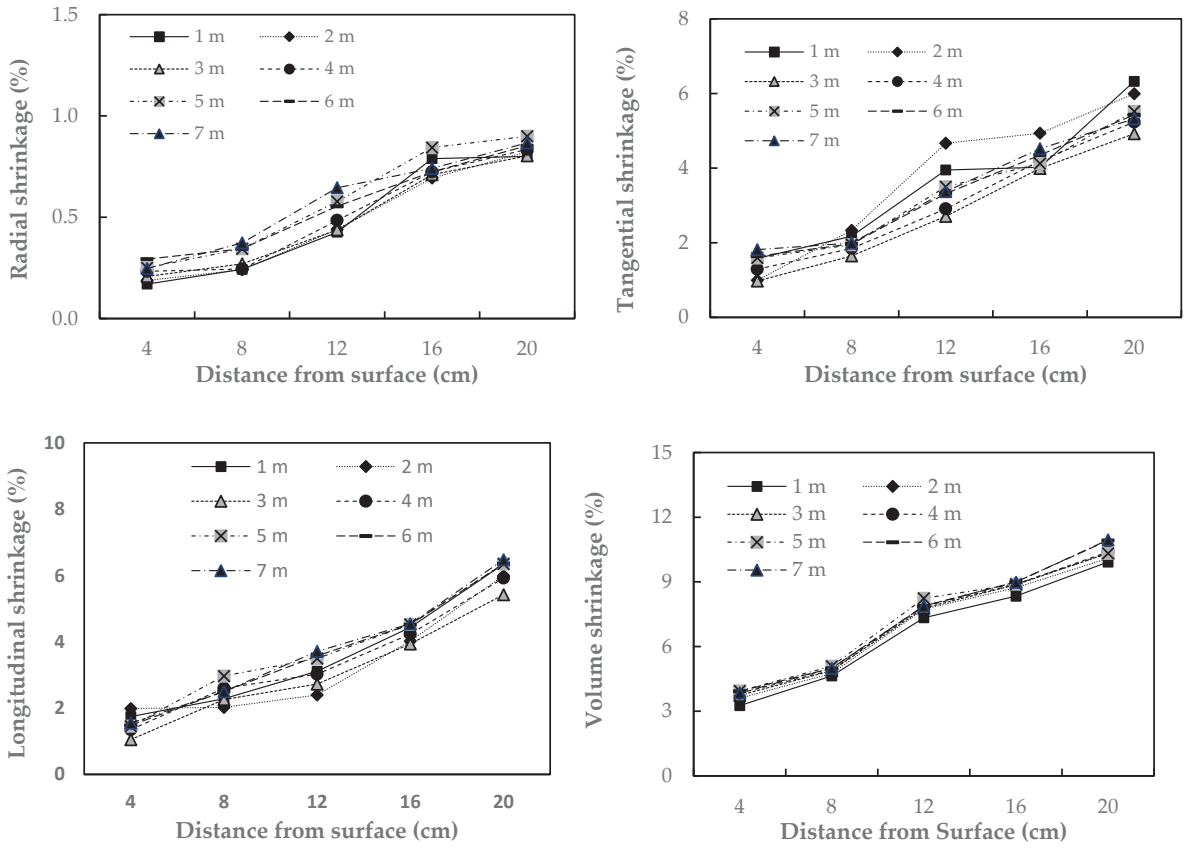

Figure 4. Dimensional shrinkage along the vertical and horizontal planes of an *A. longipes* trunk as the samples were dried from green to 12% moisture content.

decreased from the pith to the bark. These phenomena reflect the increased density *A. longipes* trunk from the bark to the pith (horizontally). Rahayu et al. (2021) reported that denser materials were more dimensionally stable. The shrinkage of wood is impacted by various factors, such as anisotropic shrinkage and alignment of the wood fibers in the trunk. In addition, the higher lignin content in the bark may have dimensional stability (Komisarz et al. 2023).

Longitudinal shrinkage was lower than tangential and radial shrinkage. This is consistent with the orientation of the fibers. Longitudinal shrinkage ranged from 0.17% to 0.87%, tangential shrinkage varied from 1.58% to 5.38%, radial shrinkage ranged from 1.74% to 6.48%, and volumetric shrinkage ranged from 3.26% to 10.95%. Shrinkage did not vary significantly from the bottom to the upper position, although shrinkage tended to increase with height. However, shrinkage tended to increase

significantly from the bark to the pith. Hartono et al. (2019) reported that volumetric shrinkage was lower, but the values were similar to those found by Nuryawan et al. (2017).

Modulus of ruptured and modulus of elasticity

The mechanical properties value of *A. longipes* at a distance greater than 12 cm from the bark was extremely low and is regarded as zero. The density value indicates that areas beyond 12 cm from the bark had lower density and exhibited twisting as a result of shrinkage. This occurred due to the presence of pores that facilitated water infiltration through capillary action, along with a significant amount of parenchyma tissue, that allowed water to be absorbed or evaporated quickly, depending on environmental conditions (Wulandari and Erwinsyah 2020). The trunk of *A. longipes* exhibits a distinct anatomical pattern regarding the horizontal orientation of the fibrovascular bundle, characterized by a decrease in FVB density as a one moves horizontally from the bark toward the pith. The reduced density of FVB will lead to a decline in strength in materials incorporating FVB tissue, such as that found in sugar palm trunks.

The outer layer of the trunk (close to the bark) exhibits a significantly higher density compared to the inner section influenced by the FVB density. The outer section is anatomically characterized by a higher composition of FVB with sclerenchyma fibers, in contrast to the parenchyma tissue that contains starch. This phenomenon results in the outer layer exhibiting greater strength than the inner layer. The values of MOR showed a notable decline as the distance from the ground increased, as well as with the distance inward from the surface at any specified height (Table 3). The observed values were generally greater than those established earlier for *A. Pinnata* (Nuryawan et al. 2017) and coconut wood (Rana et al. 2015).

In alignment with the MOR value pattern, the horizontal direction was exclusively assessed at a distance of 12 cm from the bark, with any measurement beyond this distance regarded as having value of zero (Table 4). There were no significant differences in MOE with distance from the ground nor in samples 4 and 8 cm from the outer edge; however, samples 12 cm inward did differ significantly between 1 to 3 m and 4 to 7 above ground.

A prior investigation involving *A. pinnata* indicated that the MOE value was consistently lower than that of *A. longipes* across all positions, with MOE values of *A. pinnata* ranging from 4.93 to 15.27 GPa (Nuryawan et al. 2017). When comparing the salacca palm frond, the MOE value is also lower than that of *A. longipes*: the measured value of MOE for salacca palm frond falls between 6 and 10 GPa (Hakim et al. 2021). Additionally, the MOE values comparison between *A. longipes* and coconut wood reveals distinct differences in values, with the measured values of MOE for coconut wood ranging from 1.8 to 14.03 GPa (Srivaro et al. 2018b).

In addition, the mechanical properties, including MOE and MOR, are also affected by the density of the *A. longipes* trunk. The analysis shown in Table 2, Table 3, and Table 4 illustrates the coherent relationship between density and mechanical properties. The section of the trunk exhibiting elevated density also demonstrated significant mechanical strength. The correlation between density and mechanical properties of *A. longipes* frond structure indicates that the high density of FVB tissue is associated with excellent mechanical properties compared to lower density material (Hakim et al. 2023).

3.4. Tensile and compression (parallel to grain) strength

The tensile strength and compression (parallel to grain) of *A. longipes* are summarized in Table 5 and 6. Similar to the

Table 3. MOR of *A. longipes* samples removed from selected heights above ground and distances inward from the surface.

Vertical direction	Horizontal direction (MPa)[a]		
	4 cm	8 cm	12 cm
1 m	143.49 ± 13.33 a	77.94 ± 2.69 d	19.73 ± 1.64 g
2 m	128.70 ± 15.23 a	66.98 ± 3.57 e	19.38 ± 2.75 g
3 m	122.83 ± 20.63 a	64.95 ± 5.38 e	18.01 ± 3.16 g
4 m	106.15 ± 11.48 b	63.07 ± 4.60 e	12.79 ± 3.30 h
5 m	100.32 ± 15.21 b	61.50 ± 1.78 f	12.11 ± 2.96 h
6 m	99.10 ± 17.89 b	60.77 + 1.72 f	11.25 + 1.76 h
7 m	96.79 ± 16.37 c	58.90 + 2.34 f	10.42 + 1.87 i

Note: Values represent means of five samples per location, while figures in parentheses represent one standard deviation. Values followed by same letters are not significantly different from each other by Duncan's multiple range test (α = 0.05).

Table 4. MOE of *A. longipes* removed from selected heights above ground and distances inward from the surface.

Vertical direction	Horizontal direction (GPa)[a]		
	4 cm	8 cm	12 cm
1 m	24.92 ± 1.51 a	12.98 ± 0.96 b	2.05 ± 0.52 c
2 m	22.78 ± 1.48 a	12.78 ± 0.96 b	1.59 ± 0.43 c
3 m	22.54 ± 1.32 a	12.65 ± 0.82 b	1.85 ± 0.50 c
4 m	21.31 ± 1.35 a	12.19 ± 0.96 b	0.81 ± 0.26 d
5 m	21.24 ± 1.10 a	11.77 ± 1.00 b	0.76 ± 0.21 d
6 m	17.53 ± 1.15 b	11.77 ± 1.07 b	0.73 ± 0.21 d
7 m	15.60 ± 1.33 b	9.94 ± 0.98 b	0.35 ± 0.11 d

Note: Values represent means of five samples per location, while figures in parentheses represent one standard deviation. Values followed by same letters are not significantly different from each other by Duncan's multiple range test (α = 0.05).

Table 5. Average value of variation direction (vertical and horizontal) for tensile strength of *A. longipes.*

Vertical direction	Horizontal direction (GPa)		
	4 cm	8 cm	12 cm
1 m	16.03 ± 2.29 a	8.98 ± 0.46 b	0.95 ± 0.32 c
2 m	16.01 ± 2.38 a	8.88 ± 0.46 b	0.89 ± 0.43 c
3 m	16.02 ± 2.22 a	8.52 ± 0.32 b	0.85 ± 0.20 c
4 m	16.01 ± 1.35 a	8.49 ± 0.36 b	0.78 ± 0.36 d
5 m	15.87 ± 1.10 a	8.48 ± 0.40 b	0.72 ± 0.41 d
6 m	15.77 ± 1.15 b	8.39 ± 0.37 b	0.68 ± 0.51 d
7 m	15.56 ± 1.33 b	8.38 ± 0.38 b	0.55 ± 0.21 d

Note: Values represent means of five samples per location, while figures in parentheses represent one standard deviation. Values followed by same letters are not significantly different from each other by Duncan's multiple range test (α = 0.05).

Table 6. Average value of variation direction (vertical and horizontal) for compression strength of *A. longipes.*

Vertical direction	Horizontal direction (MPa)		
	4 cm	8 cm	12 cm
1 m	6.14 + 1.19 a	1.16 + 0.52 b	0.92 + 0.12 c
2 m	5.89 + 1.48 a	1.15 + 0.46 b	0.92 + 0.23 c
3 m	5.97 + 1.32 a	1.11 + 0.42 b	0.57 + 0.15 c
4 m	5.57 + 1.35 a	1.06 + 0.56 b	0.56 + 0.16 d
5 m	5.42 + 1.10 a	1.06 + 0.39 b	0.57 + 0.11 d
6 m	5.13 + 1.15 b	1.03 + 0.47 b	0.53 + 0.18 d
7 m	5.13 + 1.33 b	1.01 + 0.48 b	0.53 + 0.13 d

Note: Values represent means of five samples per location, while figures in parentheses represent one standard deviation. Values followed by same letters are not significantly different from each other by Duncan's multiple range test (α = 0.05).

pattern for MOR and MOE, the horizontal direction was also only measured up to a distance of 12 cm from the bark, and more than 12 cm from the bark was considered to have a value of zero. Furthermore, the tensile strength and compression strength exhibited the highest value at 4 cm from the bark in the horizontal direction. The lowest value was observed at 12 cm from the bark in the horizontal direction. These phenomena are influenced by the density of the *A. longipes* trunk. Darwis et al. (2013) reported that the density influenced the mechanical properties of Palmae trunks. In addition, α-cellulose content in the bark observed in this study exceeded that of the pith of *A. longipes*. The α-cellulose serves as the primary component of the cell wall. Consequently, elevated α-cellulose content has been found to lead to thickened cell walls and enhanced mechanical properties (Ouyang and Wang 2022).

Relationships between density and mechanical properties

The correlations between density and MOR, along with MOE properties of *A. longipes,* are depicted in Figure 5a and 5b. The graph indicates a downward trend in the density, accompanied by a reduction in the MOR and MOE of the *A. longipes* trunk. The wood density of individual samples exhibits a moderate correlation with the mechanical properties of MOR and MOE. Consequently, it is feasible to accurately predict the strength of sugar palm trunks based on their density for individual samples, owing to this strong predictive capability.

The relationship between wood density and strength properties (MOR and MOE) is generally acknowledged, as density serves as an indicator of the relative quantity of solid cell wall

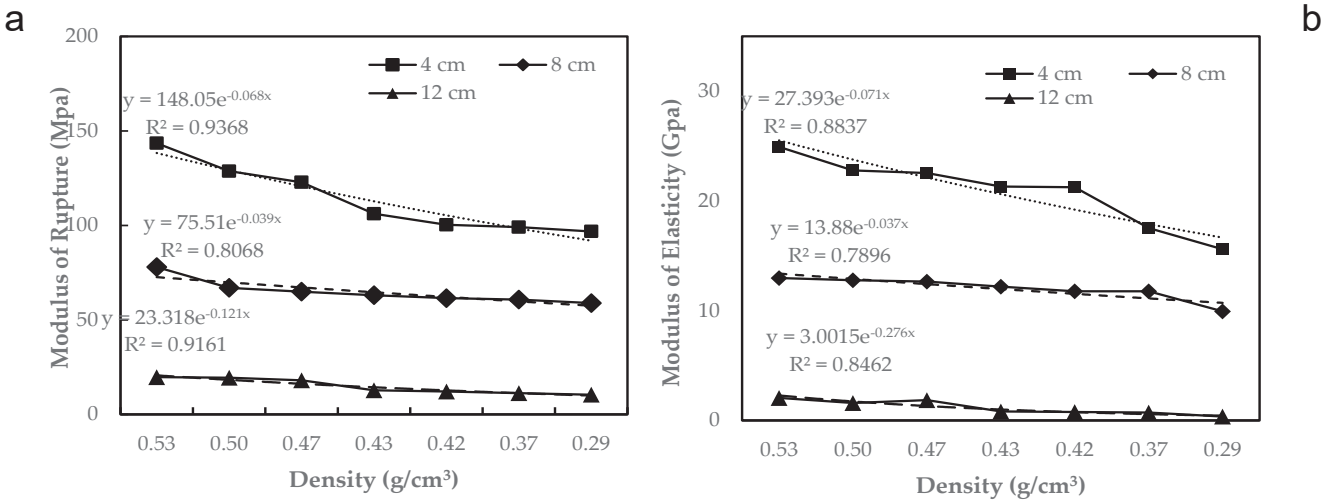

Figure 5. (a) Relationship between MOR and density; (b) Relationship between MOE and density.

(Wulandari and Erwinsyah 2020); however, the correlations are significantly influenced by the orientation, whether vertical or horizontal (Hakim et al. 2021; Srivaro et al. 2018a). In certain instance, the low-density correlations with mechanical properties were linked to the impact of the number of fibrovascular bundles (Hakim et al. 2022; Srivaro et al. 2018a). The reasoning is that as density increases, the number of FVBs also increases, which consequently affects the mechanical tests and leads to strong correlations when density is considered (Hakim et al., 2022). In addition, the previous discussion of chemical properties showed that the composition of cellulose and lignin from the outer to the inner (radial direction) *A. longipes* trunk also increased, as did MOE and MOR.

Gas chromatography–mass spectrometry analysis

The GC-MS analysis of the ethanol-benzene extract of *A. longipes* trunk resulted in the detection of 22 compounds that are presented in Table 7. Figure 6 shows the major compounds identified as hexadecanoic acid, vaccenic acid, 9-octadecenoic acid ethyl ester, tricosane, nonadecane, dodecane, 2,6,10-trimethyl-, and pentatriacontane. The components identified in this section of the trunk are nearly identical to those found in the bunch, which are mostly carboxylic acid-dominated (Hakim et al. 2024). Several linear acids such as hexadecanoic, heptadecanoic, and vaccenic were present, with significant percentage areas which are higher than the percentage areas of the acid components in the bunch (Hakim et al. 2024). The higher amount of acid in the *A. longipes* trunk may be influenced by the holocellulose content. As holocellulose decomposed between 250°C and 275°C, light oxygenates, acetic acid, furfural, and water are produced (Hamid et al., 2022). The degradation of lignin at 500°C–600°C produced phenolic compound, which was followed by esters and alkanes such as 3,7,11,15-tetramethyl-methyl ester, hexadecanoic acid ethyl ester, 9-octadecanoic acid ethyl ester, tricosane, tetracosane, nonadecane, and pentatriacontane. The esters compounds were

Table 7. The chemical compound of *A. longipes* trunk obtained in GC-MS analysis.

Peak	RT	Area (%)	Compound
1	4.898	-	1,2-Diphenylethan-1-ol
2	8.279	4.6	[Dodecanoyl(methyl)amino]Acetic Acid
3	9.79	-	Myristic Acid
4	11.22	97.98	n-Hexadecanoic acid
5	11.382	46.85	Hexadecanoic acid, ethyl ester
6	11.832	-	Heptadecanoic acid
7	12.42	84.77	cis-Vaccenic acid
8	12.57	100	9-Octadecenoic acid ethyl ester
9	12.743	27.26	Octadecanoic acid, ethyl ester
10	13.620	-	Heptadecane, 2,6,10,15-tetramethyl-
11	14.647	8.98	Tricosane
12	15.916	8.83	Nonadecane
13	17.531	11.63	Dodecane, 2,6,10-trimethyl-
14	18.523	-	1-(1-Ethoxyethoxy)-5-pentanol
15	19.596	19.73	Pentatriacontane
16	22.261	-	Tritriacontane
17	23.253	-	6,10,14-Hexadecatrienoic acid, 3,7,11,15-tetramethyl-, methyl ester, [R-(E,E)]-
18	25.71	-	Pentatriacontane
19	28.006	-	3-Acetoxypropyl trimethyl acetate
20	28.963	-	Pentatriacontane
21	31.005	-	Pentatriacontane
22	33.324	-	Tetracosane

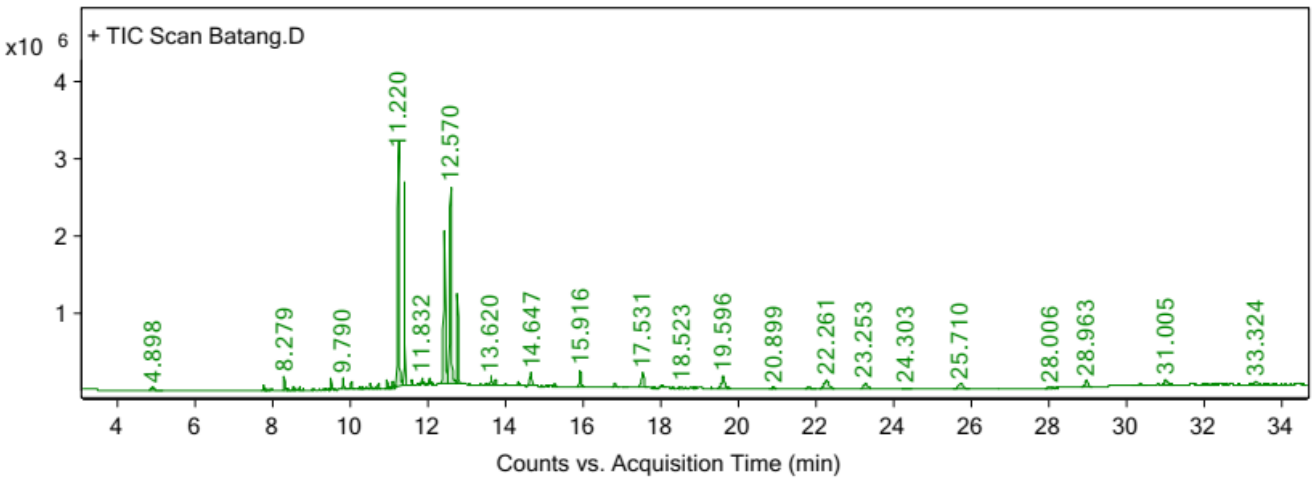

Figure 6. GC-MS chromatogram of *A. longipes* trunk.

also identified in *A. longipes* bunch and date palm biomass (Hamid et al. 2022), but the alkanes compound was unidentified in *A. longipes* bunch. This result could be due to lignin content because phenolic compounds are primarily produced through lignin decomposition, which involves cleaving ether linkages (β-O-4 and α-O-4 bonds) to generate the lignin monomer.

Fourier-transform infrared spectroscopy analysis.

Chemical studies of the functional groups found in the *A. longipes* trunk were studied using FTIR, as shown in Figure 7. A broad peak at around 3342 cm^{-1} due to stretching vibration of the O-H bond was observed in the sample, while peaks due to C-H bond stretching frequency were detected at 2851 cm^{-1}. These peaks were stronger for these samples because the cellulose content was higher, and the lignin and hemicellulose components of the raw biomass were lower. The broad absorption indicated the hydrophilic tendency of material, and it is attributed to the moisture content and hydroxyl functional group found in lignin, cellulose, and hemicellulose. The peaks at 1597 cm^{-1} indicated the presence of lignin; these are due to the stretching of C=C present in aromatic structure of lignin (Shaikh et al. 2021). Meanwhile, the peaks on 1219, 1329, and 1455 cm^{-1} could be indicated with the C-O carbonyl band in lignin and xylan units; these peaks are similar to that of *A. longipes* bunch. The peaks at 837–1162 cm^{-1} could correspond to both aliphatic and aromatic functional groups.

Thermogravimetry analysis

Thermal stability and weight loss behavior of *A. longipes* trunk was assessed by using TGA, and the result is shown in Figure 8. It is evident from Figure 8a that there was a significant weight loss at 402°C; temperature increased the mass loss of the biomass samples. Based on the graph in Figure 8b, the first phase had moisture evaporation at temperatures between 50–200°C, with a mass loss of 6.9%. This result was slightly different from that of Hakim et al. (2024), with the moisture evaporation leading to mass loss of 9.9%. The next phase was degradation of hemicellulose at around 250°C, and complete degradation at 402°C, with mass loss of 18%, reflecting carbohydrate losses loss. The *A. longipes* trunk thermal stability was illustrated by the DTG curves shown in Figure 8c. The maximum mass loss rate was at 290°C with a value of 1.08 mg/min. This result is supported by Werner et al. (2014), who found that polysaccharide decomposition occurs at a temperature range of 200–380°C, with xylan in particular experiencing a maximum mass loss rate at lower temperatures of 243°C and 292°C. However, this differed from Hakim et al. (2024), who reported that peak decomposition occurred at average temperature of 327°C (Figure 8d). According to Poletto et al. (2010), temperatures between 210°C and 300°C may be linked to the gradual breakdown of lignin and the breakdown of hemicellulose. Random cleavage of the cellulose's glycosidic bond

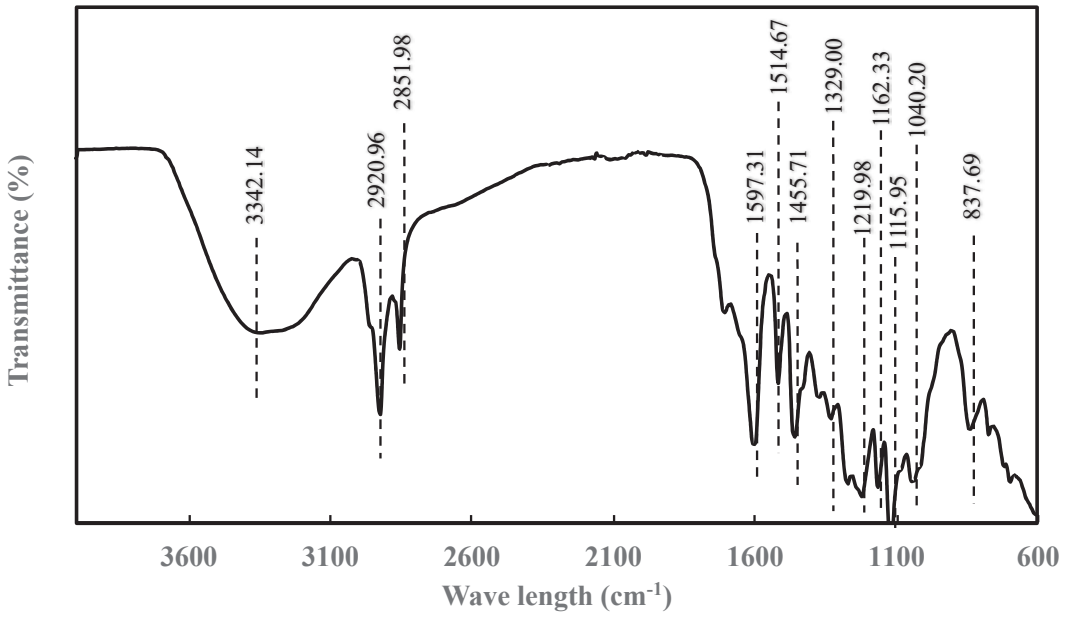

Figure 7. FTIR spectra of *A. longipes* trunk.

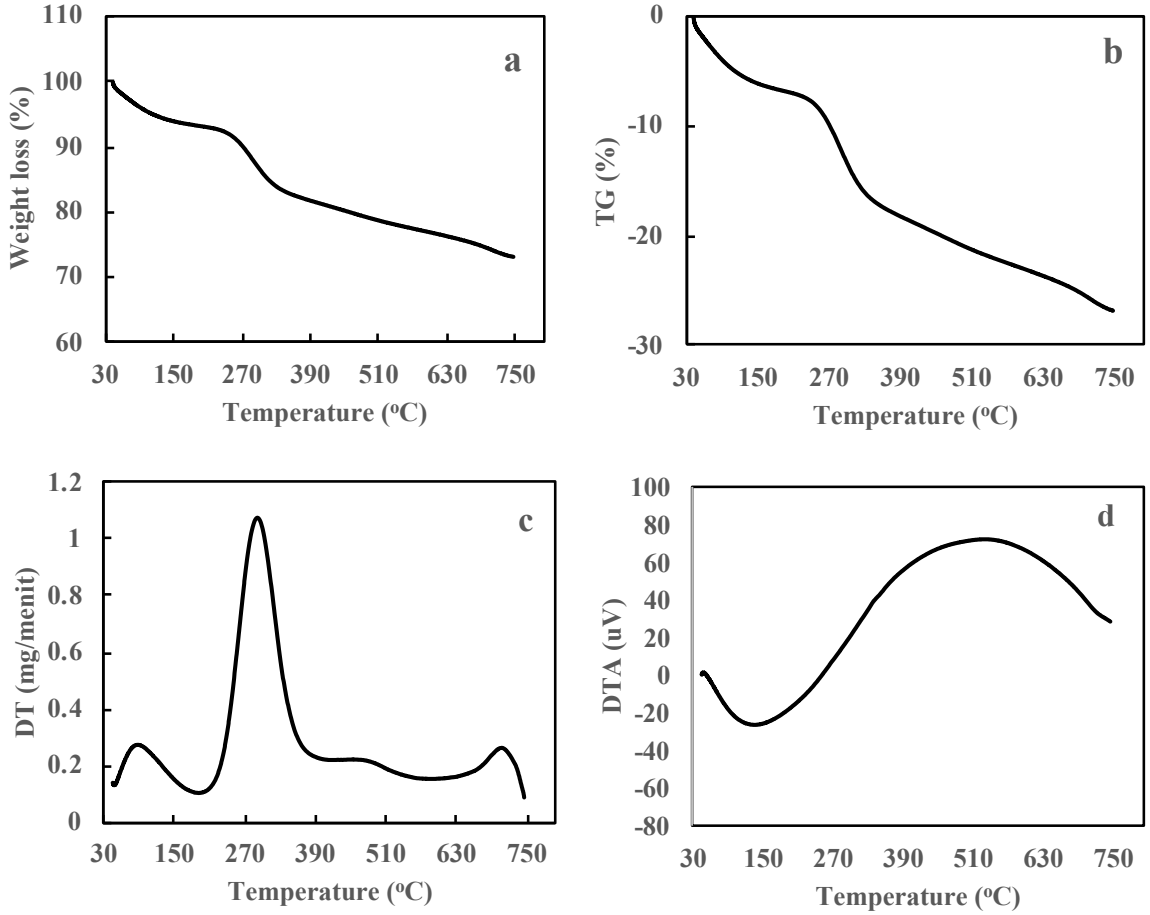

Figure 8. Thermogravimetric curve of *A. longipes* trunk. (a). Weight loss; (b). Thermo- stability; (c). Differential thermal stability; (d). Differential thermal analysis.

occurs between 275°C and 350°C, while lignin decomposes between 250°C and 500°C.

Variability of properties and utilization

Although *A. longipes* is a palm species that exhibits significant variability due to site and climatic conditions, it demonstrates high variability within individual trunks. This study examines the fundamental characteristics in both the vertical and horizontal directions. Differences in the variation of properties within the trunk of *A. longipes* are a significant factor contributing to variation in its basic characteristics. The effect of trunk position on *A. longipes* should be considered when selecting the appropriate end use. Horizontally, the potential for using *A. longipes* as construction wood would be more suitable if limited to the peripheral section, approximately 3–4 cm thick, from the bark. Material more than 4 cm from the bark is no longer suitable for use as building or construction timber under heavy loads. The influence of individual plants on various wood properties should be considered in the selection process and for improving wood quality.

Regarding within-trunk variation, horizontal variation was the most significant for all properties of the sugar palm trunk, highlighting the importance of *A. longipes* trunk characteristics in determining suitable uses. These variations follow a trend of increasing trunk quality from the pith to the outer peripheral zones (bark), which is related to chemical content and density. In this study, the horizontal position at 4 cm from the bark exhibited favorable properties (density, MOE, and MOR), with values gradually decreasing toward the pith. However, vertical variation within the trunk showed minimal range, making it less of an obstacle in quality selection and advantageous for utilizing *A. longipes* trunks along their full length, from bottom to top. GC-MS analysis revealed that the *A. longipes* trunk contains several compound categories, such as acids, esters, and alkanes. One of the acidic compounds,

vaccenic acid, may have further utility as it has been identified as a prominent compound that has antimicrobial properties.

Conclusions

The *A. longipes* palm from Sumatera, Indonesia, exhibited high-quality wood-like properties in the outermost 4 cm of its trunk diameter. The stems exhibited moderate to low density from the outermost to the innermost trunk position, which was associated with increased flexural properties closer to the outer edges. No significant differences were observed with distance above ground, and within-trunk heterogeneity was minimal. The outermost regions of the *A. longipes* trunk have potential as a substitute for industrial wood. The predominant chemicals found in the stems of *A. longipes* included n-hexadecanoic acid, 9-octadecenoic acid ethyl ester, and vaccenic acid, which are common fatty acids derived from palm plants and have potential antibacterial properties. Thermal analysis indicated that *A. longipes* stems undergo thermal degradation at temperatures up to 402°C, resulting in an 18% weight loss.

Author Contributions: All authors have contributed equally.

Funding: This research was funded by World Class University (WCU) Grant No. 40/UN5. 2.3.1/PPM/KP-WCU/2022, the Indonesian Endowment Fund for Education (LPDP), Ministry of Finance, Republic of Indonesia.

Data Availability Statement: The data presented in this study are available on request from the corresponding author.

Acknowledgments: The authors are grateful to Universitas Sumatera Utara for funding this research through the World Class University (WCU) grant, the Indonesian Endowment Fund for Education (LPDP), Ministry of Finance, Republic of Indonesia. The authors would also like acknowledge Laboratory of Forest Product Technology, Faculty of Forestry, Universitas Sumatera Utara for providing equipment to carry out the experiment.

Conflicts of Interest: The authors declare no conflict of interest.

References

ASTM (2021) D 1102. Standard test method for ash in wood. American Society for Testing and Materials, West Conshohocken, PA. USA. https://store.astm.org/d1102-84r21.html

ASTM (2001) D 1103. Standard test method for alpha cellulose in wood. American Society for Testing and Materials, West Conshohocken, PA. USA. https://www.document-center.com/standards/show/ASTM-D1103

ASTM (1978) D 1104. Standard test method for holocellulose in wood. American Society for Testing and Materials, West Conshohocken, PA. USA. https://www.document-center.com/standards/show/ASTM-D1104

ASTM (2021) D 1106. Standard test methods for acid insoluble lignin in wood. American Society for Testing and Materials, West Conshohocken, PA. USA. https://store.astm.org/d1106-21.html

Azhar I, Risnasari I, Muhdi, Srena MF, Riswan (2019) The Utilization of Sugar Palm (*Arenga pinnata*) by the People Around Batang Gadis Nasional Park Area. IOP Conf Ser: Earth Env Sci 305 012016:1–7. https://doi.org/10.1088/1755-1315/305/1/012016.

BPS (2021) Statistik Perusahaan Perkebunan Provinsi Sumatera Utara 2020. Badan Pusat Statistik Provinsi Sumatera Utara. Indonesia. https://sumut.bps.go.id/id/publication/2021/12/23/6b4fca56257b3152776ef37f/statistik-perusahaan-perkebunan-provinsi-sumatera-utara-2020.html

British Standard (1957) BS 373: Methods of testing small clear specimens of timber. https://www.en-standard.eu/bs-373-1957-methods-of-testing-small-clear-specimens-of-timber/

Darwis A, Nurrochmat DR, Massijaya Y, Nugroho N, Alamsyah EM, Bahtiar ET, Safe'i R (2013) Vascular bundle distribution effect on density and mechanical properties of oil palm trunk. Asian J Plant Sci 12(5):208–213. https://doi.org/10.3923/ajps.2013.208.213

Fadhilla S, Hakim L, Agustian A, Lubis YS, Siregar AW (2023) The diversity of utilizations, tapping flow discharge, and conservation of sugar palm (*Arenga longipes* Mogea) cultivated in Langkat, North Sumatra, Indonesia. Biodiversitas 24(1):122–132. https://doi.org/10.13057/BIODIV/D240116

Gunawan R, Ramadhan UG, Iskandar J, Partasasmita R (2018) Local knowledge of utilization and management of sugar palm (*Arenga pinnata*) among Cipanggulaan People of Karyamukti, Cianjur (West Java, Indonesia). Biodiversitas 19(1):93–105. https://doi.org/10.13057/biodiv/d190115

Hakim L, Batubara R, Manurung H, Silitonga VW (2023) Longitudinal and radial variability of anatomical properties, fiber morphology, and mechanical properties of fibrovascular bundle from Indonesian *Arenga longipes* Mogea sp. nov frond. J Nat Fibers 20(2):1–16. https://doi.org/10.1080/15440478.2023.2224978

Hakim L, Iswanto AH, Herawati E, Batubara R, Lubis YS, Aini EN (2024). Characterization of Indonesian sugar palm bunch (*Arenga longipes* Mogea) properties for various utilization purposes. Forests 15(2):1–15. https://doi.org/10.3390/f15020239

Hakim L, Widyorini R, Nugroho WD, Prayitno TA (2021) Radial variability of fibrovascular bundle properties of salacca (*Salacca zalacca*) fronds cultivated on turi agrotourism in Yogyakarta, Indonesia. Biodiversitas *22*(8):3594–3603. https://doi.org/10.13057/biodiv/d220861

Hakim L, Widyorini R, Nugroho WD, Prayitno TA (2022) Effect of vascular tissue on mechanical properties of fibrovascular bundles of *Salacca Sumatrana* Becc. fronds. J Nat Fibers 19(14):1–14. https://doi.org/10.1080/15440478.2021.1982824

Hamid FA, Zainal NH, Othman NEA, Ismail F, Wahab NA, Aziz AA (2022) Characterization of palm pyroligneous acid and its effectiveness as antifungal agent for oil palm trunk. J Oil Palm Research 34(4):678–685. https://doi.org/10.21894/jopr.2022.0007

Hartono R, Muhdi, Nainggolan JP (2019) The physical properties and the extractive content of sugar palm stem (*Arenga pinnata*). J Sylva Indonesiana 2(1): 37–46. https://doi.org/10.32734/jsi.v2i1.813

Haryoso A, Zuhud EAM, Hikmat A, Sunkar A, Darusman D (2020) Ethnobotany of sugar palm (*Arenga pinnata*) in the sasak community, Kekait village, West Nusa Tenggara, Indonesia. Biodiversitas 21(1):117–128. https://doi.org/10.13057/biodiv/d210116

Imraan M, Ilyas RA, Norfarhana AS, Bangar SP, Knight VF, Norrrahim MNF (2023) Sugar palm (*Arenga pinnata*) fibers: new emerging natural fibre and its relevant properties, treatments and potential applications. J Mater Res Technol 24 (May-Jun):4551–4572. https://doi.org/10.1016/j.jmrt.2023.04.056

Ishiguri F, Eizawa J, Saito Y, Iizuka K, Yokota S, Priadi D, Sumiasri N, Yoshizawa N (2007) Variation in the wood properties of *Paraserianthes falcataria* planted in Indonesia. IAWA J 28(3):339–348. https://doi.org/10.1163/22941932-90001645

Johnson DV (1992) Palm utilization and management in Asia: examples for the neotropics. Bulletin de l'Institut Français d'études Andines 21(2): 727–740. https://doi.org/10.3406/bifea.1992.1084

Komisarz K, Majka TM, Pielichowski K (2023) Chemical and physical modification of lignin for green polymeric composite materials. Materials 16(1):1–40. https://doi.org/10.3390/ma16010016

Lego K, Sharma C, Sharma M (2018) Axial variation of wood density in *Pinus merkusii* Jungh. & de Vriese. J Tree Sci, *37*(1):1–10. https://doi.org/10.5958/2455-7129.2018.00001.8

Longui E L, Romeiro D, Pfleger P, Lima IL, Silva FG, Garcia JN, Bortoletto G, Neto AOLF, Florsheim SMB (2014) Radial variation of anatomical features, physicomechanical properties and chemical constituents and their potential influence on the wood quality of 45-year-old *Eucalyptus propinqua*. Aust For *77*(2):78–85. https://doi.org/10.1080/00049158.2014.905739

Lovestead TM, Urness KN (2019) Gas chromatography-mass spectrometry (GC−MS). *ASM International Handbook*. National Institute of Standards and Technology. https://tsapps.nist.gov/publication/get_pdf.cfm?pub_id=926655.

Machado JS, Louzada JL, Santos AJA, Nunes L, Anjos O, Rodrigues J, Simões RMS, Pereira H (2014) Variation of wood density and mechanical properties of blackwood (*Acacia melanoxylon* R. Br.). Mater Design 56(April):975–980. https://doi.org/10.1016/j.matdes.2013.12.016

Mogea JP (2004) Four new species of Arenga (Palmae) from Indonesia. Reinwardtia, 12(2):181–189. https://archive.org/details/reinwardtia-12-181-189.

Mogea MJ, Seibert B, Smits W (1991) Multipurpose palms: the sugar palm (*Arenga pinnata*). Agroforest Syst 13:111–129. https://link.springer.com/article/10.1007/BF00140236.

Muda M, Muda NA, Awal A (2024) Sugar palm (*Arenga pinnata* Wurmb Merr.): Its potential, limitation, and impact on socio-economic development of rural communities in Malaysia. J Nat Fibre Poly Comp *3*(1)5:1–8. https://239ec624-ab30-45de-8e11-0d1c08b34d22.filesusr.com/ugd/391d16_4677fbc829f741e4857ad38be2195750.pdf.

Nirawati, Restu M, Kuswinanti T, Musa Y, Paembonan SA, Millang S, Syahidah, Larekeng SH (2020) Morphological characteristics of *Arenga pinnata* Merr. from Maros and Sinjai Provenances in South Sulawesi, Indonesia, and its relationship with brix content. IOP Conf Ser: Earth Env Sci 486 012080:1–5. https://doi.org/10.1088/1755-1315/486/1/012080.

Nuryawan A, Tarigan A, Hakim L (2017). The feasibility of sugar palm (*Arenga pinnata*) trunk for raw material of parquet (wood flooring). IOP Conf Ser: Mater Sci Eng 180 012017:1–7. https://doi.org/10.1088/1757-899X/180/1/012017.

Ouyang F, Wang W (2022) Effect of thermo-hydro-mechanical treatment on mechanical properties of wood cellulose: A molecular dynamics simulation. Forests 13(6)903:1–11. https://doi.org/10.3390/f13060903.

Pillai AR, Riyas CT, Sabu KK (2020) A review on the unexplored and underutilized Arenga species in India. Current Botany 11:226–232. https://doi.org/10.25081/cb.2020.v11.6252

Poletto M, Dettenborn J, Pistor V, Zeni M, Zattera J (2010) Materials produced from plant biomass. Part I: Evaluation of thermal stability and pyrolysis of wood. Mater Res 13 (3, Sept):375–379. https://doi.org/10.1590/S1516-14392010000300016

Rahayu I, Dirna FC, Maddu A, Darmawan W, Nandika D, Prihatini E (2021) Dimensional stability of treated sengon wood by nano-silica of betung bamboo leaves. Forests 12(11)1581:1–9. https://doi.org/10.3390/f12111581

Rana M, Das A, Ashaduzzaman M (2015) Physical and mechanical properties of coconut palm (*Cocos nucifera*) stem. Bangladesh J Sci Industr Res 50(1):39–46. https://doi.org/10.3329/bjsir.v50i1.23808.

Rizanti DE, Darmawan W, George B, Merlin A, Dumarcay S, Chapuis H, Gérardin C, Gelhaye E, Raharivelomanana P, Sari RK, Syafii W, Mohamed R, Gerardin P (2018) Comparison of teak wood properties according to forest management: short versus long rotation. Annals Forest Sci, 75(39):75–89. https://doi.org/10.1007/s13595-018-0716-8

Sahari J, Sapuan SM, Ismarrubie ZN, Rahman MZA (2012) Physical and chemical properties of different morphological parts of sugar palm fibres. Fibres Text East Eur 91(2): 21–24. http://www.fibtex.lodz.pl/article682.html.

Shaikh HM, Anis A, Poulose AM, Al-Zahrani SM, Madhar NA, Alhamidi A, Alam MA (2021) Isolation and characterization of alpha and nanocrystalline cellulose from date palm (*Phoenix dactylifera* l.) trunk mesh. Polymers 13(11)1893:1–14. https://doi.org/10.3390/polym13111893.

Srivaro S, Matan N, Lam F (2018a) Property gradients in oil palm trunk (*Elaeis guineensis*). J Wood Sci 64:709–719. https://doi.org/10.1007/s10086-018-1750-8.

Srivaro S, Rattanarat J, Noothong P (2018b) Comparison of the anatomical characteristics and physical and mechanical properties of oil palm and bamboo trunks. J Wood Sci, 64:186–192. https://doi.org/10.1007/s10086-017-1687-3.

Srivaro S, Tomad J, Shi J, Cai J (2020) Characterization of coconut (*Cocos nucifera*) trunk's properties and evaluation of its suitability to be used as raw material for cross laminated timber production. Cons Build Mater 254:1–14. https://doi.org/10.1016/j.conbuildmat.2020.119291.

Takoumbe C, Tiaya EM, Ndapeu D, Mejouyo PWH, Wagang CVK, Njeugna E, Bistac S (2023) Selected physical and mechanical properties of the oil palm pseudo-trunk: Case of the Tenera variety from Cameroon. Results in Mater 17(March):1–8. https://doi.org/10.1016/j.rinma.2022.100354

Werner K, Pommer L, Broström M (2014) Thermal decomposition of hemicelluloses. J Analytical Appl Pyrolysis, 110(1):130–137. https://doi.org/10.1016/j.jaap.2014.08.013

Wulandari A, Erwinsyah E (2020) Distribution of vascular bundles and physical properties analysis of variety DxP oil palm trunk based on various zones and trunk heights. Jurnal Penelitian Kelapa Sawit 28(1):1–14 https://jurnalkelapasawit.iopri.org/index.php/jpks/article/view/93

Empirical investigations on the wood quality assessment of five tropical species for multifarious industrial utility

*K.T. Parthiban**
Professor of Forestry / Formerly Dean (Forestry)
Forest College and Research Institute,
Tamil Nadu Agricultural University, Mettupalayam 641 301 Coimbatore, India

M.V. Jawahar Vishnu
Research Associate (Forestry)
Forest College and Research Institute,
Tamil Nadu Agricultural University, Mettupalayam 641 301 Coimbatore, India

S. Revathi
Research Associate (Forestry)
Forest College and Research Institute,
Tamil Nadu Agricultural University, Mettupalayam 641 301 Coimbatore, India

Deepshikha Singh
Ph.D. Forestry
Forest College and Research Institute,
Tamil Nadu Agricultural University, Mettupalayam 641 301 Coimbatore, India

R. Hindumathi
Junior Research Fellow
Forest College and Research Institute,
Tamil Nadu Agricultural University, Mettupalayam 641 301 Coimbatore, India

P. Kumar
Assistant Professor
Horticulture College and Research Institute, Paiyur
Tamil Nadu Agricultural University, Mettupalayam 641 301 Coimbatore, India

(Received 5 October 2024)

Abstract. Four species and one hybrid: *Khaya senegalensis, Melia dubia, Chukrasia tabularis, Toona ciliata*, and an *Acacia* hybrid were assessed for their physical, chemical, and thermo-chemical properties. *Khaya senegalensis* had the highest density (665.74 kg/m³), while *M. dubia* exhibited the highest recovery rate (80%). *Melia dubia* had the highest holocellulose content (75.50%), while lignin content in *K. senegalensis* was 28.60%. Caloric value (4380.20 kcal) was highest in *Chukrasia tabularis* while the fixed carbon (15.87%) content reached a maximum for *K. senegalensis*. The findings suggest that *K. senegalensis* and *M. dubia* are promising species for plywood, pulp, and energy applications.

Keywords: Tropical species, Physical, Chemical and thermo-chemical properties, Veneer recovery

Introduction

Wood has been used for centuries for house construction, furniture, tools for agriculture, transportation and most importantly supplying energy to peri-urban and rural communities. India is the world's largest producer and consumer of timber and timber products (Ramesh et al. 2022). Native forests were the primary source of timber until the 1980s, and forest management continues to revolve around timber production. The 1988 National Forest Policy shifted toward the conservation of forests and their management for maintaining ecological balance and ecosystem services, as well as supplying local community livelihood needs. As a result, the domestic wood supply was drastically reduced from 10 million m^3 in the 1970s to about 4 million m^3 in the 1990s (Gilbert et al. 2014). A Supreme Court 1996 order banned logging in

* Corresponding author: ktparthi2001@gmail.com

all forests unless it aligned with the State Working Plans that the national government had authorized. This led to an even greater decline in timber production. However, the rapid expansion of the economy, urbanization, industrialization, and population growth, have created a steady increase in demand for various kinds of wood and wood products. The exclusive National Agroforestry Policy by the Indian Government in 2014 has encouraged greater involvement from the wood-based industries to promote industry-specific agroforestry. The wood-based industries are attempting to revamp infrastructure and implement better processing technologies to meet the growing consumer demand.

Wood-based industries such as pulp and paper, plywood, and panel rely on a few species, creating competition for resources. *Eucalyptus* and *Casuarina* are the most commonly used pulp wood species in India, but can be problematic due to their variable adaptability and low productivity in marginal areas (Parthiban et al. 2004). The plywood industry also uses a small number of species, primarily poplars and eucalypts (Parthiban et al. 2014). Both of these genera are exotic in origin and have been criticized due to their severe water consumption (Kutnik et al. 2014) Eucalypts, in particular, can suppress the growth of other plants through allelopathy and deplete soil moisture (Desta et al. 2020). Poplar, on the other hand, faces challenges due to its low wood price, which can make it less profitable for farmers. Both species also compete with crops and intercrops for water and nutrients (Kumar et al. 2017).

Globally, high-yielding tree species are being planted to meet increasing demands for pulp and paper manufacture, plywood production, and dendroenergy (Espinoza 2004). However, not all timber species are suitable for commercial production. Density is the most significant and extensively researched wood property, correlating with several other characteristics. The increased demand for wood fiber has created a need to identify alternate species with superior wood quality coupled with high productivity and amenability for agroforestry schemes (Harper et al. 2009). The objective of this study was to assess the properties of four species and one hybrid for various industrial uses.

Materials and methods

Four tree species and one hybrid, viz., *Melia dubia*, *Chukrasia tabularis*, *Khaya senegalensis*, *Toona ciliata,* and Acacia hybrid (*Acacia auriculformis* x *Acacia mangium*) were selected based on their prolific growth, superior morphogenic characteristics, and multi-industrial utility. The three 3- to 5-year-old trees of each species were harvested from research trials established at the Forest College and Research Institute, Mettupalayam, India. The boles and large branches were debarked and chipped (chips of ~7 mm) after shade drying. The selected species along with their geographical distribution and biometric attributes are presented in Tables 1 and 2.

Table 1. Species investigated and their geographical sources.

Species	Age (years)	Location	Location
Melia dubia	5	11.2592°N, 77.0345°E	Pogalur
Chukrasia tabularis	5	11.3241°N, 76.9370°E	FC &RI
Khaya senegalensis	5	11.3241°N, 76.9365°E	FC &RI
Toona ciliata	3	11.3231°N, 76.9386°E	FC &RI
Acacia hybrid	5	11.3237°N, 76.9386°E	FC &RI

Table 2. Characteristics of trees assessed for wood properties.[a]

Species	Height (m)	GBH (cm)	Volume (m^3)
Melia dubia	15.75	99.75	0.685
Toona ciliata	10.75	52.50	0.129
Chukrasia tabularis	19.00	76.30	0.483
Khaya senegalensis	15.40	55.50	0.206
Acacia hybrid	15.00	56.50	0.209

a. Values represent means of three trees per species.

Estimation of physical properties of wood

Bulk density

The bulk density of the wood was calculated based on procedures described by Haygreen and Bowyer (1996). Chips were taken, and their volume was calculated by placing them into a suitable graduated container, then the chips were oven dried (103°C) and weighed. Bulk density was calculated based on the following formula:

$$\text{Bulk density (kg/m}^3) = \frac{m}{v} \quad (1)$$

Where, m = Oven-dry weight of chips at 100°C; and v = Volume.

Basic density

The basic density of each wood sample was calculated by using the following formula:

$$\text{Basic density (kg / m}^3) = \frac{E2}{F+G} \quad (2)$$

Where, E_2 = Green weight (after soaking in water for 48 hours); F = Oven dry weight of chips; and G = Deflection of the needle in cm due to water displacement.

Moisture content

One hundred g of wood chips were weighed, dried at 105°C for 8 hours, and weighed. Moisture content at the time of chipping was calculated using the following formula:

$$\text{Moisture content (\%)} = \frac{\textit{Initial weight} - \textit{Final weight}}{\textit{Initial weight}} \times 100 \quad (3)$$

Estimation of chemical properties of wood

Billets of each tree species were chipped, air dried, and then ground to pass a 40-mesh screen using a Wiley mill (Secon India). The milled wood was passed through a 60-mesh screen and measured for moisture, ash content, hot water solubles, 1% NaOH solubility, ethanol/benzene extractives, acid insoluble lignin, and holocellulose, as per TAPPI methods (TAPPI 1980).

Ash content

One g of oven-dry sample was placed on a tared porcelain crucible and heated in a muffle furnace at 840 ± 5°C for 1 hour. The crucible was cooled inside a desiccator and weighed. The ash content was calculated from the observed mass difference:

$$\text{Ash content (\%)} = \frac{W3 - W1}{W2 - W1} \times 100 \quad (4)$$

Where, W1 = weight of empty crucible, g; W2 = weight of empty crucible + original sample, g; and W3 = weight of empty crucible + ash sample, g.

Hot water extractives

Two g of sample was placed in conical flask with 300 ml distilled water and boiled for 2 hours. The contents were then filtered through tared Whatman filter paper, which was washed and oven-dried at 105 ± 2°C for 24 hr. The filter paper was cooled in a desiccator and weighed (W_2). The hot water solubles were calculated using the following formula:

$$\text{Hot water solubles} = \left[\frac{W2 - W1}{W2}\right] \times 100 \quad (5)$$

1% NaOH extractives

Two g of sample was placed in conical flask with 100 ml of 1% sodium hydroxide (NaOH). The sample was refluxed for 4 hours then the contents were filtered through a tared G_2 crucible (W_1). The crucible was oven-dried at 105 ± 2°C overnight and cooled in a desiccator before being weighed (W_2). Each material was tested in duplicate. NaOH solubility was calculated using the following formula:

$$\text{1\% NaOH solubility} = \left[\frac{W2 - W1}{\textit{OD weight of the sample}}\right] \times 100 \quad (6)$$

Alcohol benzene (AB) extractives

Around 7 g of oven-dried sample was placed in a tared thimble that was covered with cotton and placed in Soxhlet apparatus. The sample was then extracted in 300 ml of a 1:2 mixture of ethanol and benzene (AB extractives) for 6 hours at 70–85°C. The extracted thimble was oven-dried at 100°C and weighed (W_2). The AB extractives were calculated using the formula:

$$\text{AB Extractive \%} = \left[\frac{W2 - W1}{\textit{OD weight of the sample}}\right] \times 100 \quad (7)$$

Holocellulose (ash corrected)

Five (± 0.01) g of oven-dried sample were placed in a 250 ml conical flask and wetted thoroughly with 10 ml of distilled water. Then 150 ml of distilled water, 1.5 g of sodium chlorite, and 0.5 ml of acetic acid (glacial) were added and a smaller flask was used to cap the flask. The contents were heated in a water bath at 70°C for 1 hour, and then the supernatant was transferred to a tared crucible (W_1). The treatment was repeated with water, sodium chlorite, and acetic acid. The contents were then filtered through Whatman # 1 filter paper into a conical flask, and the filtered residue was washed with acetone. The filter paper with residues was oven-dried at 105°C overnight and weighed (W_2). The holocellulose percentage was calculated using the formula:

$$\text{Holocellulose \%} = \left[\frac{W2 - W1}{\textit{OD weight of the sample}}\right] \times 100 \quad (8)$$

Estimation of Thermochemical properties of wood

Volatile matter

The volatile content of the sample was determined using ASTM D3172 (ASTM 2002). One g of dried, powdered sample was placed in a pre-weighed crucible and heated in a muffle furnace at 600°C for 6 min. The volatile matter was calculated using the following formula:

$$\text{Volatile matter (\%)} = \frac{(W1 - W2)}{(W1 - W3)} \times 100 \quad (9)$$

Where, W_1 = Weight of the crucible + Sample; W_2 = Weight of the final ash present in the crucible + crucible; and W_3 = Weight of the empty crucible.

Fixed carbon

Fixed carbon in the sample was derived by subtracting ash content and volatile matter from the original sample mass. The fixed carbon was calculated by using ASTM D3172-84 (ASTM 2002), which follows:

$$\text{Fixed carbon (\%)} = 100 - (\text{ash content} + \text{volatile matter}) \quad (10)$$

Caloric value

The caloric value was determined using a digital bomb calorimeter (Model B.C.M – A217014, Mfg. by Advance Research Instrument Co.). A one gram sample was pelleted and fed into the calorimeter. This oxygen driven instrument burned the pellets and subsequently gave the calorific values of the samples. The amount of energy chemically bound in biomass was indicated by its caloric value, which was transformed into heat energy during combustion. Caloric value of biomass fuel significantly impacts the design of a biomass combustor (Erol et al. 2010).

Estimation of veneer recovery

The logs were transported to a nearby industrial facility and debarked. They were then fed into a 1.2 m capacity rotary lathe to produce 1.8-mm-thick veneer (Jamuna Engineering, Yamunanagar). Recovery was based upon the length of veneer produced from each log vs. the original tree diameter.

Results and discussion

Physical properties

A better understanding of how wood interacts with the environment is expected to improve processing optimization and the design of wood-based products (Avramidis 2016). In the present investigation, the wood samples collected from four species and one hybrid exhibited significant variation in physical properties (Table 3). Similarly, Izekor and Alufohai (2010) reported the mean density values of 480, 556, and 650 kg m^3 for 15-, 20-, and 25-year-old *Tectona grandis* wood, indicating that density increased with age. Similar results were reported among various *Eucalyptus* species for basic density, which ranged between 425 kg per m^3 and 542 kg per m^3 (Vennila 2009). Wood density is important for production of quality pulp and paper. The amount of wood needed to produce 1 ton of air-dried pulp is calculated from the density and pulp yield (Storebraten 1990). Therefore, the high density recorded for *Chukrasia tabularis* would make it an attractive alternate species for pulp production.

Chemical properties

The proximate chemical analysis gives an idea of potential for papermaking (Rao et al. 1999). In the present study, *T. ciliata* had lowest solubility in alcohol benzene extractive, cold water, hot water, and 1% NaOH, while *C. tabularis* had the highest alcohol benzene extractive and 1% NaOH solubility. *Melia dubia* had the highest hot water solubility when compared to other species (Table 3). Lal et al. (2010) reported low cold-water solubility (2.3%), higher hot water (5.0%), and alcohol benzene (2.4%) solubility than *E. tereticornis* (2.9%, 7.8%, and 1.4%, respectively). The lower extractives content results in fewer pitch problems and produces more homogeneous paper (Kasiviswanathan 1998). *Melia dubia, Acacia hybrid, and C. tabularis* wood will create fewer pitch problems and produce more homogeneous paper sheets. The 1% NaOH solubility measures low molecular weight carbohydrates, which were lower in *T. ciliata* when compared to the Acacia hybrid. Lower 1% NaOH solubility indicates that pulp will be less resist to UV degradation, heat and fungal decay. Hence pulp degradation will be greater in *Toona* spp. when compared to the other species. Saravanan et al. (2013) also reported similar results in 1- to 5-year-old *M. dubia* and recommended longer rotations. Holocellulose content is important for assessing the suitability of raw material for papermaking (Ona et al. 2001). Holocellulose represents the total content of carbohydrate materials and therefore, high holocellulose content is desirable for pulp and paper production because it is correlated with a higher pulp yield (Mabilangan and Estudillo 1996). *Melia dubia* was rich in holocellulose content (75.50%) when compared to the other species. This result shows that *Melia dubia* is suitable for the pulp and paper industry at early rotation.

Table 3. Physicochemical properties of wood from five different wood species.

Analysis	*Melia dubia*	*Chukrasia tabularis*	*Khaya senegalensis*	*Toona ciliata*	*Acacia* hybrid
Moisture content (%)	20.80	33.04	27.04	25.30	20.8
Bulk density (kg/m^3)	510.46	600.30	559.37	450.61	510.46
Basic density (kg/m^3)	555.14	656.43	665.74	464.45	555.84
1% NaOH solubility	6.38	6.81	5.88	3.05	9.43
Hot water solubility (%)	4.47	3.98	3.71	2.15	3.79
Alcohol-Benzene (AB) Extractive (%)	1.86	4.55	3.26	1.53	3.91
Holocellulose (%)	75.50	66.52	64.41	66.56	64.83
Acid insoluble lignin (%)	22.18	24.52	28.60	27.70	25.8
Ash content (%)	6.65	3.80	3.52	2.98	5.35

Similar results were observed in *M. dubia* and *Pinus taeda* at different ages (Saravanan et al. 2013; Mcdonough et al. 2011). Acid insoluble lignin varied from 22.18% to 28.60%. Low lignin content of a lignocellulosic material reduces pulping time and chemical consumption (López et al. 2008; Diaz et al. 2007). Furthermore, higher lignin content consumes more chemicals (Khristova et al. 2005) and results in lower pulp yield (Haygreen and Bowyer 1996) and lower pulp strength (Fengel and Wegener 1989) and requires more bleaching chemicals (Ona et al. 2001). Lignin content was lower for *M. dubia* in the current study, and similar results were obtained with *M. dubia* at different ages (Saravanan et al. 2013).

The highest ash content was found with *M. dubia* (6.65%). A high content of ash negatively impacts the chemical recovery process and, therefore, could constitute a serious drawback (Khiari et al. 2010). Similar results were reported by Saravanan et al. (2013) in *M. dubia,* with ash content decreasing with increased age.

Thermochemical properties

The energy content of wood is significantly influenced by its calorific value and is commonly considered a crucial factor for comparing different fuel types (Haygreen and Boyer 1996). Understanding the qualities of fuelwood is best achieved through assessing its calorific value, which is influenced by the chemical composition of the species (Sofer and Zaborsky 1981). The highest caloric value recorded was 4380.20 kcal (*C. tabularis*), followed by 4034.42 kcal (*K. senegalensis* and Acacia hybrid), 3974.04 kcal (*T. ciliata*), and 3745.67 kcal (*M. dubia*) (Table 4). The recent findings were more favorable than those of Mithilasri et al. (2024) who found that values in four mulberry clones ranged from 6.99 MJ Kg^{-1} to 14.13 MJ Kg^{-1}. Baqir et al. (2017) reported that the caloric value varied between 17.32 MJ Kg^{-1} and 22.56 MJ Kg^{-1} for different wood species.

Volatile matter is the biomass proportion emitted as short and long-chain hydrocarbon gases at temperatures between 400°C and 500°C (Koppejan and van Loo 2012). Fuel wood with higher quantities of volatile matter such as waxes, resins, and lignin generate more heat during combustion (Kataki and Konwer 2002). The volatile matter content in the current study ranged between 84.60% (*C. tabularis*) and 80.48% (*K. senegalensis* and Acacia hybrid). Dai et al. (2015) reported that an ideal range for volatile matter in woody biomass fuel falls between 70% and 90%. Our results are consistent with those of Baqir et al. (2019), where volatile matter of 12 wood species ranged from 76.89% (*Eucalyptus* spp.) to 85.64% (*Pithecellobium dulce*).

Table 4. Thermochemical properties of five different wood species.

Species	Caloric value (Kcal/kg)	Volatile content (%)	Fixed carbon (%)	Total biomass (Mg/ha)
Melia dubia	3745.67	83.54	9.56	303.90
Chukrasia tabularis	4380.20	84.60	11.60	171.38
Khaya senegalensis	4034.42	80.48	15.87	213.28
Toona ciliata	3974.04	82.25	14.48	90.31
Acacia hybrid	4034.42	80.48	13.31	217.27

Fixed carbon content refers to the mass remaining after volatile chemicals, ash, and moisture are removed from biomass (Marques et al. 2020). During combustion, when biomass is heated, volatile matter escapes initially and burns as gas, while fixed carbon remains as char, later burning as a solid. Increased fixed carbon content corresponds to higher energy value in plant materials (Kumar et al. 2010). Fixed carbon is also required for gasification because it is the primary source of carbon used to produce syngas. The highest fixed-carbon content was observed in *K. senegalensis* (15.87%) followed by *T. ciliata* (14.48%), Acacia hybrid (13.31%), *C. tabularis* (11.60%), and *M. dubia* (9.56%). The current findings support those of Desta and Ambaye (2020), who reported that fixed-carbon content of five wood species ranged from 5.96% to 22.39%.

Veneer recovery for plywood production

The suitability of species for plywood production is determined by their economic veneer recovery. *Eucalyptus* are the primary species used in plywood production in India, with veneer recovery ranging between 48% and 54% (McGavin et al. 2014). The recovery of veneer from the identified species (Table 5) varied from 80% (*M. dubia*) to 67% (*T. ciliata*). Kapadi (2020) reported 64% veneer recovery in *Grewia tiliaefolia*. The recovery percentage was higher than similar studies, Parthiban et al. (2019), Rahaman et al. (2012), Tenorio et al. (2011), and Rahaman et al. (2014).

Table 5. Veneer recovery (as a % of total volume for five wood species.

Species	Veneer recovery (%)	CFT	Veneer size (ft)	Sq.m
Melia dubia	80	0.5	8×27	12
Toona ciliata	67	0.3	4×27	5.7
Chukrasia tabularis	76	0.6	9×27	1.2
Khaya senegalensis	76	0.6	9×27	1.2
Acacia hybrid	76	0.4	6×27	8.6

Conclusion

Khaya senegalensis and *Melia dubia* have the best properties for plywood and pulp production based on their density and recovery rate, whereas *Chukrasia tabularis* could be used for fuel production.

Acknowledgement

The authors profusely thank the Department of Biotechnology (DBT), Government of India, New Delhi for supporting the research scheme on development of HYSR clones amenable for multifarious industrial utility (BT/PR/39385/FCB/125/42/2020) in which the current study formed a part of the programme.

References

Ahmad M, Kamke FA (2005) Analysis of Calcutta bamboo for structural composite materials: Physical and mechanical properties. Wood Sci Technol 39(4): 448–459. https://doi.org/10.1007/s00226-005-0016-y

ASTM (2002). ASTM D 3172-73(84), Standards method of proximate analysis of coal and coke, in gaseous fuels; coal and coke section 5, vol. 05.05, Annual Book of ASTM Standards 2002, p. 299.

Avramidis S (2016) Dielectric properties of four softwood species at low-level radio frequencies for optimized heating and drying. Drying Technology 34(7):753–760.

Babu S, Singh R, Avasthe RK, Yadav GS, Das A, Singh VK, Mohapatra KP, Rathore SS, Chandra P, Kumar A (2020) Impact of land configuration and organic nutrient management on productivity, quality and soil properties under baby corn in Eastern Himalayas. Sci Rep 10:220–229. https://doi.org/10.1038/s41598-020-73072-6

Baqir M, Kothari R, Singh RP (2019) Characterization and ranking of subtropical trees in a rural plantation forest of Uttar Pradesh, India, as fuel wood using fuel wood value index (FVI). Environ Dev Sustain 21(2):763–776. https://doi.org/10.1007/s10668-017-0057-z

Baqir M, Mishra AK, Kothari R, Singh RP. (2017). Calorific value and fuel wood consumption patterns of a plantation forest at Kahinure (Distt Mau), Uttar Pradesh, India by villagers. CCES 5(1, April):35–41. https://doi.org/10.5958/2320-642x.2017.00003.5

Bodnar JL, Schumacher B, Uyenaka S (1998) Garlic production in Ontario. Omafra Factsheet 1:1–8.

Catacutan D, Noordwijk Van, Nguyen T, Oborn I and Mercado A (2017) Agroforestry as part of climate change response. IOP Conf Ser: Earth Environ Sci 10: 223–226.

Dai J, Saayman J, Grace JR, Ellis N (2015) Gasification of woody biomass. Annu Rev Chem Biomol Eng 6(1):77–99.

DARC (2006) Garlic Production Management. Debrezeit Agricultural Research Centre 9:112–115.

Desta HM, Ambaye CS (2020) Determination of energy properties of fuelwood from five selected tree species in tropical highlands of southeast Ethiopia. J Energy 2020(1):3635094.

Dhyani SK, Handa AK, Uma L (2013) Area under agroforestry in India: An assessment for present status and future perspective. IJAF 15:1–11.

Diaz MJ, Garcia MM, Eugenio ME, Tapias R, Fernandez M, Lopez F (2007) Variations in fiber length and some pulp chemical properties of Leucaena varieties. Industrial Crops and Products 26:142–150.

Erol M, Haykiri-Acma H, Küçükbayrak S (2010) Calorific value estimation of biomass from their proximate analyses data. Renew Energy 35(1):170–173.

Espinoza, JA (2004) Within-tree density gradients in *Gmelina arborea* in Venezuela. New Forests 28:309–317.

Fengel D, Wegener G (1989) Wood: Chemistry, Ultrastructure, Reactions. Second edition. Walter de Gruyter and Co., Berlin.

Gessesew WS, Yemane T, Bedada S, Alemu T (2017). Evaluation of different mulching practices on garlic (*Allium sativum* L.) growth parameters under irrigated condition in Fiche, North Shoa Ethiopia. J Biol Agric Health 7:759–63.

Gilbert BP, Underhill ID, Bailleres H, El Hanandeh A, McGavin RL (2014) Veneer based composite hollow utility poles manufactured from hardwood plantation thinned trees. Construction and Building Materials 66:458–466.

Government of India (2014) *National Agroforestry Policy*. Department of Agriculture & Cooperation. Ministry of Agriculture. New Delhi. https://faolex.fao.org/docs/pdf/ind203552.pdf.

Haque S, Islam R, Karim A, Khan HA (2003) Effects of natural and synthetic mulches on garlic (*Allium sativum* L.). Asian J Plant Sci 2:83–89.

Harper SR, Patton LD, Wooden OS (2009) Access and equity for African American students in higher education: A critical race historical analysis of policy efforts. JHE 80(4):389–414.

Haygreen JG, Bowyer JL (1982) Forest Products and Wood Science – An introduction. Iowa State University Press, Ames, Iowa.

Haygreen JG, Bowyer JL (1996) Forest products and wood science: an introduction. 3rd Edition. Iowa State University Press, Ames, Iowa.

Hillis, WE (1971) Distribution, properties and formation of some wood extractives. Wood Sci Technol 5(4):272–289.

Iroc A, Sisson LC, Solidum PP (1991). Effects of different mulching materials on garlic (*Allium sativum* L.) *Horticultura* 7:104–108.

Izekor OB, Alufohai GO (2010) Assessment of cooperative societies effectiveness in agricultural credit delivery in Ikpoba Okha Local Government Area, Edo State, Nigeria. African Journal of General Agriculture, 6(3):139–142.

Jansiri S, Deenu A, Puangsin B, Sungkaew S, Kamthai S (2021) Characterization of sweet bamboo (*Dendrocalamus asper* Backer) kraft pulp filled in poly (lactic acid)/polybutylene succinate blend composite. Polym Compos 42(10):5090–5100.

Kabir MA, Rahim MA, Majumder DN (2016). Effect of different levels of organic manures on the growth and yield of garlic. J Agrofor Environ 5:73–76.

Kala PC (2010) Status of an indigenous agroforestry system in changing climate: A case study of the middle Himalayan region of Tehri Garhwal, India. J For Sci 56:373–380.

Kapadi, KA (2020) Studies on wood characterization of *Grewia tiliaefolia* vahl. For pulp, plywood and matchwood properties Master of Science in Forestry, Tamil Nadu Agricultural University, Mettupalayam.

Kar S, Pant KS, Chandel A, Roshanzada SR (2019) Trend of soil parameters under different spacings of Grewia based agroforestry system in the mid hill zones of Himachal Pradesh. Int J Chem Stud 7:1904–1907.

Kasiviswanathan KS (1998) Utilization of bagasse for paper making- An overview. IPPTA J. 10(3):9–14.

Kataki R, Konwer D (2002) Fuelwood characteristics of indigenous tree species of north-east India. Biomass Bioenerg 22(6):433–437.

Khalil HA, Yusra AI, Bhat AH, Jawaid M. (2010) Cell wall ultrastructure, anatomy, lignin distribution, and chemical composition of Malaysian cultivated kenaf fiber. Ind Crop Prod 31(1):113–121.

Khiari R, Mhenni MF, Belgacem MN, Mauret E. (2010) Chemical composition and pulping of date palm rachis and *Posidonia oceanica*–A comparison with other wood and non-wood fibre sources. Bioresour Technol 101(2):775–780.

Khristova P, Kordsachia O, Khider T (2005) Alkaline pulping with additives of date palm rachis and leaves from Sudan. Bioresour Technol 96:79–85.

Koppejan J, van Loo S, eds. (2012) *The Handbook of Biomass Combustion and Co-firing* (e-book edition). Routledge. https://doi.org/10.4324/9781849773041

Kumar R, Pandey KK, Chandrashekar N, Mohan S (2010) Effect of tree-age on calorific value and other fuel properties of *Eucalyptus* hybrid. J Forest Res 21:514–516.

Kumar Y, Thakur KT, Thakur A (2017) Socio-Cultural Paradigm of Agroforestry in India. Int J Curr Microbiol Appl Sci 6:1371–1377.

Kutnik M, Suttie E, Brischke C (2014) European standards on durability and performance of wood and wood-based products–Trends and challenges. Wood Material Science & Engineering 9(3):122–133.

Lal M, Dutt D, Tyagi CH, Upadhyay JS, Upadhyay S (2010) Characterization of *Anthocephalus cadamba* and its delignification by kraft pulping. TAPPI Journal 9(3):30–37.

Lasmini AS, Wahydi I, Rosmini R, Nasir B (2020) Combined application of mulches and organic fertilizers enhance shallot production in dryland. Agron Res 17:165–175.

Little KM, van Staden J, Clarke GPY (2003) The relationship between vegetation management and the wood and pulping properties of a Eucalyptus hybrid clone. Ann For Sci 60(7):673–680.

López F, García MM, Yánez R, Tapias R, Fernández M, Díaz MJ (2008) *Leucaena* species valoration for biomass and paper production in 1 and 2 year harvest. Biores Technol 99:4846–4853. doi:10.1016/j.biortech.2007.09.048

Mabilangan LC, Estudillo CP (1996) Philippines woods suitable for kraft pulping process. Trade Bulletin Series 5:1–9.

Marques E, Krieg CP, Dacosta-Calheiros E, Bueno E, Sessa E, Penmetsa RV, Von Wettberg E (2020) The impact of domestication on aboveground and belowground trait responses to nitrogen fertilization in wild and cultivated genotypes of chickpea (*Cicer* sp.). Front Genet 11, 576338.

Mcdonough TJ, Courchene CE, White DE, Schimleck L, Peter G (2011) Effects of loblolly pine tree age and wood properties on linerboard-grade pulp yield and sheet properties: Part 1-Effects on pulp yield. TAPPI J 9: 45-53.

McGavin RL, Bailleres H, Lane F, Fehrmann J, Ozarska B (2014) Veneer grade analysis of early to mid-rotation plantation *Eucalyptus* species in Australia. BioResources 9(4):6562–6581.

Miranda I, Gominho J, Mirra I, Pereira H (2013) Fractioning and chemical characterization of barks of *Betula pendula* and *Eucalyptus globulus*. Ind Crop Prod 41:299–305.

Mithilasri M, Parthiban KT, Kalpana R, Shankar SM (2024) Clonal evaluation and genetic divergence studies in mulberry genotypes. Asian Res J Agric 17(2):147–159. https://doi.org/10.9734/arja/2024/v17i2433

Mosquera-Losada MR, Moreno G, Pardini A, McAdam JH, Papanastasis V, Burgess PJ, Lamersdorf N, Castro M, Liagre F, Rigueiro-Rodríguez A (2012) Past, present, and future of agroforestry in Europe. In: Nair PKR, Garrity DP (eds) Agroforestry - The Future of Global Land Use. Springer, 38:234–56.

Nair PKR, Garrity D (2012) Agroforestry - The Future of Global Land Use. Springer 172:10–23.

Ngailo JA, Vieira SR (2012) Spatial patterns and correlation of soil properties of a lowland soil. J Soil Sci Environ Manage 3:287–296.

Nieschlag HJ, Nelson GH, Wolff JA, Perdue RE (1960) A Search for New Fiber Crops. TAPPI J 43:193–201.

Nwosisi S, Nandwani D, Pokharel B (2019) Yield performance of organic sweet potato varieties in various mulches. *Horticulturae 3:48–52.*

Ona T, Sonoda T, Ito K, Shibata M, Tamai Y, Kojima Y, Ohshima J, Yokota S, Yoshizawa N (2001) Investigation of relationships between cell and pulp properties in Eucalyptus by examination of within-tree variations. Wood Sci Technol 35:229–243.

Parthiban KT, Dey S, Krishnakumar N, Das A (2019) Wood and plywood quality characterization of new and alternate species amenable for composite wood production. Wood Fiber Sci 51(4):1–8.

Parthiban KT, Paramathma M, Neelakantan KS (2004) Compendium on Clonal Forestry. Directorate of Publications, Tamil Nadu Agricultural University, Coimbatore, 209.

Parthiban KT, Umarani R, Umesh Kanna S, Sekar I, Rajendran P, Durairasu P (2014). Industrial Agroforestry Perspective and Prospectives. Scientific Publisher. Jodhpur. 396 p. ISBN: 978-81-7233-905-0.

Rahaman MM, Akhter K, Biswas D, Sheikh MW (2012) Suitability of hybrid *Acacia* wood for manufacturing plywood and particleboard. J Bangladesh Acad Sci 36(2):171–176.

Rahman MK, Asaduzzaman M, Rahman MM, Das AK, Biswas SK (2014) Physical and mechanical properties of ghora neem (*Melia azedarach*) plywood. BJSIR 49(1):47–52.

Rahmani W, Salleh NM, Hamzah ZM, Abdu A, Ishak MF, Khadir AW, Awang MR, Alias AB (2021) Effect of different types of mulching on soil properties and tree growth of *Magnolia champaca* planted at the Montane Rainforest in Cameron Highlands, Pahang, Malaysia. Int J For Res 3:156–162.

Rai M, Negi RS (2021) Effects of different mulching materials, manures and bio-fertilizers on growth and yield Parameters of garlic (*Allium sativum* L.) var. Agrifound parvati in garhwal region of Uttarakhand, India. Plant Archives 21:154–159.

Ramesh M, Rajeshkumar L, Sasikala G, Balaji D, Saravanakumar A, Bhuvaneswari V, Bhoopathi R (2022) A critical review on wood-based polymer composites: Processing, properties, and prospects. Polymers 14(3):589.

Rao AR, Qu L, Ruekert RW (1999) Signaling unobservable product quality through a brand ally. Journal of Marketing Research 36(2):258–268.

Ravimycin T (2016) Effects of vermicompost (VC) and farmyard manure (FYM) on the germination percentage growth biochemical and nutrient content of Coriander (*Coriandrum sativum* L.). IJARBS 3: 91–98.

Rodrigues A, Loureiro L, Nunes LJR (2018) Torrefaction of woody biomasses from poplar SRC and Portuguese roundwood: Properties of torrefied products. Biomass Bioenerg 108:55–65.

Sanchez MD (2000) Mulberry: an exceptional forage available almost worldwide. Wld Anim Rev 93:1–21.

Saravanan V, Parthiban KT, Kumar P, Marimuthu P (2013) Wood characterization studies on *Melia dubia cav*. for pulp and paper industry at different age gradation. Res J Recent Sci 2:1–6.

Silva MFF, Silva JVF, Franco MP, Molina JC (2023) Determination of physical and mechanical properties of *Toona ciliata* and *Acrocarpus fraxinifolius* woods from Sao Paulo State. TreeDimensional 11, e2023024:1–6, 2023. DOI: doi.org/10.55746/treed.2023.07.024

Singh N, Gupta T, Dutt B (2021) Variation in physico chemical characteristics of *Toona ciliata* M. Roem provenances. Int J Chem Stud 9(1):364–368.

Sint KM, Myint CC (2005) Preliminary study on physical and mechanical properties of Yinma (*Chukrasia velutina*): The Proceedings of the 5th Annual Research Conference, Yangon, Myanmar.

Sofer SS, Zaborsky OR, eds. (1981) Biomass Conversion Processes for Energy and Fuels. New York: Plenum Press.

Storebraten S (1990) Sulfatfabrikken – virkesforsyningens soppleplass Foredrag –PTF – Oslow, Norway 25–29.

TAPPI (1980) Standard and suggested methods. Technical Association of Pulp and Paper Industry, New York. pp. 200–265.

Tazima Y (ed). (1978) Radiation mutagenesis of the Silkworm: The silkworm an important laboratory tool. *Kodansha*. Tokyo. 247–68.

Tenorio C, Moya R, Munoz F (2011) Comparative study on physical and mechanical properties of laminated veneer lumber and plywood panels made of wood from fast-growing *Gmelina arborea* trees. J Wood Sci 57:134–139.

Vennila S (2009) Pulpwood traits, genetic and molecular characterization of Eucalyptus genetic resources. Ph.D thesis. Tamil Nadu Agricultural University, Coimbatore.

Vieira TAS, Trugilho PF, Carabineiro SAC, Zanuncio AJV, Carvalho AG, Branco-Vieira M (2023) Impact of chemical composition on *Eucalyptus* wood clones for sustainable energy production. Forests 14(11):2240. https://doi.org/10.3390/f14112240

Vishnu R, Revathi R (2019) Studies on physical, chemical and fibre morphological parameters of three pulpwood species viz. *Eucalyptus, Me*lia and *Casuarina* for pulp and paper making. Int J Chem Stud 7(5):3155–3162.

Wood quality of farm grown teak (*Tectona grandis*, Linn.f) under different agroclimatic zones of Tamil Nadu, India

S. Navaneetha Krishnan
PhD Scholar
Department of Silviculture & NRM, Forest College and Research Institute
Mettupalayam – 641 301, Coimbatore, Tamil Nadu, India

A. Balasubramanian *
Professor & Dean (Forestry)
Forest College and Research Institute, TNAU
Mettupalayam – 641 301, Coimbatore, Tamil Nadu, India

M. Sivaprakash
Associate Professor (Forestry)
Department of Silviculture & NRM, Forest College and Research Institute,
Mettupalayam – 641 301, Coimbatore, Tamil Nadu, India

R. Ravi
Assistant Professor (Forestry)
Department of Forest Products and Wildlife, Forest College and Research Institute
Mettupalayam – 641 301, Coimbatore, Tamil Nadu, India

B. Sivakumar
Assistant Professor (Forestry)
Department of Forest Products and Wildlife, Forest College and Research Institute
Mettupalayam – 641 301, Coimbatore, Tamil Nadu, India

C. N. Hari Prasath
Teaching Assistant (Forestry)
Department of Silviculture & NRM, Forest College and Research Institute
Mettupalayam – 641 301, Coimbatore, Tamil Nadu, India

G. Swathiga
Senior Research Fellow
Department of Silviculture & NRM, Forest College and Research Institute
Mettupalayam – 641 301, Coimbatore, Tamil Nadu, India

V. Manimaran, K. S. Anjali, R. Ashick Rajah, and M. Ashwin Niranjan
PhD Scholars
Department of Silviculture & NRM, Forest College and Research Institute
Mettupalayam – 641 301, Coimbatore, Tamil Nadu, India

(Received 16 December 2024)

Abstract. Teak (*Tectona grandis*) is globally recognized for its exceptional wood quality, making it one of the most sought-after timbers in the world. Teak is visually appealing because of its fine grain and golden-brown hue, and its dimensional stability ensures minimal warping or cracking under various environmental conditions. Wood quality is further influenced by factors such as growth conditions, silvicultural practices, and genetic variability. Although variations in heartwood density and proportion may have an impact on its performance, plantation-grown teak has become a viable substitute for natural forests. Wood fractionation analysis was undertaken by collecting wood samples from all four agroclimatic zones in Tamil Nadu, India of both boundary and block plantations in three different age classes, viz., 5–10, 10–15, and 15–20 years. Wood density, heartwood, sapwood, and bark content were analyzed using species specific allometric equations. Wood density attained a maximum of 0.80 g cm^3 in boundary plantations of the Western agroclimatic zone in the 15- to 20-year age class. The same Western zone (WZ) registered the maximum heartwood volume of 0.433 m^3 and maximum bark content volume of 0.097 m^3 in the same age class. Similarly, maximum sapwood volume in the same age class in the Cauvery Delta zone was 0.141 m^3. Trees from the WZ had higher heartwood ratios, suggesting that these trees might more durable.

Keywords: Teak, *Tectona grandis*, Heartwood, Sapwood, Density, Correlation, Wood quality

* Author for correspondence: balasubramanian.a@tnau.ac.in

Introduction

Teak (*Tectona grandis,* Linn.; Lamiaceae) is known as the "King of Timber" and is one of the most predominant and widely used hardwood timber species across the world (Balakrishnan et al. 2021; Kidanu et al. 2005; Vongkhamho et al. 2022). Teak plantations have been widely established throughout the tropics since the 1850s (Shrivastava and Saxena 2017). Teak is predominantly native to south and southeast Asia, which contribute more than 90% of the world's teak resources (Arunkumar et al. 2024). India accounts for about 1.68 M ha of teak plantations and 6.8 M ha of natural teak forests (Kollert et al. 2024), representing about 45% of the global teak resource. Ironically, India is still a net importer of teak, with annual domestic production of only about 0.25 million cubic meters (mcm) (Shrivastava and Saxena 2017) compared with a demand of 100 mcm (Hadinata and Kozakiewicz 2020). Globally, India ranks first in teak consumption, and most of this demand is met from Africa and Latin America (Shrivastava and Saxena 2017; Gatonnou et al. 2017. One part of meeting the rising demand will be optimizing the rotation period. Short rotation teak production has been promoted, particularly on private land to bridge the supply gap and provide a revenue source to farmers (Kyaw et al. 2024).

The Government of Tamil Nadu promotes teak planting through Tree Cultivation in Patta Land (TCPL) outside forested areas (Ramar and Kannan 2016). In the past decade, Tamil Nadu accounted for nearly 8700 km^2 of trees planted through farm forestry and community plantations that are grown on waste-lands and public lands (Buvaneswaran et al. 2016). While the increasing plantation estate is a positive development, the characteristics of this resource in reference to the different edaphoclimatic conditions in Tamil Nadu are poorly understood. Previous studies suggest that the wood properties of teak can vary widely with climatic and edaphic factors (Moya et al. 2020).

The market value of teak has increased with demand, and unlike many other wood species, teak sapwood has the same physical strength and density characteristics as heartwood, making it easier to utilize the entire tree without concern for issues other than durability (Odusote et al. 2019). Teak heartwood extractives provide exceptional resistance to fungal and insect attack (Rosamah et al. 2020; Brocco et al. 2020; Colbu et al. 2021). Heartwood content of farm-grown teak wood, especially the extractives content as it affects durability, will play a major role in the value of this resource. Previous research (Nugroho et al. 2024; Rizanti et al. 2018) clearly showed that climatic and edaphic influences in addition to age play major roles in wood quality in teak. Hence understanding wood quality and heartwood proportion in farm grown trees will help growers maximize the value of this resource.

The objective of this study was to examine the proportions of heartwood, sapwood and bark in teak trees from four growing areas within Tamil Nadu, India.

Materials and methods

Study area

Farm-grown teak plantations aged 5–10, 10–15, and 15-20 years were surveyed in four agroclimatic zones of Tamil Nadu (Figure 1), namely the North Eastern (NEZ), North Western (NWZ), Cauvery Delta (CDZ), and Western zones (WZ).

Ten trees were harvested in each age group at each of the four sites. A 50-mm-thick cross section was cut 1 m above the

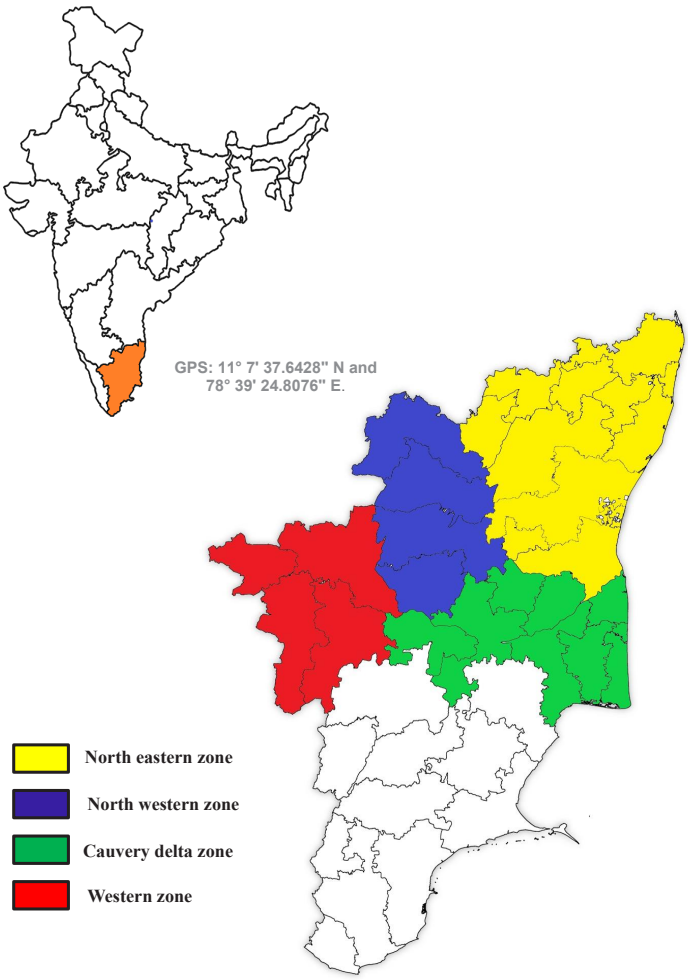

Figure 1. Locations of the study areas.

base from each tree, and the amounts of bark, sapwood, and heartwood were visually measured across two points to the nearest mm. These values were used to calculate the volume of each component. The section was then immersed in water to determine volume based upon water displacement, and the samples were oven dried at 103°C and weighed. The values were used to calculate density.

Type of plantation

The study examined trees that were both within a stand as well on the boundary of plantations in each agroclimatic zone. A total of 480 trees were examined under three age classes: 5–10, 10–15, and 15–20 years.

Estimation of wood quality parameters with reference to agroclimatic zone and age

Wood density, heartwood, sapwood, and bark content were studied for 120 wood samples in all three age classes of block and boundary plantations grown in four agroclimatic zones.

Wood density

Density is an important variable for accurate quantification of woody biomass and carbon stocks. Wood density was calculated by the ratio of the oven-dry mass of a wood sample divided by the mass of water displaced by its green volume (wood specific gravity, or WSG) (Kenzo et al. 2020) as follows:

$$WD = dm/v \quad (1)$$

where, WD = Wood density; dm = Wood dry mass; v = Volume.

Wood fractionation

The wood samples collected from three age classes belonging to boundary and block plantations grown in the four agroclimatic zones (Plates 1 to 4) were fractionated into bark, sapwood, and heartwood content. Diameter of heartwood was measured by the average of two cross-sectional measurements of each wood sample. The heartwood volume was calculated by using the geometric cylinder volume equation. Sapwood volume was estimated by subtracting the heartwood volume from the volume (inside-bark). Finally, the wood sample was converted into 2-inch billets in order to observe the exact percentage of heartwood proportion present in the wood. The total lengths of heartwood, sapwood, and outer bark of wood samples were measured using measuring tape, and the total lengths were expressed in cm (Tewari and Mariswamy 2013).

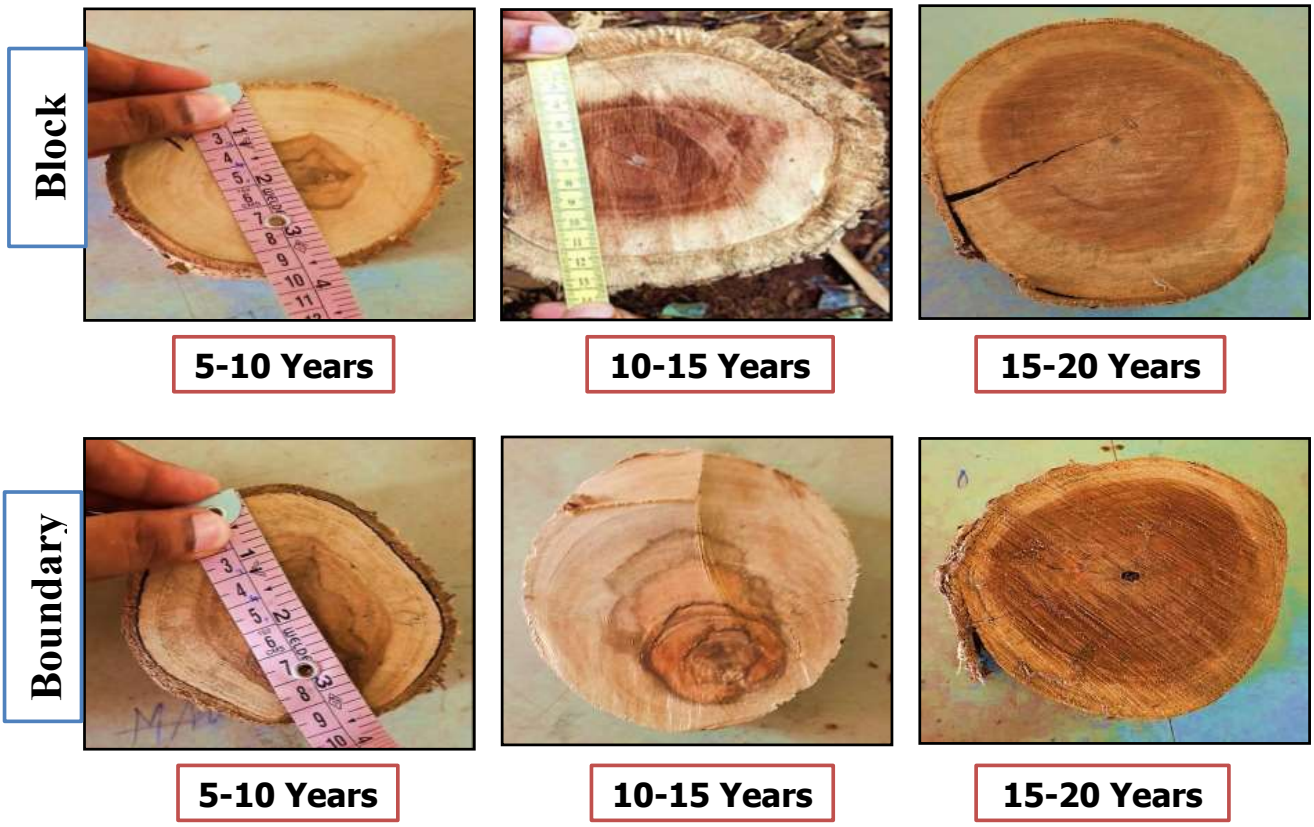

Plate 1. Wood Samples of North Eastern zone (NEZ).

Plate 2. Examples of cross cuts from tree of different ages from the North Western zone (NWZ).

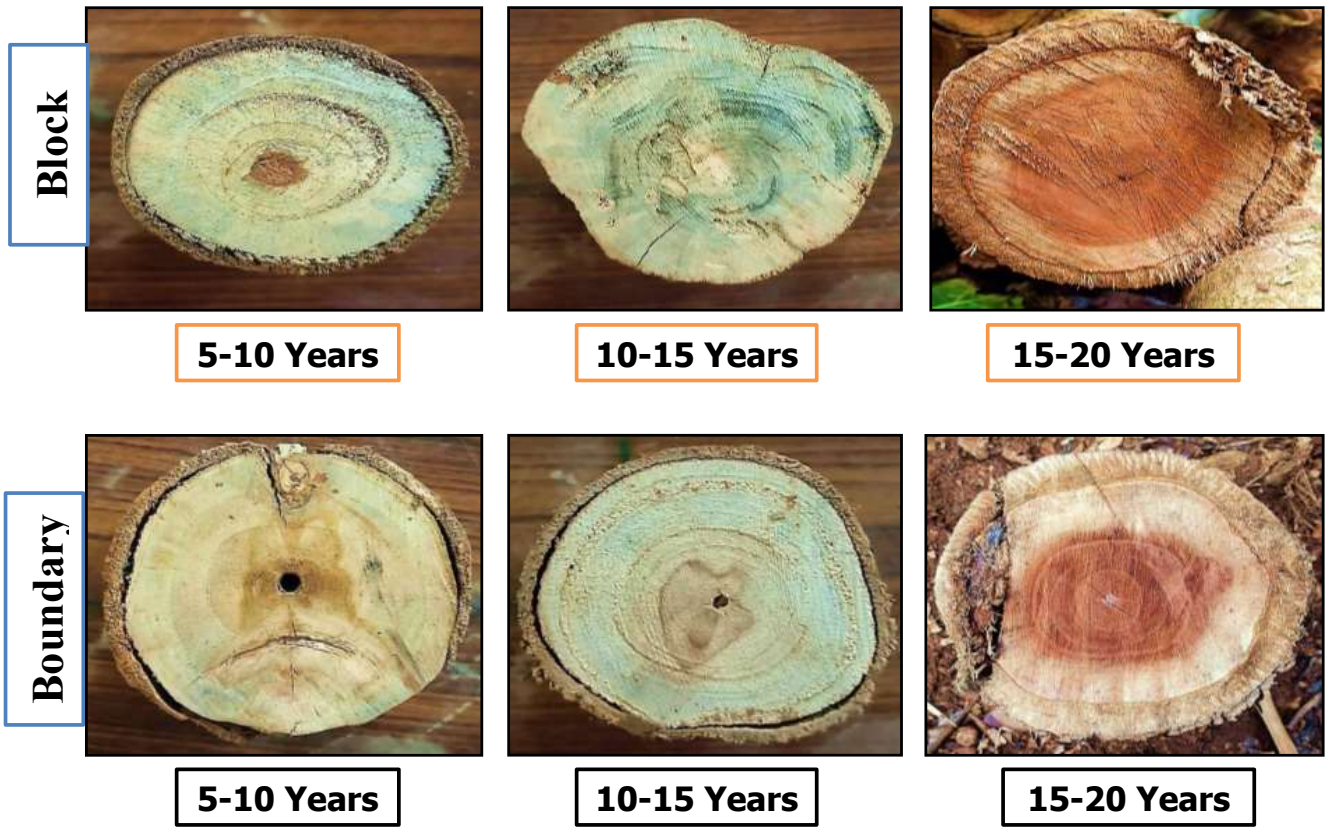

Plate 3. Examples of cross cuts from tree of different ages from the Cauvery Delta zone (CDZ).

Plate 4. Examples of cross cuts from tree of different ages from the Western zone (WZ).

Heartwood volume

The heartwood volume was estimated for each wood sample, and the average of each cross-sectional diameter was taken into account. Heartwood volume was calculated using the equation given by Moya et al. 2020:

$$hwv = g_1 + g_2/2 \times length \quad (2)$$

where, hwv is the heartwood volume, g_1 is the face area of the minor log diameter in m^2, g_2 is the face area of major log diameter m^2.

Climatic parameters

The rainfall (mm), maximum temperature (°C), minimum temperature (°C), and relative humidity (%) data for the period between 2012–2021 for Thiruvannamalai, Salem, Thanjavur, and Coimbatore districts were collected from the Agriculture Extension Center (AEC), Tamilnadu Agricultural University Coimbatore (Figure 2).

Edaphic parameters

Representative soil samples were collected from each of the four agroclimatic zones and segregated into zones 0–15 and 15–30 cm from the surface. The samples were analyzed for physicochemical and soil chemical properties (Table 1). Areas with old manure, wet spots, dead plants, furrows, and compost were excluded to minimize the differences due to the presence of soil organic matter. The soil samples were air-dried, mixed well, and passed through a 2-mm sieve for the soil physio-chemical properties like soil pH and soil electrical conductivity (Jackson, 2005) and soil chemical analysis such as soil organic carbon (Walkley and Black 1934), available nitrogen (Subbiah and Asija 1956), available phosphorous (Bray and Kurtz 1945), and available potassium (Stanford and English 1949) were analyzed.

Statistical analysis

The data were subjected to an analysis of variance and then differences were examined using Pearson's correlation coefficient with SPSS (Statistical Package of the Social Science) and Agricolae under R environment (R Core Team 2012) for correlating the wood quality of farm-grown teak with the climatic and edaphic factors. Wood quality parameters were taken as dependent variables, whereas climatic and edaphic factors were considered as independent variables.

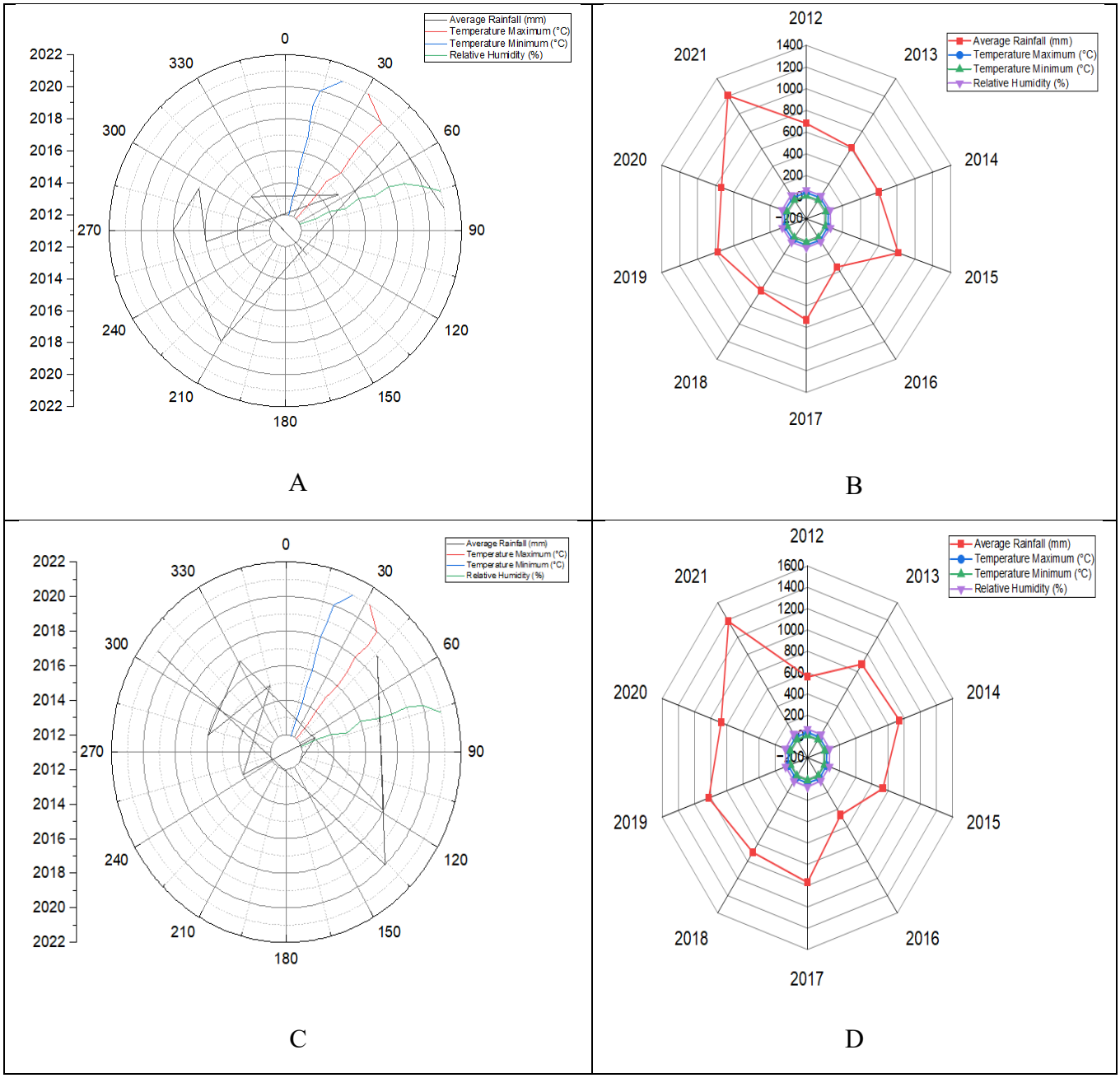

Figure 2. Climatic variables in selected agroclimatic zones: (A) North Eastern zone; (B) North Western zone; (C) Cauvery Delta zone; and (D) Western zone).

Table 1. Soil physicochemical properties evaluated in the teak plantations.

S. no.	Soil parameter	Methodology	References
1	Soil pH	Elico model pH meter	Jackson (2005)
2	Soil EC	Conductometry	Jackson (2005)
3	Available nitrogen	Alkaline permanganate method	Subbiah and Asija (1956)
4	Available phosphorus	Olsen's method	Bray and Kurtz (1945)
5	Available potassium	Neutral Normal NH4OAc, Flame photometry	Stanford and English (1949)
6	Soil organic carbon	Wet chromic acid digestion	Walkley and Black (1934)

Results

Sapwood/heartwood, bark content

North Eastern zone

Heartwood (HW), sapwood, (SW) and bark content (BC) volume varied among all three age classes. The highest heartwood (0.239 m^3), sapwood (0.114 m^3), and bark content (0.027 m^3) volumes were obtained for the age class 15–20 years in block plantations of farm-grown teak. Similarly, the lowest heartwood (0.031 m^3), sapwood (0.050 m^3), and bark content (0.007 m^3) volumes were recorded in 5- to 10-year-old stands. The average heartwood volume for plantations in the NEZ was 0.114 m^3, while average sapwood and bark content volumes were 0.072 m^3 and 0.015 m^3, respectively.

North Western zone

Maximum heartwood (0.204 m^3), sapwood (0.079 m^3), and bark content (0.021 m^3) volumes in the NWZ were obtained for the 15- to 20-year age class ($p < 0.05$) (Table 2). Similarly, minimum heartwood (0.050 m^3), sapwood (0.055 m^3), and bark content volumes (0.012 m^3) were obtained for 5- to 10-year-old timber. Average heartwood volume for NWZ plantations was 0.114 m^3, while average sapwood and bark content volumes were 0.064 m^3 and 0.015 m^3, respectively.

Cauvery Delta zone

Heartwood, sapwood, and bark content volumes in this zone varied among three age classes (Table 3**)**. The highest heartwood (0.086 m^3), sapwood (0.075 m^3), and bark content (0.014 m^3) volumes were recorded in the 15- to 20-year age class ($p < 0.05$). The lowest heartwood (0.012 m^3), sapwood (0.040 m^3), and bark content (0.003 m^3) volumes were registered in the 5- to 10-year-old timber. Irrespective of age classes, the average heartwood volume for block plantations was 0.048 m^3, and the average sapwood volume and bark content volume were 0.056 m^3 and 0.009 m^3, respectively.

Western zone

Heartwood, sapwood, and bark volumes of trees from the three age classes of block plantations are given in Table 4. Maximum heartwood volume (0.139 m^3) was found in 15- to 20-year-old trees ($p < 0.05$), which also had the maximum sapwood (0.073 m^3) and bark (0.090 m^3) volumes. Average volumes of heartwood, sapwood, and bark volumes for all age classes were 0.082 m^3, 0.047 m^3, and 0.057 m^3, respectively.

Boundary plantations

North Eastern zone

The highest heartwood volume obtained in boundary plantations in this zone was 0.342 m^3 for 15- to 20-year-old trees ($p < 0.05$) (Table 5). This age class also has the highest sapwood (0.074 m^3) and bark (0.030 m^3) volumes. The lowest heartwood (0.070 m^3), sapwood (0.047 m^3), and bark content (0.010 m^3) volumes were registered in the 5- to 10-year age class. Average heartwood, sapwood, and bark content volumes for all three age classes in the NEZ were 0.197 m^3, 0.060 m^3, and 0.020 m^3, respectively.

North Western zone

The 15- to 20-year age class had maximum heartwood (0.303 m^3), sapwood (0.067 m^3), and bark content (0.022 m^3) volumes in this zone, while the 5- to 10-year age class had the lowest ($p < 0.05$) heartwood (0.099 m^3), sapwood (0.040 m^3), and bark content (0.017 m^3) volumes. The average heartwood, sapwood, and bark content volumes in all age classes were 0.210 m^3, 0.052 m^3, and 0.019 m^3, respectively.

Cauvery Delta zone

The lowest heartwood (0.037 m^3), sapwood (0.024 m^3), and bark content (0.008 m^3) volumes in this zone were observed in the 5- to 10-year-old trees, while 15- to 20-year-old trees had significantly higher heartwood (0.312 m^3), sapwood (0.141 m^3), and bark content (0.034 m^3) volumes ($p < 0.05$). Average volumes for all age classes in boundary plantations for heartwood, sapwood, and bark content volumes were 0.154 m^3, 0.078 m^3, and 0.020 m^3, respectively.

Western zone

Maximum heartwood, sapwood and bark volumes in 15- to 20-year-old trees were 0.433 m^3, 0.120 m^3 and 0.097 m^3, respectively, while heartwood, sapwood, and bark contents in 5- to 10-year-old trees were 0.113 m^3, 0.083 m^3, and 0.054 m^3, respectively.

Significantly higher heartwood volumes were found in 15- to 20-year-old teak plantations grown in this zone.

Pearson correlations for wood quality vs. climate in block plantations

Climatic factors including average annual rainfall were positively correlated with wood density, heartwood, sapwood, and bark content, with correlation coefficients of $r = 0.412$, 0.792, 0.755 and 0.103, respectively (Table 6). Similarly, relative humidity was positively correlated with wood density, heartwood, sapwood, and bark content volumes, with correlation coefficients of $r = 0.354$, 0.597, 0.442, and 0.456, respectively. Maximum temperature was negatively correlated with heartwood volume ($r = -0.085$) in trees aged 5–10 years to 15–20 years, reflecting the negative effects of higher temperatures on tree growth. Minimum temperature was also positively correlated with wood density, heartwood, and sapwood volumes. There was a strong positive correlation between heartwood volume and average rainfall ($r = 0.792$).

Table 2. Volumes of bark (BC), sapwood (SW) and heartwood (HW) in boundary and block plantations in the North Western zone (NWZ).

Age class (yr)	Block				Boundary			
	Wood density (g/cm³)	HW volume (m³)	SW volume (m³)	BC volume (m³)	Wood density (g/cm³)	HW volume (m³)	SW volume (m³)	BC volume (m³)
5-10	0.61	0.050	0.055	0.012	0.70	0.099	0.040	0.017
10-15	0.69	0.088	0.059	0.013	0.74	0.228	0.050	0.018
15-20	0.74	0.204	0.079	0.021	0.79	0.303	0.067	0.022
Mean	0.68	0.114	0.064	0.015	0.74	0.210	0.052	0.019
S.Ed	0.04	0.027	0.004	0.002	0.03	0.034	0.005	0.001
CD	0.08	0.059	0.009	0.004	0.05	0.075	0.011	0.002

Table 3. Volumes of bark (BC), sapwood (SW) and heartwood (HW) in boundary and block plantations in the Cauvery Delta zone (CDZ).

Age class (yr)	Block				Boundary			
	Wood density (g/cm³)	HW volume (m³)	SW volume (m³)	BC volume (m³)	Wood density (g/cm³)	HW volume (m³)	SW volume (m³)	BC volume (m³)
5-10	0.60	0.012	0.040	0.003	0.66	0.037	0.024	0.008
10-15	0.70	0.046	0.054	0.011	0.72	0.112	0.067	0.018
15-20	0.75	0.086	0.075	0.014	0.76	0.312	0.141	0.034
Mean	0.68	0.048	0.056	0.009	0.71	0.154	0.078	0.020
S.Ed	0.04	0.012	0.006	0.002	0.03	0.047	0.020	0.005
CD	0.09	0.026	0.013	0.004	0.06	0.103	0.044	0.011

Table 4. Volumes of bark (BC), sapwood (SW) and heartwood (HW) in boundary and block plantations in the Western zone (WZ).

Age class (yr)	Block				Boundary			
	Wood density (g/cm³)	HW volume (m³)	SW volume (m³)	BC volume (m³)	Wood density (g/cm³)	HW volume (m³)	SW volume (m³)	BC volume (m³)
5-10	0.63	0.025	0.021	0.023	0.68	0.113	0.083	0.054
10-15	0.68	0.083	0.048	0.059	0.74	0.238	0.096	0.094
15-20	0.74	0.139	0.073	0.090	0.80	0.433	0.120	0.097
Mean	0.68	0.082	0.047	0.057	0.73	0.261	0.100	0.082
S.Ed	0.03	0.033	0.015	0.019	0.03	0.093	0.011	0.014
CD	0.07	0.069	0.032	0.041	0.06	0.196	0.023	0.029

Table 5. Volumes of bark (BC), sapwood (SW), and heartwood (HW) in boundary and block plantations in the North Eastern zone (NEZ).

Age class (yr)	Block				Boundary			
	Wood density (g/cm³)	HW volume (m³)	SW volume (m³)	BC volume (m³)	Wood density (g/cm³)	HW volume (m³)	SW volume (m³)	BC volume (m³)
5-10	0.62	0.031	0.050	0.007	0.67	0.070	0.047	0.010
10-15	0.71	0.071	0.054	0.012	0.73	0.180	0.061	0.019
15-20	0.75	0.239	0.114	0.027	0.78	0.342	0.074	0.030
Mean	0.69	0.114	0.072	0.015	0.73	0.197	0.060	0.020
S.Ed	0.04	0.037	0.012	0.003	0.03	0.046	0.005	0.003
CD	0.08	0.081	0.026	0.007	0.07	0.101	0.011	0.007

Pearson correlation for wood quality vs. climate in boundary plantations

Average rainfall was positively correlated with wood density, heartwood volume, sapwood volume, and bark content volume, with correlation coefficients (r) of 0.859, 0.816, 0.384, and 0.196 at $p < 0.01$, respectively. Similarly, relative humidity was positively correlated with wood density, heartwood, sapwood, and bark content volumes, with correlation coefficients of $r = 0.831$, 0.899, 0.685, and 0.632, respectively. Maximum temperature was negatively correlated with all the wood quality parameters. A strong positive correlation ($r = 0.899$) was found between heartwood volume and relative humidity (Table 7).

Table 6. Pearson Correlations coefficients for wood quality vs. climate in block plantations.

Pearson's correlation	Wood density (g/cm^3)	Heartwood volume (m^3)	Sapwood volume (m^3)	Bark content volume (m^3)	Average rainfall (mm)	Maximum temperature (°C)	Minimum temperature (°C)	Relative humidity (%)
Wood density (g/cm^3)	1							
Heartwood volume (m^3)	0.774	1						
Sapwood volume (m^3)	0.753	0.891	1					
Bark content volume (m^3)	0.389	0.363	0.193	1				
Average rainfall (mm)	0.412	0.792	0.755	0.103	1			
Maximum temperature (°C)	0.120	-0.085	0.055	-0.502	-0.295	1		
Minimum temperature (°C)	0.338	0.347	0.535	-0.249	0.491	-0.144	1	
Relative humidity (%)	0.354	0.597	0.442	0.456	0.797	-0.694	0.365	1

Table 7. Pearson Correlation coefficients for wood quality vs. climate in boundary plantations.

Pearson's correlation	Wood density (g/cm^3)	Heartwood volume (m^3)	Sapwood volume (m^3)	Bark content volume (m^3)	Average rainfall (mm)	Maximum temperature (°C)	Minimum temperature (°C)	Relative humidity (%)
Wood density (g/cm^3)	1							
Heartwood volume (m^3)	0.957	1						
Sapwood volume (m^3)	0.612	0.721	1					
Bark content volume (m^3)	0.433	0.565	0.681	1				
Average rainfall (mm)	0.859	0.816	0.384	0.196	1			
Maximum temperature (°C)	-0.553	-0.503	-0.095	-0.190	-0.841	1		
Minimum temperature (°C)	0.320	0.229	-0.183	-0.390	0.635	-0.719	1	
Relative humidity (%)	0.831	0.899	0.685	0.632	0.840	-0.690	0.318	1

Pearson correlation for wood quality vs. edaphic factors in block plantations

Available phosphorous showed positive correlations with all wood density (r = 0.579), heartwood volume (r = 0.290), sapwood volume (r = 0.441), and bark content volume (r = 0.142) (Table 8). Similarly, soil pH was negatively correlated with wood density (r = -0.389), heartwood volume (r = -0.334), sapwood volume (r = -0.537), and bark content volume (r = -0.364). Positive correlations were also observed between available nitrogen and available potassium with wood density, with correlation coefficients of r = 0.053 and r = 0.343, respectively. Heartwood volume was negatively correlated with soil electrical conductivity (EC), organic carbon, and available nitrogen, with the correlation coefficients of r = -0.035, -0.275, and -0.362 in all four agroclimatic zones in the block plantation age classes of 5–10, 10–15, and 15–20 years (Table 9).

Pearson correlation for wood quality vs. edaphic factors in boundary plantations

Electrical conductivity and organic carbon were positively correlated with wood density (r = 0.225 and r = 0.352), heartwood volume (r = 0.300 and r = 0.436), sapwood volume (r = 0.493 and r = 0.376), and bark content volume (r = 770 and r = 0.493) (Table 10). pH was negatively correlated with wood density, heartwood volume, sapwood volume, and bark content volume, with correlation coefficients of r = -0.554, -0.635, -0.563, and -0.204, respectively. Available nitrogen, phosphorus, and potassium were negatively correlated with wood density, with coefficients of r = -0.099, -0.118, and -0.129, while correlations for these three elements with heartwood volume were r = -0.124, -0.078, and -0.275, respectively.

Discussion

Wood fractions of teak in block plantations

As expected, heartwood volume increased with increasing age and diameter (Tables 3 to 6), while bark content decreased. Tewari and Mariswamy (2013) also found that heartwood volume increased and bark volume decreased with increasing age and diameter at breast height (DBH).

The highest heartwood volume in block plantations was 0.239 m^3 (age class of 15–20 years) was recorded from the northeastern zone. A previous study at Karnataka found that maximum heartwood volume of 0.167 m^3 was recorded in a 36-year-old plantation. The studies show that heartwood volume increased with increasing age and diameter (Tewari and Mariswamy (2013). Similar studies were reported in teak with 20-year-old plantations in Thailand (Wanishdilokratn et al. 2024) and Indonesia (Nugroho et al. 2024).

Table 8. Soil physicochemical properties of four agroclimatic zones.

			Surface soil (0-15 cm)					
SI. No.	Location	Age class (yr)	Soil pH	EC (dS/m)	Organic carbon (%)	Available nitrogen (Kg/ha)	Available phosphorus (Kg/ha)	Available potassium (Kg/ha)
1	Arani (NEZ)	10-15	8.13	0.12	0.60	177	16.0	268.0
2	SU Vanam (NEZ)	5-10	7.17	0.16	0.56	173	20.0	295.0
3	Uthangarai (NWZ)	15-20	8.10	0.12	0.60	165	11.0	235.0
4	Naduvur (CDZ)	5-10	8.43	0.18	0.48	153	17.0	275.0
5	Pudur (WZ)	15-20	7.60	0.18	0.83	172	13.0	264.0
					Subsurface soil (15-30 cm)			
1	Arani (NEZ)	10-15	8.70	0.18	0.62	185	18.3	358.0
2	SU Vanam (NEZ)	5-10	7.01	0.17	0.59	180	25.0	312.0
3	Uthangarai (NWZ)	15-20	8.44	0.22	0.84	173	15.0	257.0
4	Naduvur (CDZ)	5-10	8.47	0.21	0.52	161	20.0	290.0
5	Pudur (WZ)	15-20	6.72	0.25	1.11	179	16.4	276.0

Table 9. Pearson correlation coefficients for wood quality vs. edaphic factors in block plantations.

Pearson's Correlation	Wood density (g/cm^3)	Heartwood volume (m^3)	Sapwood volume (m^3)	Bark content volume (m^3)	pH	Electrical conductivity (dSm^{-1})	Organic carbon (%)	Nitrogen ($kg\ ha^{-1}$)	Phosphorus ($kg\ ha^{-1}$)	Potassium ($kg\ ha^{-1}$)
Wood density (g/cm^3)	1									
Heartwood volume (m^3)	0.765	1								
Sapwood volume (m^3)	0.826	0.899	1							
Bark content volume (m^3)	0.296	0.299	0.157	1						
pH	-0.389	-0.334	-0.537	-0.364	1					
Electrical conductivity (dSm^{-1})	-0.111	-0.035	-0.193	0.717	-0.180	1				
Organic carbon (%)	-0.272	-0.275	-0.280	0.501	-0.474	0.624	1			
Nitrogen ($kg\ ha^{-1}$)	0.053	-0.362	-0.046	-0.038	-0.357	0.061	0.431	1		
Phosphorus ($kg\ ha^{-1}$)	0.579	0.290	0.441	0.142	-0.285	0.171	-0.326	0.239	1	
Potassium ($kg\ ha^{-1}$)	0.343	0.027	0.238	-0.035	0.056	0.155	-0.221	0.502	0.681	1

Table 10. Pearson correlation coefficients for wood quality vs. edaphic factors in boundary plantations.

Pearson's correlation	Wood density (g/cm^3)	Heartwood volume (m^3)	Sapwood volume (m^3)	Bark content volume (m^3)	pH	Electrical conductivity (dSm^{-1})	Organic carbon (%)	Nitrogen ($kg\ ha^{-1}$)	Phosphorus ($kg\ ha^{-1}$)	Potassium ($kg\ ha^{-1}$)
Wood density (g/cm^3)	1									
Heartwood volume (m^3)	0.944	1								
Sapwood volume (m^3)	0.445	0.601	1							
Bark content volume (m^3)	0.313	0.479	0.626	1						
pH	-0.554	-0.635	-0.563	-0.204	1					
Electrical conductivity (dSm^{-1})	0.225	0.300	0.493	0.770	-0.180	1				
Organic carbon (%)	0.352	0.436	0.376	0.493	-0.473	0.624	1			
Nitrogen ($kg\ ha^{-1}$)	-0.099	-0.124	0.324	-0.072	-0.357	0.061	0.431	1		
Phosphorus ($kg\ ha^{-1}$)	-0.118	-0.078	0.511	0.108	-0.285	0.171	-0.326	0.239	1	
Potassium ($kg\ ha^{-1}$)	-0.129	-0.275	0.172	-0.104	0.056	0.155	-0.221	0.502	0.681	1

The proportions of sapwood, heartwood, and bark varied with age in the selected agroclimatic zones of Tamil Nadu (Figure 3). Heartwood percentages in the present study ranged from 22.39% to 83.51%, sapwood percentages ranged from 11.23% to 71.64%, and bark content percentages ranged from 5.26% to 32.78% in the three age classes. Conversely, Kollert et al. (2024) found that heartwood percentage varied from 37.05% to 56.33%, sapwood percentage varied from 12.95% to 23.04%, and bark content percentage varied from 27.77% to 43.52% in different ages (11–36 years). The studies all concluded that heartwood percentage increased and bark content decreased with increasing age and diameter, whereas the sapwood proportion remained relatively similar. A stable sapwood proportion would be consistent with the need for the trees to maintain sufficient transport capacity to maintain the foliage.

Wood density and specific gravity are both used to indicate the amount of actual wood substance present in a unit volume of wood, and both terms can be calculated from one another (Zobel and Talbert 1984). Wood density or wood specific gravity is considered as one of the most important wood properties contributing to wood quality.

Wood density in block plantations ranged from 0.60 g/cm^3 to 0.75 g/cm^3 in the three age classes. Shukla et al. (2007) reported that the average wood density of *Acacia auriculiformis* was highest in 13-year-old trees (0.62 g/cm^3), followed by 12-year-old (0.60 g/cm^3) and 8-year-old trees (0.57 g/cm^3).

Wood fractions of teak in boundary plantations

Teak grown in boundary plantations had the highest heartwood volumes when compared to block plantations. This may be

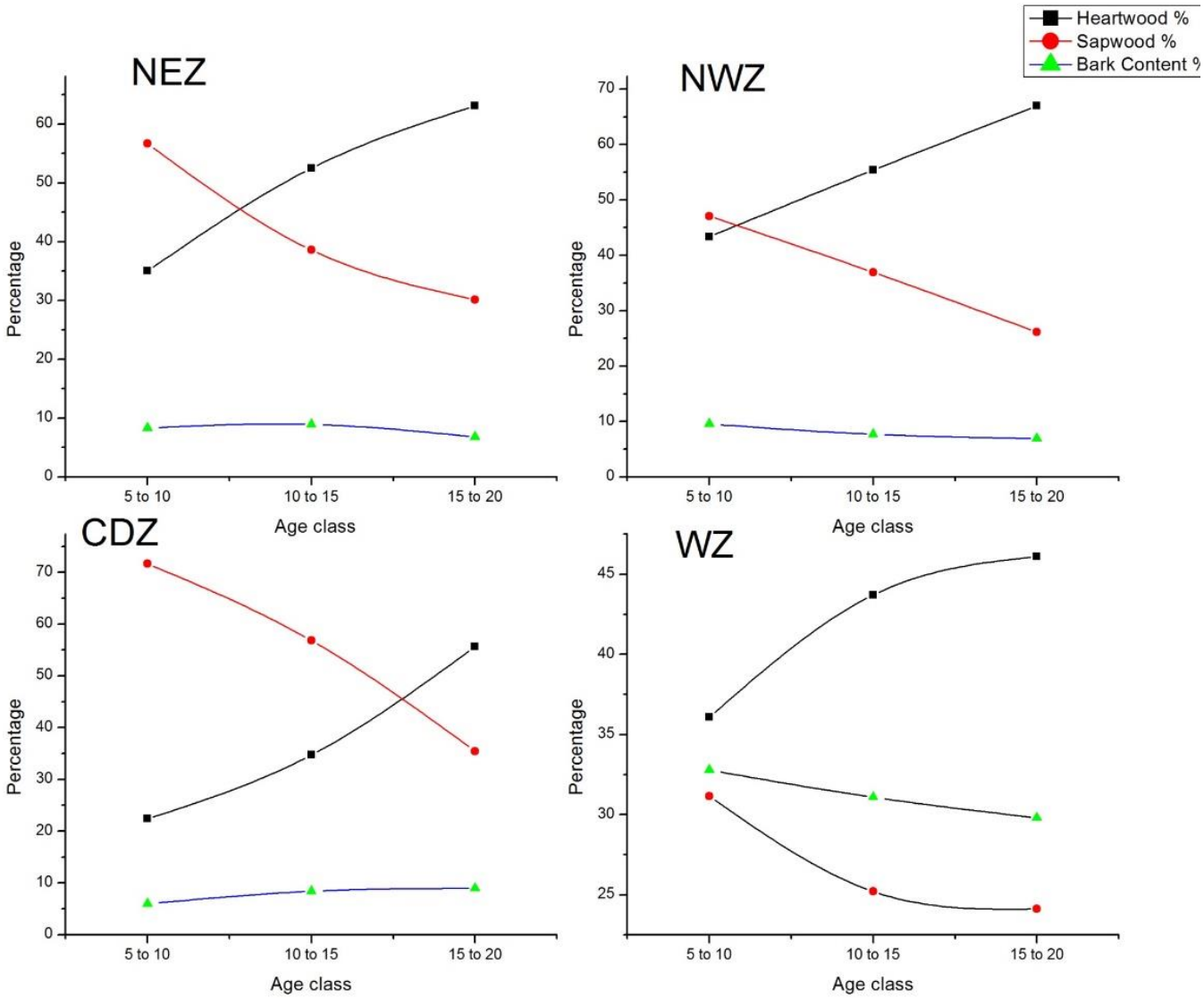

Figure 3. Wood fractions of teak in block plantations

attributed to wider spacing adaptability for boundary planting (5 m × 5 m, 7 m × 7 m, or 10 m × 10 m) compared to closer spacing (2 m × 2 m or 3 m × 3 m) of block planting. Zahabu et al. (2015) also concluded that wider spacing was more favorable for teak grown in boundary plantations in farmlands of Tanzania. Enhanced wood production from teak boundaries has been attributed to low competition for light, water, and nutrients from neighboring trees (Pandey and Brown 2000).

Teak grown in boundary plantation in selected agroclimatic zones had the maximum heartwood volume in 15- to 20-year-old trees in terms of cubic meter and percentage (Figure 4). The highest heartwood volume (0.433 m^3) was registered in the western zone with the spacing of 5 × 5 m. The present findings were in line with Zahabu et al. (2015) and showed increased heartwood proportion as planting spacing increased in boundary plantations. Bhat (1995) and Kokutse et al. (2004) also found an increase in the heartwood proportion of teak with increased spacing in farm plantations of Kerala, India and Togo, respectively.

Wood density of teak gradually increased (0.66 g/cm^3 to 0.80 g/cm^3) with increased age, from 5 to 20 years. Cordero and Kanninen (2003) also observed that wood density increased (0.73 g/cm^3 to 0.77 g/cm^3) as age increased from 10 to 47 years, but growth rate declined. The results were positively correlated with those of Wanneng et al. (2014) who compared density of three age groups (5, 10, and 15 years) of teak and found that density with the maximum age group of 15 years would be acceptable for industrial utilization.

Edaphoclimatic influence on wood quality in block plantations

Integrating trees on farms is beneficial for farmers, especially those struggling to cope with the impacts of climate change (Gonsalves 2014). Rainfall, relative humidity, and maximum

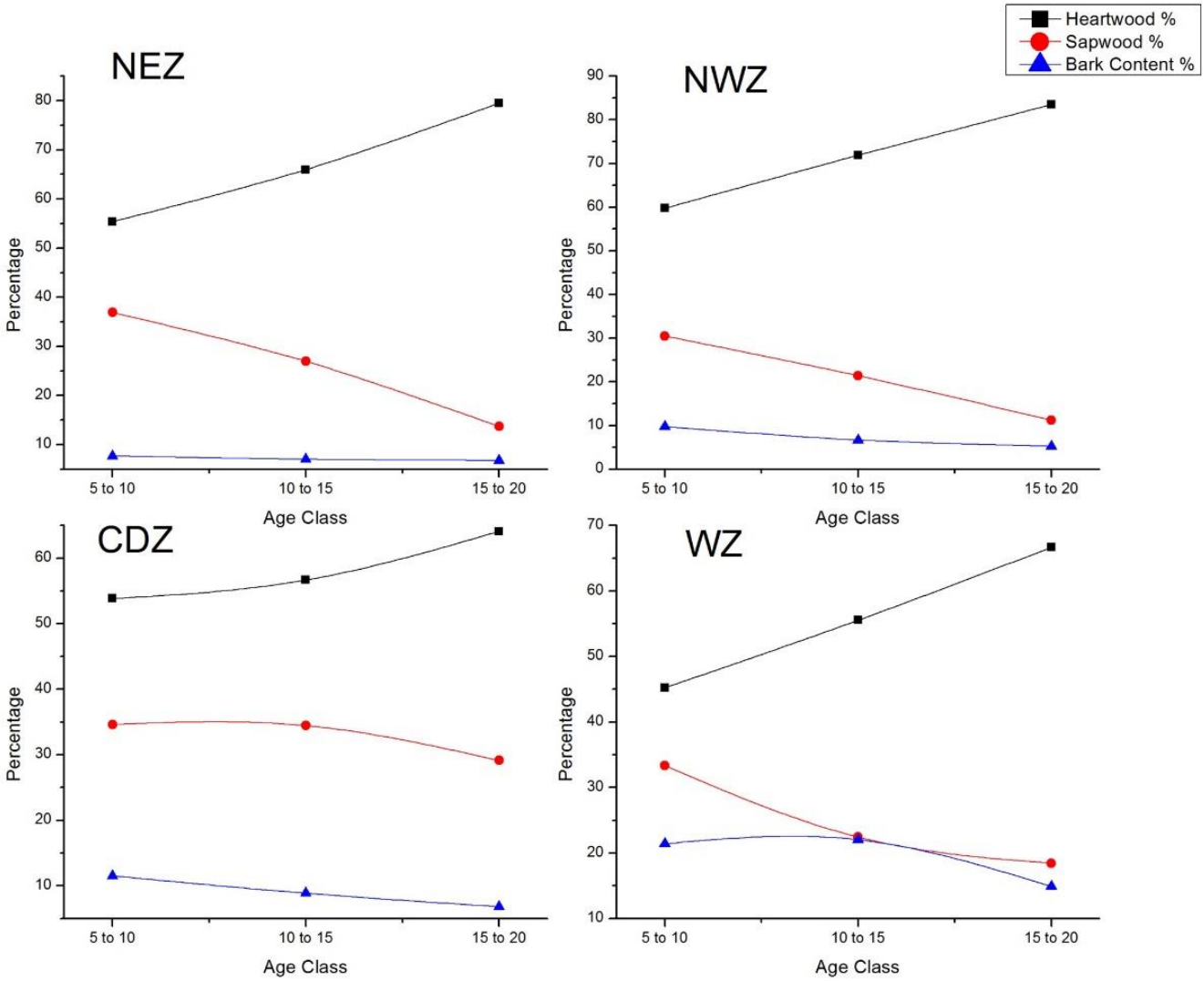

Figure 4. Wood fractions of teak in boundary plantations

and minimum temperature were correlated with heartwood volume in all three age classes in all four zones in Tamil Nadu (Figure 5). Climatic factors were positively correlated with heartwood volume under the average rainfall (r = 0.792), minimum temperature (r = 0.347), and relative humidity (r = 0.597). The present study confirms the findings of Pimpale et al. (2000), who found that the highest increase in mean annual increment (MAI) of a 5-year-old teak plantation was registered in 1999 at Akola, Maharashtra, where maximum annual rainfall was above average. Mean growth rate of teak ranged from 4.5 mm/year/tree (initial years) to 5.2 mm/year/tree (30 years onwards); however, slower growth was observed when annual rainfall was less than 800 mm (Palanisamy et al. 2009). Previous studies indicate that teak grows well in areas with 800-2500 mm rainfall annually at an elevation of about 1200 m (Sabastian et al. 2018).

Previous studies have also shown that teak grows well on deep, well-drained alluvial soils but poorly on dry sandy, shallow or hard pan, acidic, laterite, black cotton or waterlogged soils. It tolerates heat and drought and soil pH's ranging from 5.0 to 8.0 (Kulkarni 2000). Soil pH (r = -0.334), soil EC (r = -0.035), soil organic carbon (r = -0.275), and soil available nitrogen (r = -0.362) were all negatively correlated with the heartwood volume of teak (Figure 6). Conversely, available phosphorus (r = 0.290) and potassium (r = 0.027) were positively correlated with the heartwood volume. Watanabe et al. (2016) found positive correlations with available phosphorus and potassium and negative correlations with pH, soil EC, and available nitrogen and the quality of teak heartwood. Zhang et al. (2016) found that shallow soils were an important factor limiting tree heartwood ratios, while deeper soils were associated with higher tree growth and improved wood quality.

Edaphoclimatic influence on wood quality in boundary plantations

Tree growth is strongly influenced by climatic factors like rainfall, temperature (maximum and minimum), and relative humidity. In the current study, teak heartwood volume was highly positively correlated with rainfall (r = 0.816) and relative humidity (r = 0.899). The results are in line with 5-year-old *Pinus radiata* (Alvarez et al. 2012) that exhibited positive correlations between heartwood volume and mean annual rainfall. In the present study, maximum temperature was negatively correlated with heartwood volume (r = -0.503). Similar negative correlations between maximum temperature and heartwood volume were recorded in *Pinus radiata* plantations (Yang et al. 2018). The results illustrate the obvious influences of mean annual rainfall, temperature, and relative humidity on tree growth and heartwood volume of teak (Figure 7).

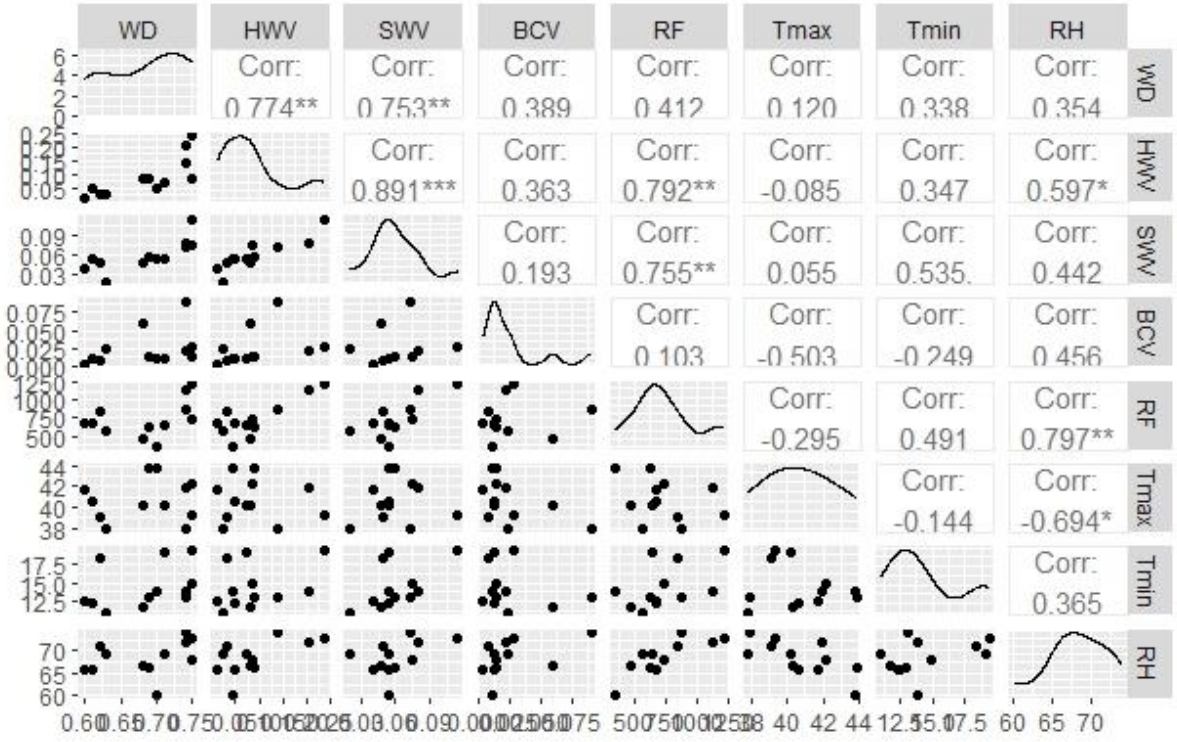

Figure 5. Relationships between wood quality and climate factors in block plantations.

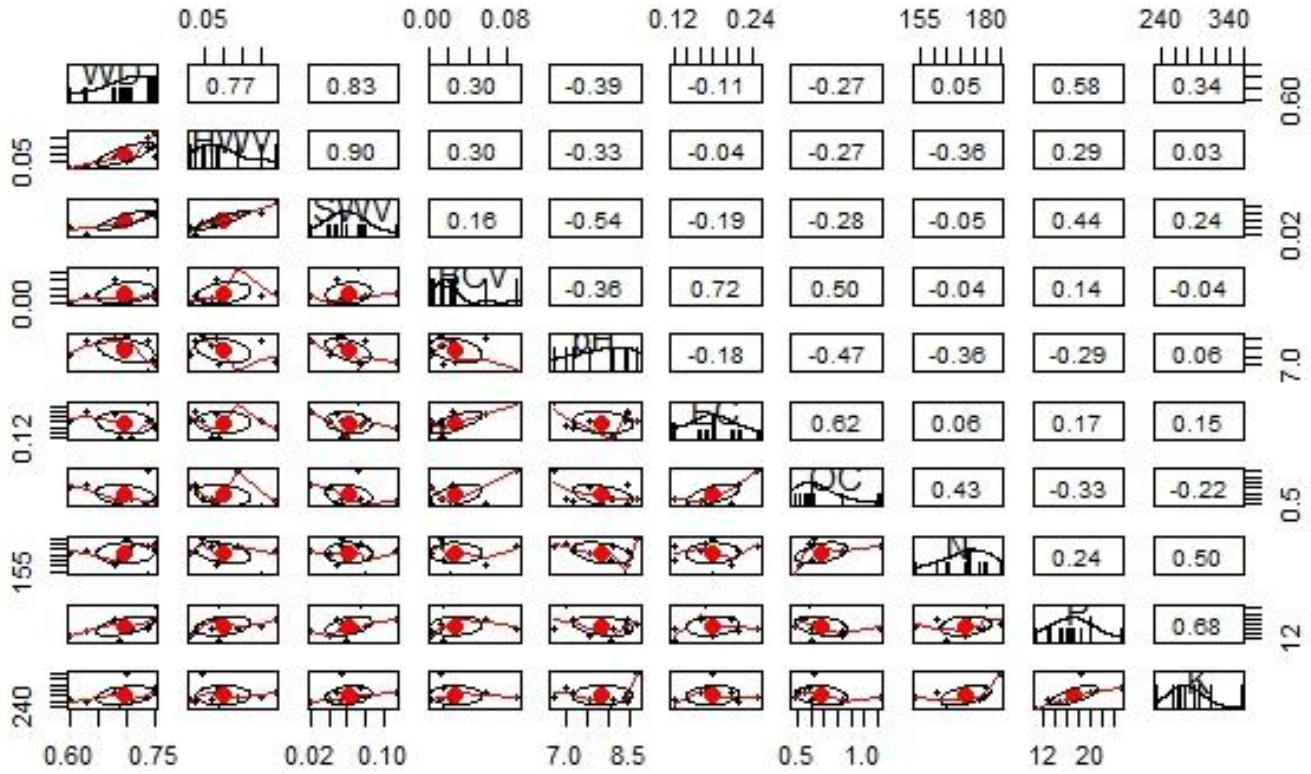

Figure 6. Relationships between wood quality and soil characteristics in block plantations.

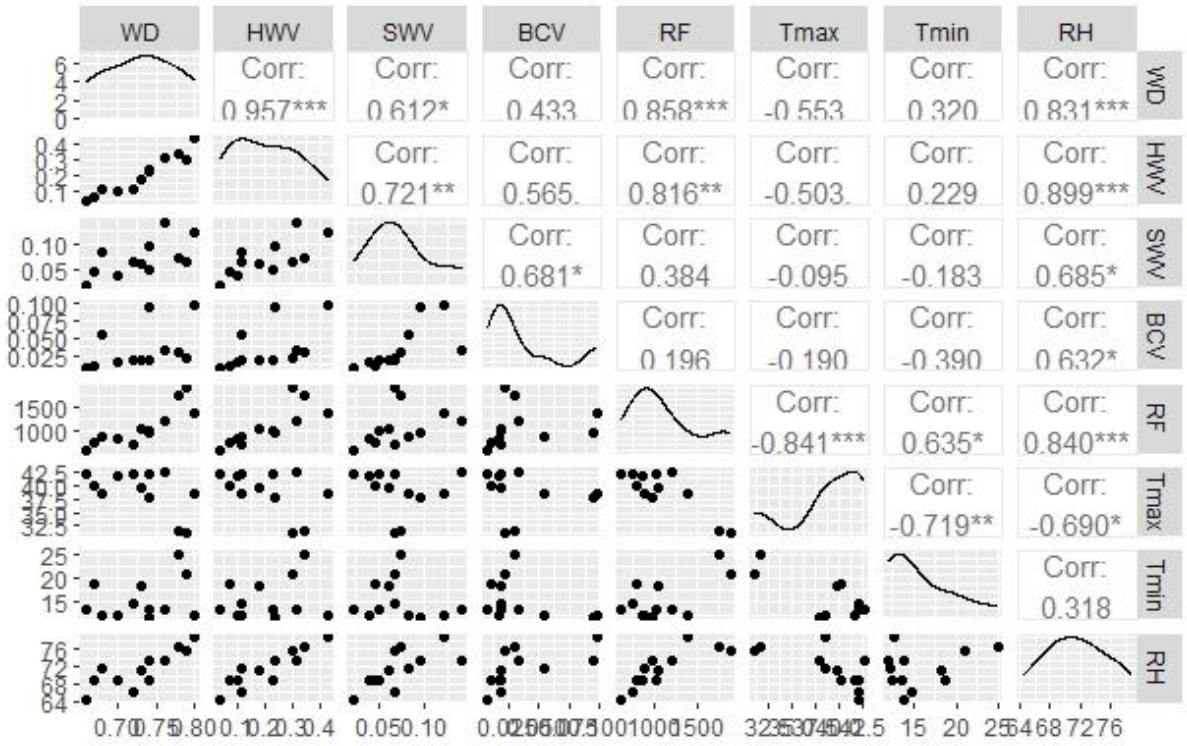

Figure 7. Relationships between wood quality and climate in boundary plantations.

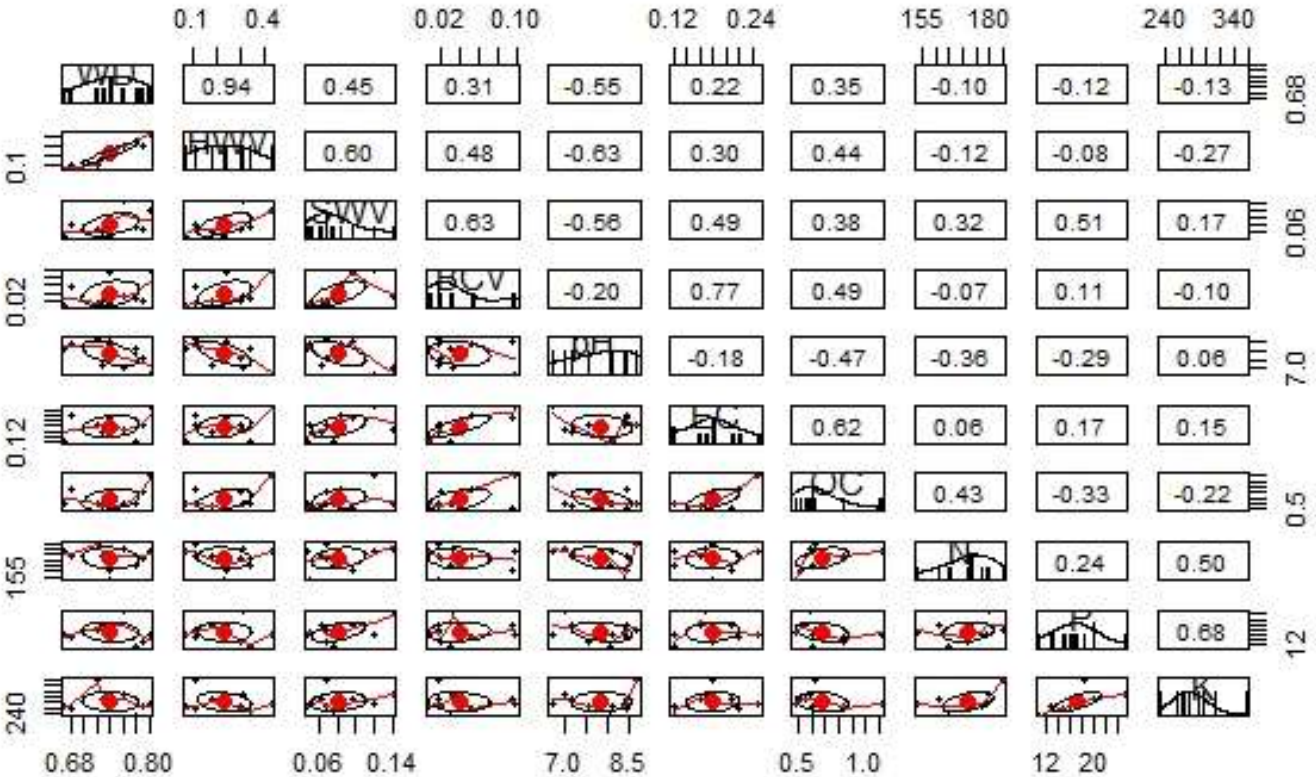

Figure 8. Relationships between wood quality and Soil characteristics in boundary plantations

Soil physicochemical and chemical properties strongly influenced the growth parameters in the boundary plantations. Soil macronutrients such as available nitrogen, phosphorus, and potassium play significant roles in the wood quality of farm-grown teak. Increasing soil pH was negatively correlated with all wood quality attributes, while soil EC exhibited a significant positive correlation. Previous studies have found that soil pH and EC influence growth, wood quality, and tree distribution. Aparanji (2000) found significant relationships between the volume increment of teak and soil physicochemical properties. The soil organic carbon was positively correlated with heartwood volume in radiata pine (Gunaga et al. 2011 and Alvarez et al. 2012).

Available nitrogen, phosphorus and potassium were all negatively correlated with all wood quality parameters (Figure 8). These results support previous studies with other species (Watanabe et al. 2016 and Gunaga et al. 2011). The positive influence of soil factors on wood quality and productivity of tree species have also been previously reported for teak (Aparanji 2000), *Pinus radiata* (Alvarez et al. 2012), *Ailanthus excelsa* (Rajasugunasekar et al. 2017) and *Picea abies* (Johansson et al. 2014).

Conclusion

Heartwood, sapwood, and bark volumes all varied among all three age classes and also with all four agroclimatic zones. Teak grown in block plantations had the highest heartwood and sapwood volumes in the northeastern zone for 15- to 20-year-old trees. However, maximum bark content was obtained in the western zone for 15- to 20-year-old trees. The northeastern zone registered the maximum clear bole volume, indicating that this zone was well-suited in terms of wood yield and quality. Maximum heartwood and bark volumes in boundary plantations were observed in 15- to 20-year-old trees in the western zone. Maximum sapwood volume was observed for 15- to 20-year-old trees in the Cauvery Delta. Boundary plantations in the western zone tended to have higher wood volumes and heartwood content, suggesting that this area is the most suitable zone for growing teak in boundary plantations.

Acknowledgements

The authors would like to thank the Indian Council of Forestry Research and Education, Dehradun for providing financial support through the All India Coordinated Research Project on

Silvicultural interventions for productivity enhancement and carbon sequestration in plantations of important tree species.

References

Alvarez E, Duque A, Saldarriaga J, Cabrera K, de Las Salas G, del Valle I, Lema A, Moreno F, Orrego S, Rodríguez L (2012) Tree above-ground biomass allometries for carbon stocks estimation in the natural forests of Colombia. For Ecol Manag 267:297–308. https://doi.org/10.1016/j.foreco.2011.12.013

Aparanji SL (2000) Influence of site factors on growth of teak stands in the Western Ghats. MSc Thesis. Sirsi, University of Agricultural Sciences Dharwad. http://krishikosh.egranth.ac.in/handle/1/5810128611

Arunkumar AN, Warrier, KCS, Warrier, RR (2024) The Timeless Legacy of Teak: Unveiling Its History, Importance, and Enduring Relevance. In Uthup TK, Karumamkandathil R (eds) Economically Important Trees: Origin, Evolution, Genetic Diversity and Ecology. Sustainable Development and Biodiversity, vol 37. Springer, Singapore. pp. 173–205. https://doi.org/10.1007/978-981-97-5940-8_5

Balakrishnan S, Dev SA, Sakthi AR, Vikashini B, Bhasker TR, Magesh NS, Ramasamy Y (2021) Gene-ecological zonation and population genetic structure of *Tectona grandis* Lf in India revealed by genome-wide SSR markers. Tree Genet Genomes 17 (4):1–14. https://doi.org/10.1007/s11295-021-01514-x

Bhat KM (1995) A note on heartwood proportion and wood density of 8-year-old teak Indian For 121 (6):514–517.

Bray RH, Kurtz, LT (1945) Determination of total, organic, and available forms of phosphorus in soils. Soil Sci 59(1), 39–46. https://dx.doi.org/10.1097/00010694-194501000-00006

Brocco VF, Paes JB, Costa LGD, Kirker GT, Brazolin S (2020) Wood color changes and termiticidal properties of teak heartwood extract used as a wood preservative. Holzforschung 74 (3):233–245. https://doi.org/10.1515/hf-2019-0138

Buvaneswaran C, Masilamani P, Senthilkumar S (2016) Windbreaks of casuarina for tailoring growth and branching pattern of teak trees in bund planting system. Int J Appl Agric Res 15 (1):33–42.

Colbu DE, Sandu I, Vasilache V, Earar K, Paraschiv ED, Sandu IG, Bulgaru DI, Sandu AV (2021) Study on the chemical composition of teak wood extracts in different organic solvents. iFor-Biogeosci For 14 (4):329. https://doi.org/10.3832/ifor3717-014

Cordero LP, Kanninen M (2003) Heartwood, sapwood and bark content, and wood dry density of young and mature teak (*Tectona grandis*) trees grown in Costa Rica. Silva Fenn 37 (1):45–54.

Gatonnou KM, Kokutse AD, Kokou K, Koffi-Tessio EM, Agbodji AED (2017) Analysis of the competitiveness of teak wood export in Togo (West Africa). Eur Sci J 13(1):134. http://dx.doi.org/10.19044/esj.2017.v13n1p134

Gonsalves A (2014) Lessons learned on consortium-based research in climate change and development. CARIAA working paper; 1. https://assets.publishing.service.gov.uk/media/57a089aaed915d3cfd000384/CARIAA_WP1.pdf

Gunaga RP, Kanfade AH, Vasudeva R (2011) Soil fertility status of 20 seed production areas of *Tectona grandis* Linn. f. in Karnataka, India. J For Sci 57 (11):483–490.

Hadinata ME, Kozakiewicz P (2020) An investigation of selected properties of teak wood from 9-year-old plantation forest in Indonesia. Ann. of WULS-SGGW 110 (2020):61–72.

Jackson ML (2005) Soil Chemical Analysis: Advanced Course. 2nd ed, rev. Madison, WI: UW-Madison Libraries Parallel Press.

Jackson ML (1973) Soil Chemical Analysis. Prentice Hall of India (P) Ltd, New Delhi.

Johansson U, Sönströd C, Linusson H, Boström H (2014) Regression trees for streaming data with local performance guarantees. IEEE International Conference on Big Data (Big Data) , Washington, DC, USA, 2014, pp. 461–470, doi: 10.1109/BigData.2014.7004263.

Kenzo T, Himmapan W, Yoneda R, Tedsorn N, Vacharangkura T, Hitsuma G, Noda I (2020) General estimation models for above-and below-ground biomass of teak (*Tectona grandis*) plantations in Thailand. For Ecol Manag 457:117701. https://doi.org/10.1016/j.foreco.2019.117701

Kidanu S, Mamo T, Stroosnijder L (2005) Biomass production of Eucalyptus boundary plantations and their effect on crop productivity on Ethiopian highland Vertisols. Agrofor Syst 63 (3):281–290. https://doi.org/10.1007/s10457-005-5169-z

Kokutse AD, Bailleres H, Stokes A, Kokou K (2004) Proportion and quality of heartwood in Togolese teak (*Tectona grandis* Lf). For Ecol Manag 189 (1–3):37–48. https://doi.org/10.1016/j.foreco.2003.07.041

Kollert W, Sandeep S, Sreelakshmy MP, Kokutse A, Reis CA, Bedijo NG, ... Thulasidas PK (2024) Global Teak Resources and Market Assessment 2022.

Kulkarni JR (2000) Wavelet analysis of the association between the southern oscillation and the Indian summer monsoon. Int J Climatol 20 (1):89–104. https://doi.org/10.1002/(SICI)1097-0088(200001)20:1%3C89::AID-JOC458%3E3.0.CO;2-W

Kyaw HY, Kainyande A, Van Hiep T (2024) Profitability Analysis of *Tectona grandis* and *Chukrasia tabularis*: Evidence from Smallholder Forest Plantations in Northwest Vietnam. https://doi.org/10.5152/forestist.2024.23050

Moya R, Gaitán-Álvarez J, Ortiz-Malavassi E, Berrocal A, Fernández-Sólis D (2020) Equations for predicting heartwood merchantable volume and tradable sawlog in *Tectona grandis*. J Trop For Sci 32(4):379–390.

Nugroho E, Ihle R, Heijman W, Oosting SJ (2024) The role of forest user group membership in the extraction of teak forest resources for smallholder cattle farming. Land Use Policy 139:107053. https://doi.org/10.1016/j.landusepol.2024.107053

Odusote JK, Adeleke AA, Lasode OA, Malathi M, Paswan D (2019) Thermal and compositional properties of treated *Tectona grandis*. Biomass Convers Biorefin 9 (3):511–519. https://doi.org/10.1007/s13399-019-00398-1

Palanisamy K, Gireesan K, Nagarajan V, Hegde M (2009) Selection and clonal multiplication of superior trees of teak (*Tectona grandis*) and preliminary evaluation of clones . J Trop For Sci:168–174.

Pandey D, Brown C (2000) Teak: a global overview. UNASYLVA-FAO:3–13. https://www. apps.fao.org.

Pimpale AR, Hiwase SS, Gawande PA, Patil PG (2000) Probability models for prediction of annual maximum daily rainfall at Akola, Maharashtra. PKV Res J 24(2):97–98.

R Core Team (2012) R: A language and environment for statistical computing. – R Foundation for Statistical Computing, Vienna, Austria. https://www.R-project.org/.

Rajasugunasekar D, Menason E, Subramaniyan P, Palanisamy K (2017) Correlation coefficient analysis of germination and seed parameters in *Ailanthus excelsa* Roxb. A multipurpose tree species. Status and recent researches on important timber trees of India. Coimbatore: Institute of Forest Genetics and Tree Breeding, pp. 422–442.

Ramar A, Kannan A (2016) Status and scenario of forest resources in Tamil Nadu. In, Tracking Indian Economy: Issues and Prospects, Mayas Publications, Tamil Nadu, p. 66.

Rizanti DE, Darmawan W, George B, Merlin A, Dumarcay S, Chapuis H, Gérardin C, Gelhaye E, Raharivelomanana P, Sari RK (2018) Comparison of teak wood properties according to forest management: short versus long rotation. Ann For Sci 75 (2):1–12. https://doi.org/10.1007/s13595-018-0716-8

Rosamah E, Ferliyanti F, Kuspradini H, Dungani R, Aditiawati P (2020) Chemical content in two teak woods (*Tectona grandis* Linn. F.) that has been used for 2 and 60 years. J Biol Sci Technol Manag 2:15–19. https://doi.org/10.5614/3bio.2020.2.1.3

Sabastian GE, Kanowski P, Williams E, Roshetko JM (2018) Tree diameter

performance in relation to site quality in smallholder timber production systems in Gunungkidul, Indonesia. Agrofor Syst 92 (1):103–115. https://doi.org/10.1007/s10457-016-0018-9

Shrivastava S, Saxena AK (2017) Wood is Good: But, is India doing enough to meet its present and future needs. Centre for Science and Environment, New Delhi.Shukla SR, Rao RV, Sharma SK, Kumar P, Sudheendra R, Shashikala S (2007) Physical and mechanical properties of plantation-grown *Acacia auriculiformis* of three different ages. Aust For 70 (2):86–92. https://doi.org/10.1080/00049158.2007.10675007

Stanford G, English L (1949) Use of the flame photometer in rapid soil tests for K and Ca. – Agron J 41(9, Sept):446–447. https://doi.org/10.2134/agronj1949.00021962004100090012x.

Subbiah BV, Asija GL (1956) A rapid method for the estimation of nitrogen in soil. Curr Sci 25:259-260.

Tewari VP, Mariswamy KM (2013) Heartwood, sapwood and bark content of teak trees grown in Karnataka, India. J For Res 24 (4):721–725. https://doi.org/10.1007/s11676-013-0410-5

Vongkhamho S, Imaya A, Yamamoto K, Takenaka C, Yamamoto H (2022) Influence of topographic conditions on teak growth performance in mountainous landscapes of Lao PDR. Forests 13 (1):118. https://doi.org/10.3390/f13010118

Walkley A, Black IA (1934) An examination of the Degtjareff method for determining soil organic matter, and a proposed modification of the chromic acid titration method. Soil Sci *5*37(1):29–38. https://doi.org/10.1097/00010694-193401000-00003

Wanishdilokratn T, Sukjareon S, Howpinjai I, Yotapakdee T, Wirojanarome W, Kamton R, ... Asanok L (2024) Comparison of the yield and quality of teak wood from different plantations in Phrae Province, Thailand. Environ Nat Resour J 22(5):431–436. https://doi.org/10.32526/ennrj/22/20240069

Wanneng PX, Ozarska B, Daian MS (2014) Physical properties of *Tectona grandis* grown in Laos. J Trop For Sci:389–396.

Watanabe K, Kohzu A, Suda W, Yamamura S, Takamatsu T, Takenaka A, Koshikawa MK, Hayashi S, Watanabe M (2016) Microbial nitrification in throughfall of a Japanese cedar associated with archaea from the tree canopy. SpringerPlus 5(1):1–15. https://doi.org/10.1186/s40064-016-3286-y

Yang Y, Ding J, Zhang Y, Wu J, Zhang J, Pan X, Gao C, Wang Y, He F (2018) Effects of tillage and mulching measures on soil moisture and temperature, photosynthetic characteristics and yield of winter wheat. Agric Water Manag 201:299–308. https://doi.org/10.1016/j.agwat.2017.11.003

Zahabu E, Raphael T, Chamshama SAO, Iddi S, Malimbwi RE (2015) Effect of spacing regimes on growth, yield, and wood properties of *Tectona grandis* at Longuza Forest Plantation, Tanzania. Int J For Res 2015. https://doi.org/10.1155/2015/469760

Zhang C, Li X, Chen L, Xie G, Liu C, Pei S (2016) Effects of topographical and edaphic factors on tree community structure and diversity of subtropical mountain forests in the lower Lancang River Basin. Forests 7(10):222. https://doi.org/10.3390/f7100222

Zobel BJ, Talbert J (1984) Applied Forest Tree Improvement, New York. John Wiley. 505 p.

Drying *Ochroma pyramidale* from Costa Rican plantations using kiln, solar and air drying: time, moisture content, color and drying defects

Roger Moya *†
Professor - Research Scientist
Escuela de Ingeniería Forestal
Instituto Tecnológico de Costa Rica
Apartado 159-7050, Cartago-Costa Rica,
Email: rmoya@itcr.ac.cr
ORCID: 0000-0002-6201-8383

Carolina Tenorio
Professor - Research Scientist
Escuela de Ingeniería Forestal
Instituto Tecnológico de Costa Rica
Apartado 159-7050, Cartago-Costa Rica,
Email: ctenorio@itcr.ac.cr
ORCID: 0000-0003-2901-7079

Verónica Villalobos-Barquero
Professor - Research Scientist
Escuela de Ingeniería Forestal
Instituto Tecnológico de Costa Rica
Apartado 159-7050, Cartago-Costa Rica,
Email: vvillalobos@itcr.ac.cr
ORCID: 0000-0003-3449-6721

Alejandro Meza-Montoya
Professor - Research Sc Professor - Research Scientist
Escuela de Ingeniería Forestal
Instituto Tecnológico de Costa Rica
Apartado 159-7050, Cartago-Costa Rica,
Email: almeza@itcr.ac.cr
ORCID: 0000-0002-8233-9571

(Received 20 February 2025)

Abstract. Balsa (*Ochroma pyramidale)* holds significant market importance due to its rapid growth and the low density (<0.2 g/cm³) of its wood. Extensive areas of balsa have been established in many tropical regions; however, knowledge about drying wood from this species remains limited. This study evaluated kiln drying (KD), solar drying (SD), and air drying (AD)—in terms of drying time, wood color, and the presence of defects such as warp, splits, and cracks—of 6-cm-thick lumber from 1.7- and 4.5-year-old balsa plantations in Costa Rica. Drying time was shortest for KD, while SD required an intermediate duration between KD and AD. Balsa wood dried using KD exhibited statistically significant differences in all three color parameters, with the highest overall color change. Conversely, wood dried using SD and AD displayed similar values for the three color parameters, with minimal color change. Boards exhibited varying levels of warping (crook, bow, cup, and twist), splits, and checking before drying. SD resulted in similar defect levels (incidence, magnitude, and quality index) to AD. However, KD caused the greatest changes in wood quality and the highest defect incidence. While KD allowed for drying balsa wood with fewer defects in the shortest time, the highest wood quality was achieved with SD and AD, albeit requiring longer drying durations.

Keywords: Balsa wood, *Ochroma pyramidale,* Drying process, Drying defects, Tropical wood, Low density, Quality

Introduction

Ochroma pyramidale (balsa) is a tropical species that grows naturally from southern Mexico to Bolivia, covering latitudes from 22° N to 15° S (Francis 2000). This species is widespread across tropical regions of the Americas, and is particularly abundant in Ecuador, where it is highly commercialized (Condoy et al. 2023). Following the Second World War, *O. pyramidale* was cultivated in commercial plantations across various countries in Asia and Oceania (Francis 2000). More recently, it has been established as a fast-growing plantation species in tropical America and other tropical regions worldwide (Business Research Insights 2024), with the primary

* Author for correspondence: rmoya@itcr.ac.cr
† Society of Wood Science & Technology member

objective of producing sawlogs in the shortest time possible, while maintaining the appropriate density (Francis 2000).

Balsa wood is characterized by its low density, ranging from 50 to 350 kg/m³ (Borrega et al. 2015). Balsa wood has diverse applications in engineering products for civil infrastructure (e.g., wind turbines and bridges), transportation (e.g., cars, trucks, caravans, trains, aircraft, and boats), industrial uses (e.g., packaging and storage), and leisure (e.g., sports equipment and musical instruments) (Galos et al. 2022). The wood must achieve a moisture content (MC) of 10%–12% for these applications, which can be attained using various drying processes (Thybring et al. 2022).

The purpose of drying is to reduce the moisture content to an optimal level, enabling maximum performance during the final use of the wood (Elustondo et al. 2023). Different drying methods are available, and various classifications exist. Teischinger et al. (2023) provided a classification based on heat and energy transfer mechanisms, which included convection, conduction, and radiation/electric field drying. The most common convection-based methods are air drying (AD), solar drying (SD), and conventional kiln drying (KD).

These drying methods are widely used in tropical regions and for plantation-grown wood in Costa Rica (Salas and Moya 2014; Tenorio et al. 2016; Moya et al. 2013; Moya and Tenorio 2022). However, most studies have focused on KD, with limited research examining the behavior of wood in other drying methods (Salas and Moya 2014). An exception was research on *Gmelina arborea* and *Tectona grandis*, where the performance under KD, SD, and AD conditions was studied across varying periods and climatic conditions in Costa Rica (Salas and Moya 2014).

Research on drying balsa remains limited, particularly for plantation-grown wood, as most studies have focused on trees from natural forests. For instance, the USDA Forest Products Laboratory (Boone et al. 1988) recommended kiln drying schedules T10-D4S for lumber up to 2.5 cm thick and T8-D3S for thicker lumber. Similarly, the French Agricultural Research Centre for International Development (CIRAD 2024) proposed drying schedules where balsa wood could achieve a moisture content of 10%–14% within 2–3 days, although the thickness of the wood was not specified (Midgley et al. 2010). Eddowes (Eddowes 2005) highlighted the need to evaluate the applicability and profitability of solar drying systems to achieve high-quality drying outcomes and cost efficiency. Additionally, Jenkin et al. (2019) emphasized that logs must be processed and kiln-dried within 48 hours of harvesting to minimize drying defects and improve wood quality.

Although some studies have explored balsa wood drying methods in Ecuador and Peru, they often lack methodological details about the behavior of wood under KD, SD, and AD conditions. For example, Guevara (1996) used AD to dry lumber (15 cm wide, 20 mm thick, and 1.2 m long) from secondary forest trees in Peru and reported an initial MC of 286%. However, drying times varied widely, ranging from 30 to 45 days, and the wood was classified as fast-drying with type A warping defects. Meanwhile, Utia (2012) studied AD using triangle crib piling and inverted "V" end-racking methods for wood (2.5 cm thick, 10 cm wide, and 1.3 m long) from natural forests. While drying defects were assessed at different tree heights, additional drying data were limited.

The objective of this study was to compare KD, SD, and AD—in terms of drying time, wood color, and the presence of defects such as warping, splitting, and cracking in 6 cm thick lumber from 1.7- and 4.5-year-old plantations in Costa Rica. The findings of this study will provide valuable insights into producing balsa wood for use in wind turbine blades, where international markets demand wood with a thickness of 5 cm.

Methodology

Tree sampling

Two different provenances were sampled: one plantation located near the Pacific Coast and the other near the Caribbean Coast (Figure 1a). The tree characteristics for each site are presented in Table 1. The Pacific plantation consisted of naturally regenerated balsa, covering approximately 0.25 ha in Parrita (10º 52' 41" N, 84º 21' 88" W). This site contained 25 naturally regenerated trees, of which 10 were sampled. Stand density at sampling time was approximately 600 six-year-old trees/ha. The Caribbean plantation, was a 4.5-year-old managed stand located in Guácimo (10º 52' 41" N, 84º 21' 88" W), established with a 2 × 2 m spacing (initial stand density of 2,500 trees/ha). At the time of sampling, the stand density had decreased to 2,080 trees/ha. No thinning was applied to either plantation, and weed control was conducted manually. Fertilization was carried out at the time of establishment and subsequently at the beginning of each rainy season in May. Six to eight 1.25 m-long sawlogs were extracted from each sampled tree. Sawlog diameter ranged from 18 cm to 25 cm for trees from the natural regeneration area and 14 cm to 18 cm for those from the managed plantation.

Sawing pattern

The logs were through-sawn into 60-mm-thick planks using a pattern commonly employed by the Costa Rican furniture

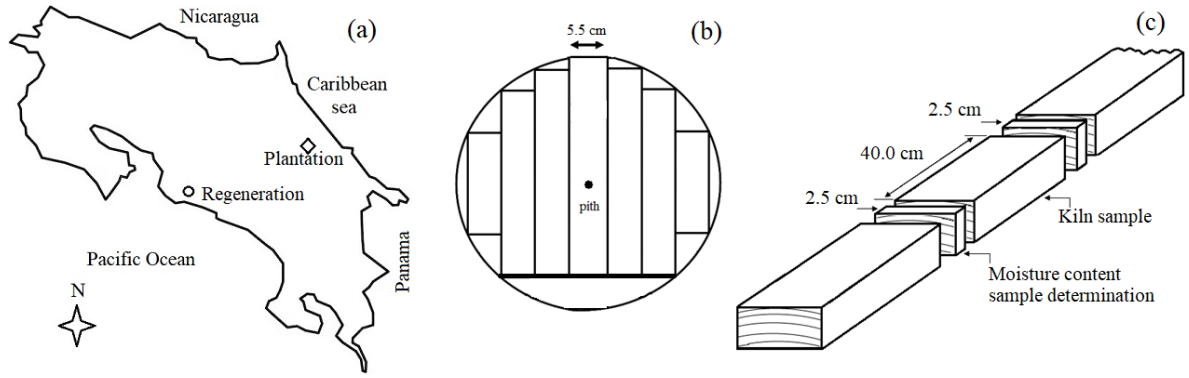

Figure 1. Geographic location (a), sawing pattern (b) and sample extracted for moisture content determination (c) used for *Ochroma pyramidale* lumber.

Table 1. Characteristics of *Ochroma pyramidale* trees used to produce lumber used in different methods of drying.

Precedence	Age (months)	Diameter at breast height (cm)	Commercial height (m)	Total height (m)	Type of drying		
					Kiln	Solar	Air
Regeneration	4.5	20.26	6.64	16.52	x		
Plantation	1.7	15.66	6.50	14.13		x	x

industry; however, the initial cut was varied. This initial cut was made to relieve growth stresses, and then the log was rotated to rest on the straight face (Figure 1b). The thickness was selected because the international market requires dried lumber with a final thickness of 50 mm and this allowed for shrinkage and planning (Condoy et al. 2023; Moya and Muñoz 2008), The boards included flat sawn, quarter sawn, rift sawn, and double rift sawn material. All boards were edged, ensuring that each had four finished edges.

Drying processes

The balsa wood drying was evaluated using three different drying schedules:

- AD—dried by stacking outdoors on stickers and protecting from sun and rain
- SD—dried using a solar dryer based on the design of Salas and Moya (2014)
- KD—dried in a Nardi chamber (San Bonifacio, Italy) following T10-D4S program (Table 2) proposed by Boone et al. (1988) with a target MC of 10%.

Air and solar drying were carried out in Cartago, Costa Rica (09º 50’ 56” N, 83º 54’ 38” W). The three drying methods were evaluated between December 2024 and January 2025. Cartago had an average temperature of 18.16ºC, daily precipitation of 0.91 mm, and an average solar radiation of 19.12 MJ/m²/day (Figure 2a).

Stacking

Green lumber was stacked in packages measuring 1.0 m wide, 1.3 m high, and 1.2 m long. Each of the 12 layers was 5 to 10 boards wide, depending on the drying method. Stickers (2.5 cm × 2.5 cm in cross-section) were placed between the layers.

Table 2. Kiln schedules used for the conventional drying of *Ochroma pyramidale* wood.

Step	Chamber condition				
	TBS °C	TBH	EMC %	MC %	HR
Heating	60	-	-	-	-
	60	-	16.0	-	-
Drying	60	56	14.2	Above 50	82
	60	54.5	12.0	50-40	75
	60	51.5	9.6	40-35	64
	60	49.0	8.0	35-30	55
	65.5	51.5	6.8	30-25	49
	71.0	54.5	5.8	25-20	43
	76.5	57.0	5.1	20-15	39
	82.0	54.5	3.5	15-12	26
Equalization	82	-	10	10	-
Conditioning	82	-	10	-	-
Cooling	40	-	-	-	-

Legend: TBS = Dry-bulb temperature; TBH =Wet-bulb temperature; EMC = equilibrium moisture content; MC = lumber moisture content, HR = Relative humidity.
Source: Boone et al. (1988)

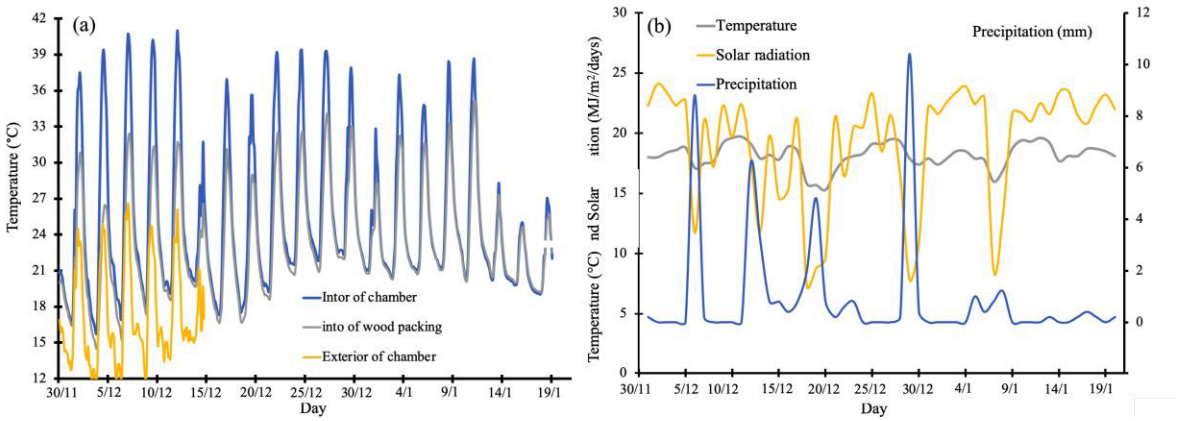

Figure 2. Temperature, solar radiation, and precipitation in Cartago during air drying and (a) and temperature variations in the solar chamber during solar drying of balsa wood(b).

Single stacks were prepared for AD and KD, while two stacks were used for SD to maximize the chamber capacity.

Moisture control

Moisture content during the drying process was monitored using six samples from six representative boards in each drying batch placed at different heights on each side of the pile. Kiln samples (400 mm long) were obtained from the middle of six representative boards in each lumber stack (Simpson 1991). A 2.5-cm-thick cross-section was removed from each end of kiln samples for MC determination, "Initial Moisture Content" (Figure 1c). The end cross-sections of each kiln sample were sealed with silicon paint to retard longitudinal drying. Two samples were placed 20 cm from the ground, two were placed 15 cm from the top, and the remaining two were positioned 25 cm away from the other samples. The target MC was set to 10% for KD, and the drying was considered complete when the MC reached 12% for AD and SD samples. The SD and AD samples were weighed once a day until the control sample reached constant MC. The KD samples were weighed twice a day.

The MC before drying, referred to as "initial moisture content" (Initial-MC), was measured in two 2.5-cm-thick cross-section extracted from each end (Figure 1c). The Initial-MC was determined by weighing, oven drying at 103°C, and weighing according to ASTM D4442-20 (ASTM 2020). The final moisture content (Final-MC) was determined by removing a 6.0-cm-thick cross-section from each board after drying and following the same procedure (ASTM 2020).

Color evaluation

Wood color was determined on a marked area before drying using 30 pieces randomly selected for each drying method. A MiniScan XE Plus spectrophotometer (Hunter Lab Corporate Headquarters, VI, USA) was used to obtain color parameters in the CIE L* a* b* color space. The measurement range of the device was from 400 to 700 nm, with a measurement aperture of 11 mm. For the reflection observation, the specular component (SCI mode) was included at a 10° angle, which is normal to the specimen surface (D65/10), with a field of vision of 2° (Standard observer, CIE 1931) and D65 illumination standard (corresponding to daylight at 6500 K). Color was remeasured on the same locations after drying.

The MiniScan XE Plus generated three parameters for each measurement: L* (luminosity), a* (color tendency from red to green), and b* (color tendency from yellow to blue). ΔE* was calculated from the values of the L*, a*, and b* parameters before and after drying, following the formula outlined in ASTM D2244-23 (ASTM 2023).

Drying defects

Warp (twisting, curvature, bowing, and cupping), cracks, and splits were measured before and after drying following procedures detailed by Moya and Tenorio (2022). All defects were measured using rulers with an accuracy of ± 0.05 mm.

The severity of warping and other drying defects was quantified using Chilean standard NCh993EO72 as described by Pérez et al. (2007), which establishes quality limit values for different parameters. A quality index (QI) was established for each parameter as outlined in equation (1):

$$QI = \frac{(Na * 0) + (Nb * 0{,}5) + (Nc * 2) + (Nd * 2{,}5)}{M} \quad (1)$$

Where: QI is the quality index, which can be QI_{Crook}, QI_{Bow}, QI_{Cup}, or QI_{Twist}; Na is the number of pieces without warp or other defects; Nb is the number of pieces with slight warp or

other defects; Nc is the number of pieces with moderate warp or other defects; Nd is the number of pieces with severe warp or other defects; and M is the total number of pieces.

It is important to note that the magnitude of splits and checks was not measured if the length was shorter than 1 cm. An increase in the QI index indicated a higher severity of drying defects, while a decrease in the QI indicated a reduction in the defects.

Statistical analysis

The average values of Initial-MC, Final-MC, air dry density, color parameters, ΔE*, and drying defects (warp, split, and crack) were determined for each drying method. The variation of the two MC parameters over time was graphed for each drying method. A one-way ANOVA was applied to the different parameters (Initial-MC, Final-MC, air density, color parameters, ΔE*, and drying defects of warp, split, and crack) to determine statistical differences between the drying methods. A Tukey modified least significant difference test was used to identify statistical differences at $p < 0.01$ between the averages of each drying method. The statistical software SAS 8.1 for Windows (SAS Institute Inc., Cary, NC, USA) was used for analysis. Each quality index (QI) parameter was analyzed based on the percentage of incidence and the magnitude of severity before and after drying.

Results and discussion

Moisture content and dried density of wood utilized

The Initial-MC of KD balsa wood was lower than that of SD or AD wood. The KD wood also reflected the provenance of the trees (Table 3). The wood used for kiln drying came from a natural regeneration plot, whereas the wood for solar drying and air drying came from fast-growth plantation trees (Table 1).

The differences in wood density and Initial-MC between wood from natural regeneration and fast-growth plantations can be attributed to two main factors. Tree age plays a significant role, with trees from naturally regenerated stands tending to be older (4.5 years old) and containing denser wood than those from fast-growth plantations (Table 1). As trees age, in addition to an increase in diameter, there is variation in the anatomical features across the diameter (Zobel and Van Buitenen 1989). Generally, the diameter of vessels decreases with age, but their frequency increases. Fibers, which are the anatomical tissue with the highest variation, experience an increase in cell wall thickness as the tree ages (Bucur 2016). This results in an increase in specific gravity (SG) or wood density, and a decrease in Initial-MC (Zobel and Van Buitenen 1989).

Table 3. Initial and final moisture content (MC), density at 12% MC and time to the final MC of *Ochroma pyramidale* wood dried using three different methods.

Type of drying	Initial MC (%)	Final MC (%)	Dried density 12 % (g/cm^3)	Time (hours)
Kiln	104.34	10.16	0.23	136.5
Solar	134.64	12.17	0.11	480
Air	134.64	15.11	0.11	1081

The second factor is the growing conditions, which vary between natural forests and fast-growth plantations. Compared to natural forests, conditions in plantation forests are generally more favorable for tree growth, which leads to faster growth and lower density. These trees produce a higher percentage of juvenile wood, which has thinner cell walls, compared to natural forest wood. Decreased wood density, and an increase in voids are also likely to result in a higher Initial-MC (Moya et al. 2025).

Thus, older trees from natural regeneration exhibit higher density due to their greater age. Numerous studies on balsa wood (Moya et al. 2025; Williamson and Wiemann 2010; Wiemann and Williamson 1988; Whitmore 1973; Rueda and Williamson 1992; Baker 2000; Pertiwi et al. 2017, 2022; Listyanto et al. 2021) confirm that density increases with tree age. Baker (2000) concurred that wood from balsa plantations tended to have lower density than that from natural forest trees.

Moisture content variation and time of drying

As expected, the drying time to reach the target final moisture content was shortest with KD (Table 2, Figure 3). The drying time for SD was intermediate between KD and AD, with AD requiring the longest drying time. The highest Final-MC was observed in AD, while SD resulted in an intermediate value for Final-MC (Table 3).

The decreasing of MC with drying time across the three drying methods (Figure 3) are attributed to the degree of control over temperature, relative humidity, and wind speed conditions (Yin and Liu 2021). For KD, drying conditions can be regulated within the chamber and are not dependent on external environmental factors (Elustondo et al. 2023). In contrast, AD is slower due to the effects of environmental conditions, such as temperature, rain events, and relative humidity where the green lumber is stacked (Lingayat et al. 2021). Solar drying exhibited shorter drying times than AD (Figure 3), likely because SD benefits from better control of temperature and relative humidity (Figure 2b). These conditions in SD were driven by solar radiation hitting the collector, which increased

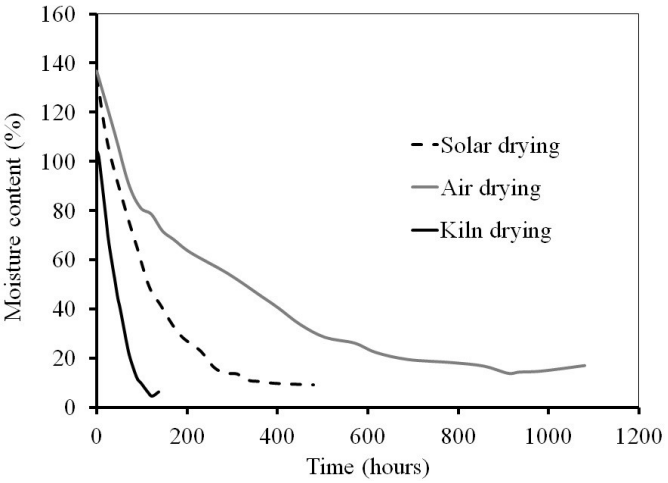

Figure 3. Moisture content variation in *Ochroma pyramidale* lumber during air, solar and kiln drying.

the internal temperature within the chamber (Lamrani et al. 2023; Kamarulzaman et al. 2021).

A key advantage of AD is that the Final-MC tends to be higher than that seen in Costa Rica for other drying methods, such as KD and SD. Air drying can result in EMC values ranging from 13% to 14% (Salas and Moya 2014), which are higher than those for KD and SD. This higher Final-MC likely reflects the low temperatures (below 20°C), rain events and elevated humidity during the drying process (Figure 2b). However, the Final-MC condition in AD may vary depending on the season. In the same region where balsa wood for this study was dried, Salas and Moya (2014) found that balsa wood could be dried to a Final-MC of less than 15% during the dry season, although Final-MC may exceed 16% at other times of the year.

Wood color variation

The color of KD balsa wood differed significantly from that of the AD and SD materials in all three color parameters, with lower values in L* and b*, but a higher value in the a* parameter. In contrast, the SD and AD wood presented similar values for all three parameters (Table 4). The differences between KD and SD or AD can be attributed to the origin of the material and tree age (Table 1).

Wood color variation can be influenced by several factors, including the presence of sapwood and heartwood, tree age, wood origin, growth conditions (natural forest or plantation forest), soil type, and grain pattern (Hu et al. 2020). Thus, the differences in color parameters between KD and AD or SD materials may reflect tree age and wood origin (Table 1). Wood used for KD came from older trees than the wood used for SD and AD and was sourced from naturally regenerated

Table 4. Color variation of *Ochroma pyramidale* lumber before and after air drying, kiln drying, and solar drying.

Drying type	Color parameter before			Color parameter after			ΔE*
	L*	a*	b*	L*	a*	b*	
Kiln	68.4^{A}	12.8^{A}	28.8^{A}	64.8^{A}	11.4^{A}	26.1^{A}	5.7^{A}
Solar	80.2^{B}	7.1^{B}	26.0^{B}	73.2^{B}	8.1^{B}	24.4^{A}	8.3^{B}
Air	82.6^{B}	5.9^{B}	25.5^{B}	73.8^{B}	6.9^{B}	23.5^{A}	10.2^{B}

Legend: Different letters for each parameter color mean statistical difference at 99% level of confidence.

trees, (Table 1). The aging process of trees tends to reduce the L* and b* parameters, while the a* parameter increases (Bessa et al. 2023), which is consistent with the results observed in this study (Table 4).

Well-managed forest plantations typically offer more favorable growth conditions compared to natural forests (Eddowes 2005; Bredemeir et al. 2015). Higher growth rates generally result in a greater proportion of sapwood, which tends to have a lighter color (Quiñonez-Piñón and Valeo 2018). Additionally, the production of extractives increases with tree age, contributing to a reddish color in the wood (Yang et al. 2024). Therefore, wood from natural forests is generally darker than wood from plantations.

During drying, the wood undergoes color changes, showing decreases in the L* and b* parameters, and an increase in the a* parameter (Keey 2005). This behavior was observed in balsa wood across all three drying methods (Table 4). The variations in color parameters have been attributed to loss of the C=O group, which is linked to the aromatic skeleton of lignin. The C=O group is associated with the L* and b* parameters, causing these values to change, while lignin, which is more associated with the a* parameter, remains in the wood (Zelinka et al. 2022). Consequently, the a* parameter is relatively consistent across the different drying methods (Table 4).

Color parameters and color change (ΔE*) after drying followed a similar trend to those before drying. Kiln-dried wood exhibited color parameters that were different from those of wood dried in SD and AD (Table 4). This result supports the premise that dried lumber will experience a color change regardless of the drying method used, and that this change is related to the origin of the wood and tree age (Hu et al. 2020). However, the greatest color change (ΔE*) was observed in wood dried using KD or sourced from natural regeneration, which likely indicates that older wood and KD wood was more affected by the drying process compared to wood from fast-growing plantations, which maintained a lighter color.

The change in wood from older trees or through KD leads to a lower loss of the C=O group, which was associated with the L* and b* parameters (Zelinka et al. 2022). In contrast, wood from younger trees tends to have a lighter color, and the C=O group is lost during drying, resulting in an increase in lignin. As a result, the L* and b* parameters decrease, but the a* parameter increases, leading to a greater change in color (ΔE*) (Table 4).

Drying defects

The wet (green) boards had warping (crook, bow, cup, and twist), splitting, or checking before drying. Among the warping defects, cup and twist had the lowest incidence, and, in fact, these defects were absent in both SD and AD materials (Table 5). However, crook and bow, as well as splitting and checking, showed a high incidence, with crook reaching 100% in SD, for example. After drying, an increased warping was observed across all three drying methods (Table 5). Incidence of crook and bow was lower than that of cup and twist, increased with drying.

The effect of drying method on defects was not prominent; the increases in crook and bow were similar across methods. However, cup and twist defects increased more in SD and AD compared to KD (Table 5). Incidence of splits and checks was lower than that of warping defects, and in fact, the incidence of the splits either remained the same or decreased in AD (Table 5).

Cupping and twisting were present at low levels before drying (Table 5). Warping was present after drying, with the greatest change in the magnitude of the four drying defects occurring with KD. Crook, bow, and cup defects had the smallest increases in magnitude in SD and AD, but twisting saw the greatest increase in magnitude in comparison to KD (Table 5). As noted, the magnitude of split and check defects was not measured.

Warping defects (crook, bow, cup, and twist) before drying, assessed with the Quality Indices (QI), varied across the different drying methods. The QI for crook (QI_{Crook}), QI for bow (QIB_{Bow}), and cup (QI_{Cup}) were lowest in KD compared to AD or SD (Figure 4a-c). QI_{Crook} and QI_{Twist} both increased across all three drying methods tested (Figure 4a,d), indicating a decrease in wood quality. In contrast, the QI_{Bow} and QI_{Cup} decreased in KD, suggesting a slight improvement in wood quality, while they increased in SD and AD wood, reflecting a decrease in quality (Figure 4b-c).

Table 5. Incidence and magnitude for different defects before and after kiln, solar, and air drying of *Ochroma pyramidale* lumber.

Type	Parameter	Time	Drying defect					
			Crook	Bow	Cup	Twist	Split	Check
Kiln	Incidence (%)	Before	41.7	86.1	19.4	38.9	33.4	38.9
		After	91.7	91.7	27.22	100	16.7	41.7
		Change	↑ 50.0	↑ 5.6	↑ 7.82	↑ 61.1	↓ 16.7	↑ 2.8
	Magnitude (mm)	Before	2.4	3.4	1.7	2.8	*	*
		After	4.0	2.7	14.5	14.0	*	*
		Change	↑ 50	↑ 5.6	↑ 12.8	↑ 11.2		
Solar	Incidence (%)	Before	100	36.7	0.0	0.0	40.0	36.7
		After	100	43.4	53.4	90.0	43.4	43.4
		Change	↑ 50	↑ 5.6	↑ 53.4	↑ 90	↑ 3.4	↑ 6.7
	Magnitude (mm)	Before	4.4	1.9	0.0	0.0	*	*
		After	4.5	1.9	1.7	21.7	*	*
		Change	↑ 50	↑ 5.6	= 1.7	= 21.7		
Air	Incidence (%)	Before	83.3	26.7	0.0	0.0	36.7	33.4
		After	96.7	56.7	36.7	93.4	36.7	30
		Change	↑ 50	↑ 30.0	↑ 36.7	↑ 93.4	= 0	↓ 3.4
	Magnitude (mm)	Before	4.6	2.6	0.0	0.0	*	*
		After	4.8	2.9	1.6	22.4	*	*
		Change	↑ 0.2	↑ 0.3	↑ 1.6	↑ 22.4		

Legend: * split and check magnitudes were not measured. ↑ : drying defects increased after drying; ↓ drying defects decreased after drying; and = drying defects was similar before and after drying.

The increases in incidence, magnitude, or QI of defects after drying (Figure 4, Table 5) can be attributed to shrinkage within the boards due to the presence of juvenile wood (Elustondo et al. 2023; Tomad et al. 2023), growth stresses (Moya et al. 2025), and internal stresses produced during the drying process (Elustondo et al. 2023; Tomad et al. 2023; Srisuchart et al. 2023). These three factors are likely the main causes of warping in wood after drying. Juvenile wood in the balsa trees sampled in this study (Table 1), is characterized by a higher microfibril angle in the S2 wall. This type of wood is more prone to warping and splitting, both during sawing and drying processes (Elustondo et al. 2023; Tomad et al. 2023). As trees age, the microfibril angle of newly formed wood on the exterior decreases, but the core wood remains more prone to different shrinkage rates, resulting in warping, splitting, or checking in dried lumber (Tenorio et al. 2012; Moya et al. 2025).

Growth stresses in balsa wood, as in other fast-growing species, are caused by mechanical stress in the xylem tissue during growth, and these stresses tend to be more intense in young trees (Kojima et al. 2009; Gril et al. 2017). These stresses result from the maturation of the cell wall and the increase in canopy load on the stem (Jarvis 2024). The deformation of fibers in axial and transversal directions during the maturation process leads to mechanical stress at the outermost surface of the secondary xylem, just beneath the layer of differentiating xylem (Gril et al. 2017; Thibaut and Gril 2021). Growth stresses in balsa logs are released when the trunk is sawn and manifest in the lumber through warping (crook, bow, and twist), split, and check (Entwistle et al. 2012), as observed in the lumber (Figure 4). Residual growth stresses are further released during drying, causing an increase in distortions such as warping, splitting, and cracking in the lumber (Elustondo et al. 2023; Tomad et al. 2023).

Another cause of distortion in balsa lumber can be attributed to stress tensions during drying. Lumber does not dry uniformly throughout its thickness, as the outer layers dry faster than the inner layers. This discrepancy causes internal stress tensions that can lead to warping, splitting, or cracking, and particularly cup defects (Moya et al. 2017; Tomad et al. 2023; Srisuchart et al. 2023).

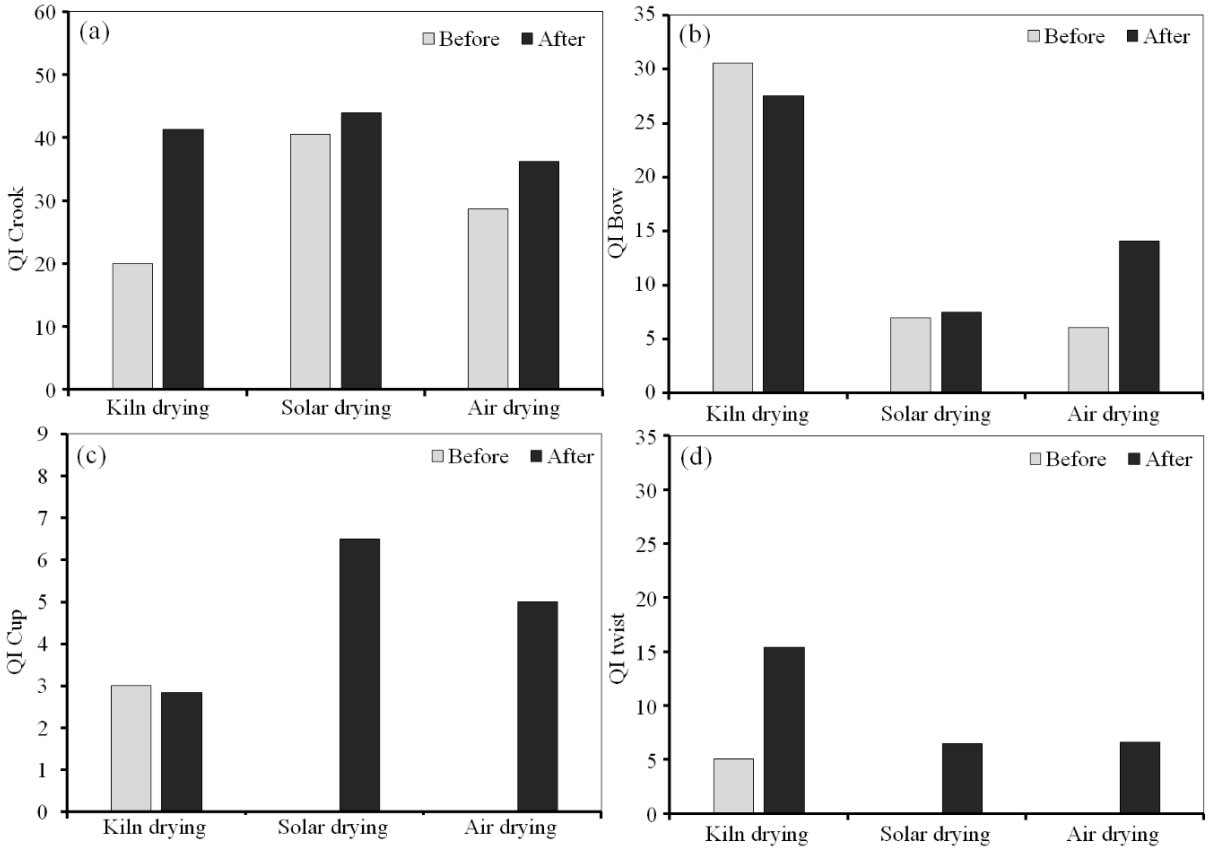

Figure 4. Quality indices of *Ochroma pyramidale* lumber before and after kiln drying.

Cupping was absent, and twist had low incidence prior to drying (Table 5). These defects are linked to the dimensions of the boards (Bond and Espinoza 2016). In the case of cup, narrower boards, like those in this study (less than 10 cm), do not show cupping before drying. However, cupping becomes more pronounced after drying. These results align with findings in other tropical woods from fast-growing forest plantations in Costa Rica (Boone et al. 1988; Tenorio et al. 2012; Salas and Moya 2014; Moya et al. 2017; Moya and Tenorio 2022). Cupping increases after drying due to differences in shrinkage between the two faces of the boards (Bond and Espinoza 2016), which are not present in the green condition. Twist results from longitudinal shrinkage of the board (Bond and Espinoza 2016), and the curvature of the growth ring greatly impacts this defect after drying (Straze et al. 2011). However, the boards used in this study were less than 1.3 m in length and had few growth rings (1-2 per thickness), resulting in less twist. In contrast, twist defects would be more pronounced in longer boards (Bond and Espinoza 2016; Straze et al. 2011). The greatest increase in cup and twist defects in balsa wood (Table 5, Figure 4) was likely due to the influence of juvenile wood, growth stresses in young trees, and internal stress tensions during drying—factors that strongly contribute to the development of drying defects (Tomad et al. 2023; Srisuchart et al. 2023).

Splitting and cracking are also caused by growth stresses in standing trees (Gril et al. 2017), and these stresses are more prominent in wood from fast-growing plantations (Kojima et al. 2009). The high incidence of growth stresses before drying (Table 5) clearly indicated that the balsa trees had a significant amount of internal stress. Splitting and cracking increased after drying, although the levels were lower than those of other defects in dried lumber. This slight increase can be explained by the relatively low variation in temperature observed across different drying methods. These defects tend to develop when there is significant variation in the surface temperature of the boards (Bond and Espinoza 2016). Kiln-dried wood exhibited the greatest temperature fluctuations, whereas SD and AD wood showed more consistent temperatures (Figure 2b), which minimized the development of splitting and cracking (Table 2).

Different drying methods produced distinct effects on the presence of warping, splitting, and checking in balsa wood (Table 5, Figure 3). Kiln-dried wood exhibited the highest incidence and magnitude of defects. Air-dried wood, on the other hand, had the least defects, and SD wood exhibited intermediate values between that of KD and AD. According to Youngs (Youngs 1997), tensions generated during drying are more pronounced in KD because it is a short-term method with drastic changes in temperature and relative humidity inside the chamber. This behavior has also been observed in other tropical woods from natural forests (De Souza-Mendes et al. 1995) or fast-growing plantations, where twisting, cupping, and splitting were the drying defects most easily induced by KD (Moya et al. 2013).

An important distinction was that KD lumber showed different values for crook and bow compared to SD and AD, but these differences may also reflect either tree age or the different growing site (Table 1). This resulted in differences in QI values, incidence percentages, and the magnitude of drying defects.

Meanwhile, SD presented intermediate values for incidence, magnitude, and QI (Table 5, Figure 4). Intermediate temperatures and relative humidities in the solar chamber were maintained, with cyclic variations throughout the day (Figure 2b), as well as a constant air speed, which could have contributed to defect formation (Lamrani et al. 2023). However, the severity of defects in SD was lower than that in KD (Lamrani et al. 2023; Kumar et al. 2023). SD reached higher temperatures and wind speeds than AD, leading to more defects that were more severe (Elustondo et al. 2023). The slower drying process in AD allowed for the gradual release of wood stresses (Yin and Liu 2021).

Conclusion

As expected, KD had the shortest drying time, followed by SD and finally AD. The evaluation of the color and drying defects of balsa wood revealed that KD resulted in the greatest color changes and produced the highest incidence percentages, magnitude values, and changes in QI for various drying defects. Warping defects (crook, bow, cup, and twist), as well as splitting and cracking, were present after the sawing process and became more pronounced after drying. Crook and bow showed the greatest increase in intensity after drying, regardless of the drying method, followed by twisting, while the cupping, splitting, and cracking exhibited the least intensity increase.

Air drying presented the best drying quality, with the fewer defects, but it had the disadvantage of the longest drying time. Solar drying produced similar values for defects (incidence, magnitude, and QI) to AD, but with shorter drying times. Kiln-drying, on the other hand, resulted in the greatest changes in wood quality and a higher incidence of defects. Kiln-drying can be used to dry lumber in the shortest possible time, but this comes with higher costs and a greater number of defects. For the best wood quality, AD and SD are more favorable, offering superior results, albeit with longer drying times.

References

ASTM-American Society for Testing and Materials (2020) Standard test methods for direct moisture content measurement of wood and wood-base materials. ASTM D4442-20. ASTM: West Conshohocken, PA, USA. https://doi.org/10.1520/D4442-20

ASTM-American Society for Testing and Materials (2023) Standard practice for calculation of color tolerances and color differences from instrumentally measured color coordinates; ASTM D2244-23. ASTM: West Conshohocken, PA. USA. https://doi.org/10.1520/D4442-20

Baker DC (2000) Wood density patterns of young Costa Rican trees in planted and natural forests. Thesis of Master and Science. Oregon State University. Oregon, USA. 161 p.

Bessa F, Sousa V, Quilhó T, Pereira H (2023) Diversity of wood colour in tropical timber species and its relationship with wood density and anatomical features. IAWA J 45(3):335–357. doi: 10.1163/22941932-bja10148

Bredemeier M, Busch G, Hartmann L, Jansen M, Richter F, Lamersdorf NP (2015) Fast growing plantations for wood production–integration of ecological effects and economic perspectives. Front Bioeng Biotechnol 3:72. doi: 10.3389/fbioe.2015.00072

Bond BH, Espinoza O (2016) A Decade of improved lumber drying technology. Curr Forestry Rep 2:106–118. doi: 10.1007/s40725-016-0034-z

Boone RS, Kozlik CJ, Bois PJ, Wengert EM (1988) Dry kiln schedules for commercial woods: temperate and tropical. FPL-GTR-57. U.S. Department of Agriculture, Forest Service, Forest Products Laboratory, Madison, WI. 158 p.

Borrega M, Ahvenainen P, Serimaa R, Gibson L (2015) Composition and structure of balsa (*Ochroma pyramidale*) wood. Wood Sci Technol 49:403–420. doi: 10.1007/s00226-015-0700-5

Bucur V (2016) Ageing of Wood. In: Bucur V (eds) Handbook of Materials for String Musical Instruments. Springer, Cham, Springer International Publishing Switzerland. doi: 10.1007/978-3-319-32080-9_7

Business Research Insights (2024) Balsa wood market size, share, growth, and industry analysis by type (grain A, grain B, and grain C) By Application (Aerospace & defense, marine, road & rail, and industrial construction), Regional Forecast To 2031. Accessed 28 May 2024. https://www.businessresearchinsights.com/market-reports/balsa-wood-market-100512

Condoy VGS, Chuchuca IPB, Romero KHP (2023) Análisis de las exportaciones de madera de balsas y su influencia en ámbitos económico-ambiental. Polo del Conocimiento: Rev Cient-Prof 8(11):1275–1302.

CIRAD (2024) Balsa. In: Tropix 5.0. CIRAD: Paris. Accessed 15 January 2025. http://www.cirad.fr/en/index.php

De Souza-Mendes A, Simpson WT, Verrill SP (1995) Laboratory test for grouping tropical species for kiln drying. Wood Sci Technol 29:353–362. doi: 10.1007/BF00202583

Elustondo D, Matan N, Langrish T, Pang S (2023) Advances in wood drying research and development. Drying Tech 41(6):890–914. doi: 10.1080/07373937.2023.2205530

Eddowes PJ (2005) Balsawood. In: Solomon Islands Timber. Solomon Islands Forestry Management Project: Honiara, Solomon Islands. Accessed 2 January 2025. http://www.solomon-timbers.com.sb/altHome/brochures/Balsawood.pdf

Entwistle K, Chauhan S, Sharma M, Walker J (2012) The effect of saw kerf width on the value of the axial growth stress measured by slitting a log along its axis. Wood Mater Sci Eng 11:1–12. doi: 10.1080/17480272.2014.929176

Francis JK (2000) *Ochroma pyramidale* Cav. balsa. In: Francis JK, Lowe CA (eds) Silvics of Native and Exotic Trees of Puerto Rico and the Caribbean Islands. General Technical Report IITF-GTR-15 U.S. Department of Agriculture, Forest Service, International Institute of Tropical Forestry, Río Piedras, pp 371–376. https://www.fs.usda.gov/research/treesearch/2862#

Galos J, Das R, Sutcliae MP, Mouritz AP (2022) Review of balsa core sandwich composite structures. Mater Des 221:111013. doi: 10.1016/j.matdes.2022.111013

Guevara L (1996) Comportamiento al secado natural de cuatro especies maderables de bosques secundarios. Folia Amazónica 8(1):79–90

Gril J, Jullien D, Bardet S, Yamamoto H (2017) Tree growth stress and related problems. J Wood Sci 63:411–432. doi: 10.1007/s10086-017-1639-y

Hu J, Liu Y, Wu Z (2020) Structural color for wood coloring: A Review. BioRes 15(4):9917. doi: 10.15376/biores.15.4

Jarvis MC (2024) Forces on and in the cell walls of living plants. Plant Physiol 194(1):8–14. doi: 10.1093/plphys/kiad387

Jenkin B, Minimulu J, Kanowski P (2019) Improving the smallholder balsa value chain in East New Britain Province, Papua New Guinea. Aust For 82(sup1):23–31. doi: 10.1080/00049158.2018.1537541

Kamarulzaman A, Hasanuzzaman M, Rahim NA (2021) Global advancement of solar drying technologies and its future prospects: A review. Sol Energy 221:559–582. doi: 10.1016/j.solener.2021.04.056

Keey RB (2005) Colour development on drying. Maderas Cienc Tecnol 7(1):03–16. doi: 10.4067/S0718-221X2005000100001

Kojima M, Yamamoto H, Okumura K, et al (2009) Effect of the lateral growth rate on wood properties in fast-growing hardwood species. J Wood Sci 55:417–424. doi: 10.1007/s10086-009-1057-x

Kumar B, Raj AK, Szepesi G, Szamosi Z (2023) A conspectus review on solar drying of wood: regional and technical contrivances. J Therm Anal Calorim 148(17):9237–9261. doi: 10.1007/s10973-023-12093-5

Lamrani B, Bekkioui N, Simo-Tagne M, Ndukwu MC (2023) Recent progress in solar wood drying: An updated review. Drying Technol 41(5):605–627. doi: 10.1080/07373937.2022.2112048

Lingayat A, Balijepalli R, Chandramohan VP (2021) Applications of solar energy based drying technologies in various industries–A review. Sol Energy 229:52–68. doi: 10.1016/j.solener.2021.05.058

Listyanto T, Poedyastanto EPF, Abqoriah SM, Lukmandaru G (2021) Specific gravity, extractive content, and natural durability of balsa (*Ochroma pyramidale*) wood at 3 and 4 years old. IOP Conf Ser: Earth Environ Sci 891:012013. doi: 10.1088/1755-1315/891/1/012013

Midgley S, Blyth M, Howcroft N, Midgley D, Brown A (2010) Balsa: biology, production and economics in Papua New Guinea. ACIAR Technical Reports No. 73. Australian Centre for International Agricultural Research, Canberra, 98 pp. https://www.aciar.gov.au/sites/default/files/legacy/node/12685/balsa_biology_production_and_economics_in_papua__40057.pdf

Moya R, Muñoz F (2008) Wet pockets in kiln-dried *Gmelina arborea* lumber. J Trop For Sci 22(3):317–328

Moya R, Ureña E, Salas C, Muñoz F, Espinosa O (2013) Kiln drying behavior of lumber from ten fast-growth plantation species in Costa Rica. Wood Mater Sci Eng 8:37–45. doi: 10.1080/17480272.2012.707686

Moya R, Berrocal A, Rodriguez-Solis M, Muñoz F (2017) Effect of steam-drying treatment on moisture content, drying rate, color, and drying defects in juvenile wood of *Tectona grandis* from fast-growth plantations. Drying Technol 35(15):1832–1842. doi: 10.1080/07373937.2017.1280503

Moya R, Tenorio C (2022) Application of the steaming step during kiln drying of lumber of two tropical species with high growth stress presence. Drying Technol 40(15):3231–3240. doi: 10.1080/07373937.2021.2017299

Moya R, Tenorio C, Villalobos-Barquero V, Meza-Montoya (2025) Variation of physical wood properties and effect of dasometric variables in *Ochroma pyramidale* trees growing in plantation. Heliyon 11(1):e41210. doi: 10.1016/j.heliyon.2024.e41210

Pérez P, Ananías RA, Hernández G (2007) Estudio experimental del secado de renovales de canelo *Drimys winteri*. Maderas Cienc Tecnol 9:59–70.

Pertiwi YAB, Ishiguri F, Nezu I, Aiso H, Hiraoka Y, Marsoem SN, Ohshima J (2022) Evaluation of xylem maturation process and effects of radial growth rate on cell morphologies in wood of balsa (*Ochroma pyramidale*) trees. Wood Fiber Sci 54(2):149–159. doi: 10.22382/wfs-2022-15

Pertiwi YAB, Ishiguri F, Aiso H, Ohshima J, Yokota S (2017) Wood properties of 7-year-old balsa (*Ochroma pyramidale*) planted in East Java. Inter Wood Prod J 8(4):227–232. doi: 10.1080/20426445.2017.1394560

Quiñonez-Piñón MR, Valeo C (2018) Assessing the translucence and color-change methods for estimating sapwood depth in three boreal species. Forests 9(11):686. doi: 10.3390/f9110686

Rueda R, Williamson GB (1992) Radial and vertical wood specific gravity in *Ochroma pyramidale* (Cav. ex Lam.) Urb. (Bombacaceae). Biotropica 24(2):512–518. doi: 10.2307/2389013

Salas C, Moya R (2014) Kiln-, solar-, and air-drying behavior of lumber of *Tectona grandis* and *Gmelina arborea* from fast-grown plantations: Moisture content, wood color, and drying defects. Drying Technol 32(3):301–310. doi: 10.1080/07373937.2013.829087

Simpson, W (1991) Properties of wood related to drying. In Dry Kiln Operator's Manual Handbook AH-188, Simpson, WT, ed.; USDA Forest Service, Forest Products Laboratory: Madison, WI: 1–42.

Srisuchart K, Tomad J, Leelatanon S, Jantawee S, Matan N (2023) Internal stress development within wood during drying: A master curve concept and its application on drying stress evaluation. Drying Technol 41(15):2516–2532. doi: 10.1080/07373937.2023.2259467

Straze A, Kliger R, Johansson M, Goriek Z (2011) The influence of material properties on the amount of twist of spruce wood during kiln drying. Eur J Wood Wood Prod 69:239–246. doi: 10.1007/s00107-010-0422-1

Teischinger A, Avramidis S, Hansmann C, Mayrhofer A (2023) Sawn Timber Steaming and Drying. In: Niemz P, Teischinger A, Sandberg D (eds) Springer Handbook of Wood Science and Technology. Springer Handbooks, Springer, Cham. doi: 10.1007/978-3-030-81315-4_23

Tenorio C, Moya R, Salas C (2016) Kiln drying behavior utilizing drying rate of lumber from six fast-growth plantation species in Costa Rica. Drying Technol 34(4):443–453. doi: 10.1080/07373937.2015.1060493

Tenorio C, Moya R, Quesada-Pineda H (2012) Kiln drying of *Acacia mangium* wood: colour, shrinkage, warp, split and check in lumber before and after drying. J Trop For Sci 24:125–139.

Thibaut B, Gril J (2021) Tree growth forces and wood properties. Peer Community J 1:e446. doi: 10.24072/pcjournal.48

Thybring EE, Fredriksson M, Zelinka SL, Glass SV (2022) Water in wood: A review of current understanding and knowledge gaps. Forests 13(12):2051. doi: 10.3390/f13122051

Tomad J, Leelatanon S, Jantawee S, Srisuchart K, Matan N (2023) Internal stress development within wood during drying: regime and kinetics. Drying Technol 41(1):77–88. doi: 10.1080/07373937.2022.2084750

Utia KY (2012) Secado al natural en métodos de apilado en triangulo y caballete de la especie forestal Topa (*Ochroma pyramidale* (Cave. Ex Lam) Urban). Tesis Ing en Recursos Naturales Renovables Mención: Forestales, Universidad Nacional Agraria de la Selva, Tingo María, Perú.

Wiemann MC, Williamson GB (1988) Extreme radial changes in wood specific gravity in some tropical pioneers. Wood Fiber Sci 20(3):344–349.

Williamson GB, Wiemann MC (2010) Age-Dependent Radial Increases in Wood Specific Gravity of Tropical Pioneers in Costa Rica. Biotropica 42(5):590–597. doi: 10.1111/j.1744-7429.2009.00618.x

Whitmore JL (1973) Wood density variation in Costa Rican Balsa. Wood Sci 5:223–229.

Yang H, Huang X, Gu Y, et al (2024) Influence of tree age on the wood color and compounds involved in the "golden-thread" wood color formation in *Phoebe zhennan*. Ind Crops Prod 221:119406. doi: 10.1016/j.indcrop.2024.119406

Yin Q, Liu HH (2021) Drying stress and strain of wood: A Review. Appl Sci 11(11):5023. doi: 10.3390/app11115023

Youngs RL (1997) Present methods of drying and conditioning wood for use. Economy Botany 21:46–50. doi: 10.1007/BF02897174

Zelinka SL, Altgen M, Emmerich L, Guigo N, Keplinger T, Kymäläinen M, Thybring EE, Thygesen LG (2022) Review of wood modification and wood functionalization technologies. Forests 13(7):1004. doi: 10.3390/f13071004

Zobel BJ, Van Buitenen JP (1989) Wood variation and wood properties. In: Wood Variation. Springer Series in Wood Science. Springer, Berlin, Heidelberg. doi: 10.1007/978-3-642-74069-5_1

Support vector regression-based grid localization method for acoustic emission sources from Chinese fir boards

GuoFeng Wang
Beijing Forestry University
E-mail: wangguofengbjfu@163.com

*Dong Zhao**
Beijing Forestry University
E-mail: zhaodong68@bjfu.edu.cn

(Received 20 December 2024)

Abstract. Wood is an anisotropic composite material, whose variation can make it difficult to locate surface damage using non-destructive testing. In order to solve the problem of sound source localization on the surface of wood, this study used a first localization method combining grid-based feature mapping and machine learning. Chinese fir boards (*Cunninghamia lanceolata*) were divided into a grid and acoustic emission signals were generated through a pencil-lead break test. These signals were processed using wavelet packet decomposition (WPD) to create a database of energy feature vectors. Localization was then achieved by applying support vector regression (SVR), which compared the feature vectors from the experimental points with those in the database to determine the sound source location. The average absolute error of this localization method was 7.51 mm, the average relative error was 3.79%, and the positioning accuracy was 91.84%, which can effectively locate the sound source on the wood surface.

Keywords: Acoustic emission, Signal processing, Machine learning, Signal prediction, Grid localization

Introduction

The evaluation of wooden members is crucial for the proper functioning of the entire wooden structure (Lamy et al. 2015; Han et al. 2022). Although many methods for structural non-destructive testing (NDT) exist (Nocetti et al. 2023; López et al. 2023; Xu et al. 2023; Guo et al. 2017), few can achieve real-time dynamic assessment (Ji et al. 2023), i.e., structural damage monitoring and localization under normal working conditions. In particular, wood exhibits varying moduli of elasticity in different directions (Dinçkal 2011), which affects sound source localization. Low localization accuracy remains a key challenge for using acoustic emission as a non-destructive testing technology.

Sound source localization refers to the process of determining the origin of acoustic emissions by analyzing the characteristics of sound waves (Qin et al. 2024; Zhou et al. 2023; He and Zhu 2024; Li et al. 2018). In the context of wooden structures, this technique is particularly valuable for detecting damage, such as cracks or voids (Aicher et al. 2001; Pan et al. 2024; Boccacci et al. 2022). It plays a critical role in ensuring the structural integrity and safety of wooden components, especially in applications such as wooden buildings (Rescalvo et al. 2018), furniture (Ai et al. 2024), and cultural heritage preservation (Cruz et al. 2022; Xu et al. 2021). The ability to accurately locate sound sources in wood is essential for real-time structural health monitoring and damage assessment. Despite its potential, the anisotropic nature of wood poses significant challenges to achieving high localization accuracy, which limits the widespread adoption of this technology.

At present, there are two main research methods for sound source localization: signal arrival time-based research and signal processing-based research. In arrival time-based sound source localization, Kundu et al. (2007) used multiple sensors to obtain the arrival time differences of sound source signals and used additional information, such as the angle between the sensors and the sound source, to determine signal location. Yin et al. (2021) improved the relative positioning of the sensors to further enhance the accuracy of the arrival time-based localization method. They also constructed a composite material model through finite element simulation to verify the effectiveness of the proposed method. Park et al. (2012) used four sensors to collect signals, construct arrival time differences, and build a neural network database to predict signal position. However, propagation speed of the stress wave signals in anisotropic

* Corresponding author

materials varies depending on the direction, so it is difficult to accurately detect the arrival time of the signals in each direction, and ultimately making it difficult to determine the exact location of the sound source generation. Therefore, researchers proposed a sound source localization method based on stress wave signal processing. In the research of sound source localization based on stress wave signal processing: Shrestha et al. (2015) constructed a signal database by processing the signals collected by traversing each sound source point, and then determining the location of the sound source by comparing the correlation coefficients; Zhao et al. (2017) proposed a wood energy attenuation model to determine the location of damage to the wood structure; Su et al. (2012) constructed a support vector regression (SVR) model based on acoustic emission signal features for the spatial 3D structural localization of anisotropic materials; Ebrahimkhanlou and Salamone (2018) proposed a method that combined dispersion and modal characteristics of signals with a neural network. In this approach, only a single transducer was used to locate the sound source region. This method effectively overcame the effects of wave velocity attenuation and reduced the number of sensors required. However, the localized object was structurally simple, limiting the method's generalizability.

Since wood is an orthogonal anisotropic material (Bucur 2023), the performance differences were smaller when structural neighboring positions were closer. Therefore, this paper proposes a grid localization method for wood sound sources. This method leverages the fact that as the distance between the acoustic emission source positions decreases, the influence of wood texture diminishes, and the frequency-domain features of the signals received by the sensors become more similar. It employs wavelet packet decomposition (WPD) for energy feature extraction and combines it with SVR to achieve accurate sound source localization. The main process of the research is as follows (Figure 1): ① Divide a limited number of grids into sample points on the wood. Break the lead at these sample points and extract the energy of each frequency band from the signals collected by the acoustic emission sensors using wavelet packet noise reduction and transformation. ② Apply principal component analysis (PCA) for dimensionality reduction to enhance feature vector differentiation, then input the low-dimensional feature vectors into a SVR to build a model. ③ Break the lead at various positions on another board, collect acoustic emission signals, and perform WPD to extract the wavelet packet energy feature vector. ④ Use the SVR to complete the localization of the acoustic emission source. The main advantage of this method is that grid division reduces the influence of wood anisotropy within a local range, and when combined with wavelet packet feature extraction, it further minimizes the impact of wood anisotropy on positioning accuracy. At the same time, using only a single sensor avoids the problems of multi-sensor signal interference and wave velocity attenuation, thereby significantly improving the accuracy and practicality of positioning. This method provides a new

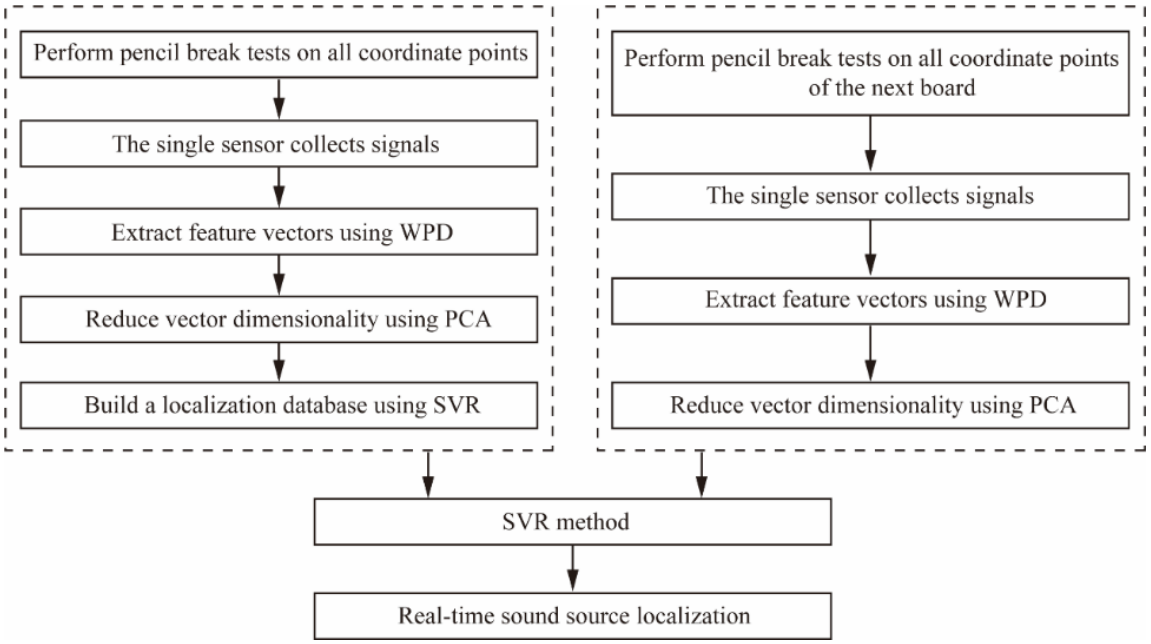

Figure 1. Sound source localization flowchart.

solution for non-destructive testing of wood, with potential applications in real-time structural health monitoring, quality control in wood processing, and cultural heritage preservation.

Material and methods

Test system

The acoustic emission signal acquisition system consisted of a DS2 acoustic emission analyzer, an RS-2A acoustic emission sensor, and a front amplifier with adjustable gain (40 dB, 5 V output). According to the Shannon-Nyquist sampling theorem, the sampling frequency was set to 500 kHz (Li et al. 2020). When the acoustic emission signal propagates in the wood, the value of its energy decreases with increased distance from the source; the distance between the sound source and the acoustic emission sensor was 0–200 mm (Zhao et al. 2017). Therefore, the maximum distance between the transducer and the excitation point should not be more than 200 mm from the surface of the wood. High temperature vacuum grease was used to connect the transducer to the wood sample.

Two rectangular defect-free boards of Chinese fir (*Cunninghamia lanceolata*) from adjacent areas of the same parent board (named "fir board 1" and "fir board 2"). The boards had similar ratios of sapwood and heartwood, and were used to construct the training samples and test samples, respectively. The experiment used a rectangular board with fixed support on all four sides, which measured 185 mm × 140 mm × 20 mm (length × width × thickness) with a density of 0.306 g/cm^3. A 140 mm × 140 mm square was used for the lead-breaking experiments (Figure 2). Taking 7 × 7 grids as an example, the coordinate system was established (Figure 2b), and the planks were aligned with the y-axis and x-axis directions in the down-grain direction and cross-grain direction, respectively.

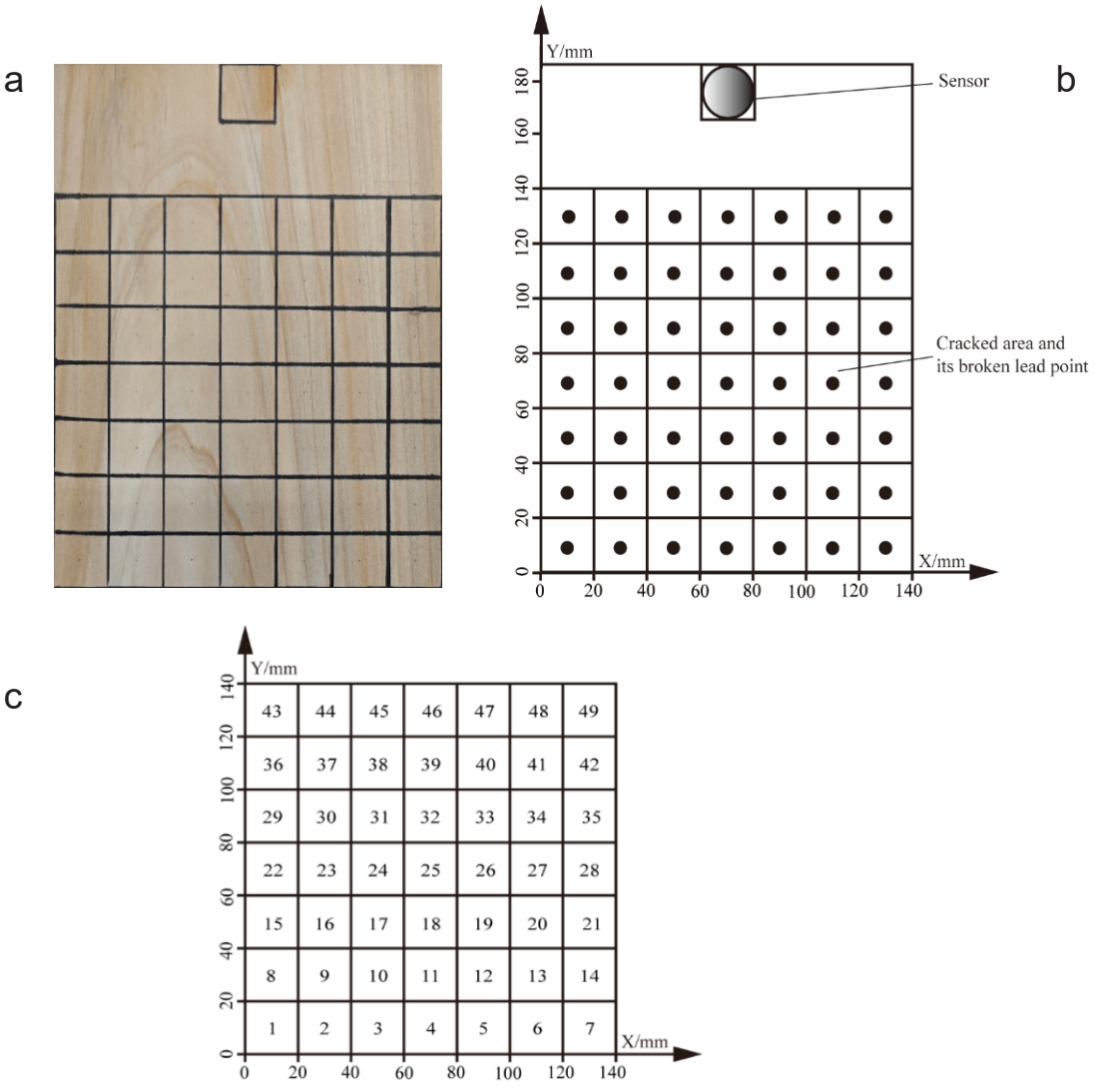

Figure 2. (a) Grid division, (b) sensor layout, and (c) lead breakage point location of fir boards.

In accordance with the ASTM standard (American Society for Testing and Materials), the geometric center of each grid area was broken with a Hsu-Nisisen quill (2H/0.5 mm), and a signal excitation was applied to generate an acoustic source, i.e., the signal generated by the simulated crack. The coordinates of the geometric center point of a single transducer were 70 mm by 175 mm. The minimum distance between the transducer and the signal excitation point was 35 mm, and the maximum distance was 175.57 mm.

Wavelet packet energy feature vector extraction

The wavelet packet method decomposes both high-frequency and low-frequency components of the signal layer by layer until reaching the predetermined decomposition level. A 3-level WPD of the original signal S yielded the signal components S_{3-0}, and S_{3-1} … S_{3-7} (Figure 3).

The Daubechies (db) wavelet has the advantages of orthogonality, tight support, approximate symmetry, and the ability to perform discrete wavelet transform, which can be fully reconstructed. Through layer-wise decomposition, acoustic emission signals yield increasingly detailed wavelet packet energy feature vectors; however, beyond a certain number of layers, the increase in sensitivity to the acoustic emission signal of wood is not obvious. For comprehensive consideration, this paper adopted the db5 wavelet to calculate the energy feature vectors of each frequency band of the wavelet packet in the 9th layer, which was used as the input index of the SVR:

$$[\lambda_1, \lambda_2, \lambda_3, \lambda_4, \lambda_5, \lambda_6, \cdots] \quad (1)$$

For every λ there is:

$$\lambda_j = \frac{E_{9,j}}{\sum_{i=1}^{n} E_{9,j}} \quad (2)$$

Where: $E_{9,j}$ stands for the energy of the 9th component of the 9th layer wavelet packet j. In addition, the energy ratio of the wavelet packet is characterized as:

$$\int_0^{+\infty} \frac{da}{a^2} \int_{-\infty}^{+\infty} |WT_x(a,b)|^2 \, db = C_\Psi \int_{-\infty}^{+\infty} |x(t)|^2 dt \quad (3)$$

$$C_\Psi = \int_{-\infty}^{+\infty} \frac{|\Psi(\omega)|^2}{\omega} d\omega \quad (4)$$

Where: $WT_\chi(a,b)$ is the wavelet packet coefficients; C_ψ is the coefficient that converts the wavelet packet energy to the time domain energy; $\Psi(\omega)$ is the wavelet tolerance condition; ω is the frequency.

The energy of each wavelet packet component is the sum of the squares of the coefficients of that wavelet packet, i.e.:

$$E = \sum (d_i)^2 \quad (5)$$

Where: d_i is the coefficient of the wavelet packet in which it is located.

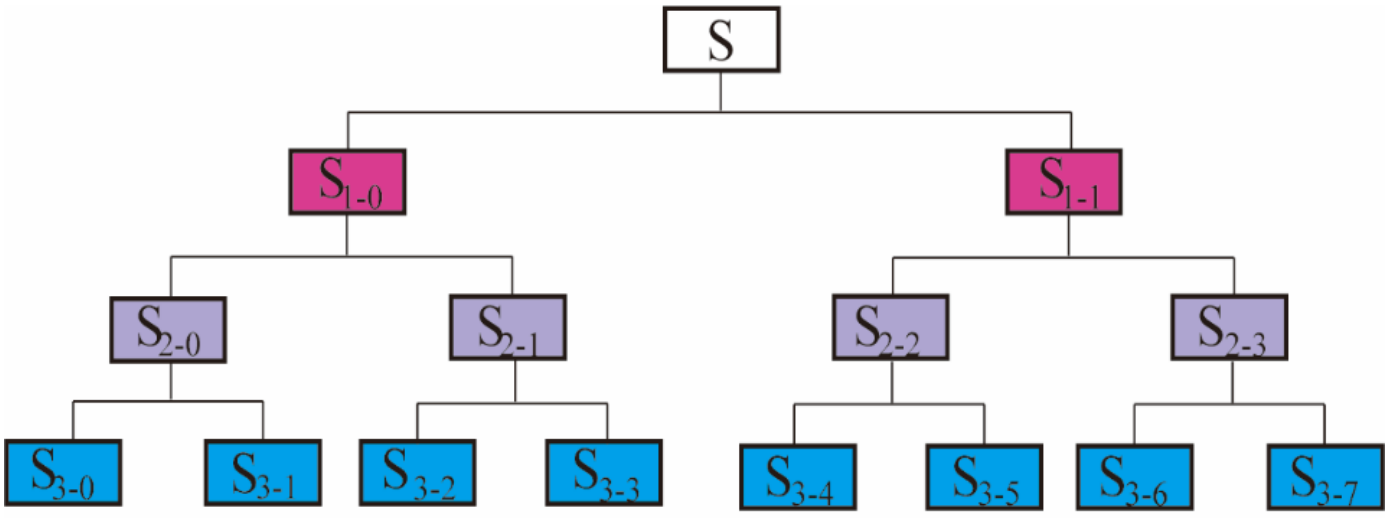

Figure 3. 3-level Wavelet packet decomposition.

So, the wavelet packet energy $E_{9,j}$ can also be expressed as:

$$E_{9,j} = \sum (d_{9,j,i})^2 \quad (6)$$

Where: $d_{9,j,i}$ represents the $S_{9,j}$ coefficient.

Support vector regression principle

Acoustic emission signals were decomposed into energy feature vectors by wavelet packet methods, and the feature dimensions were usually between tens and hundreds, which needed to be reduced to be used as inputs to the localization model. Considering the number of samples and feature dimensions, this paper chose the SVR algorithm to construct the acoustic emission localization model.

The SVR algorithm was a supervised learning algorithm used to predict discrete values. The samples were assumed to be *(x,y)*; *f(x)* was the output; *y* was the desired outcome; ω and *b* were the parameters to be determined; ε was the maximum permissible deviation; the solid and hollow circles denoted the samples with no loss computed and the samples with loss computed (Figure 4). The objective function of SVR is:

$$\min_{\varepsilon,b} \frac{1}{2}||\omega||^2 + C\sum_{i=1}^{m} l_\varepsilon(f(x_i) - y_i) \quad (7)$$

C is the regularization parameter and l_ε is the ε-insensitive loss function:

$$l_\varepsilon(y - f(x)) = \begin{cases} 0, |y - f(x)| \le \varepsilon \\ |y - f(x)| - \varepsilon, \text{else} \end{cases} \quad (8)$$

Introducing the slack variables ξ_i and $\hat{\xi}_i$ yields:

$$\min_{\omega,b,\xi,\hat{\xi}} \frac{1}{2}||\omega||^2 + C\sum_{i=1}^{m}(\xi_i + \hat{\xi}_i) \quad (9)$$

$$\text{s.t. } f(x_i) - y_i \le \varepsilon + \xi_i$$

$$y_i - f(x_i) \le \varepsilon + \hat{\xi}_i$$

The SVR function is obtained according to the KKT condition:

$$f(x) = \sum_{i=1}^{m}(\hat{\alpha}_i - \alpha_i)\kappa(x, x_i) + b \quad (10)$$

Where: $\kappa(x_i, x_j) = \varphi(x_i)^T(x_j)$ is the kernel function.

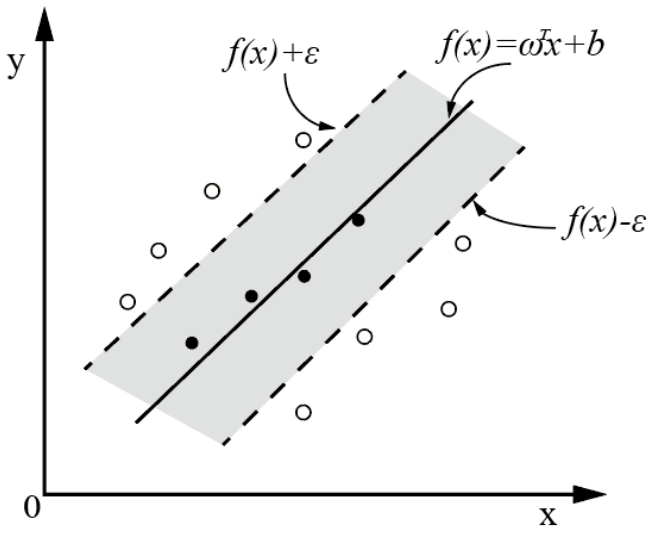

Figure 4. Schematic diagram of support vector regression.

Grid localization method

The principle of SVR method for Chinese fir board sound-source grid localization was as follows: firstly, a suitable SVR model was selected according to the prediction object, and the regression model was trained by training samples. According to the training samples in the delineated grid, a regression function was expressed as

$$f(x) = \sum_{i=1}^{m}(\hat{\alpha}_i - \alpha_i)\kappa(x, x_i) + b$$

The SVR training model based on radial basis kernel function was obtained, at this time, the predicted value of the sample points was determined by the regression function and loss function.

Constructing an energy feature vector localization model

Wavelet packet denoising was implemented using a MATLAB-based signal processing program. The original signal underwent 4-level decomposition using the db5 wavelet, followed by removal of the noise-dominated low-frequency band. The remaining frequency components, free from fundamental frequency interference, were then reconstructed, resulting in a denoised signal with enhanced robustness for source localization. The original acoustic emission signal in grid region 1 was given (Figure 5a), as well as the signal after noise reduction by removing disturbances such as environmental and electromagnetic noise (Figure 5b).

Each signal after the noise reduction process was subjected to a 9-layer WPD of db5 wavelets to obtain a 512-dimensional

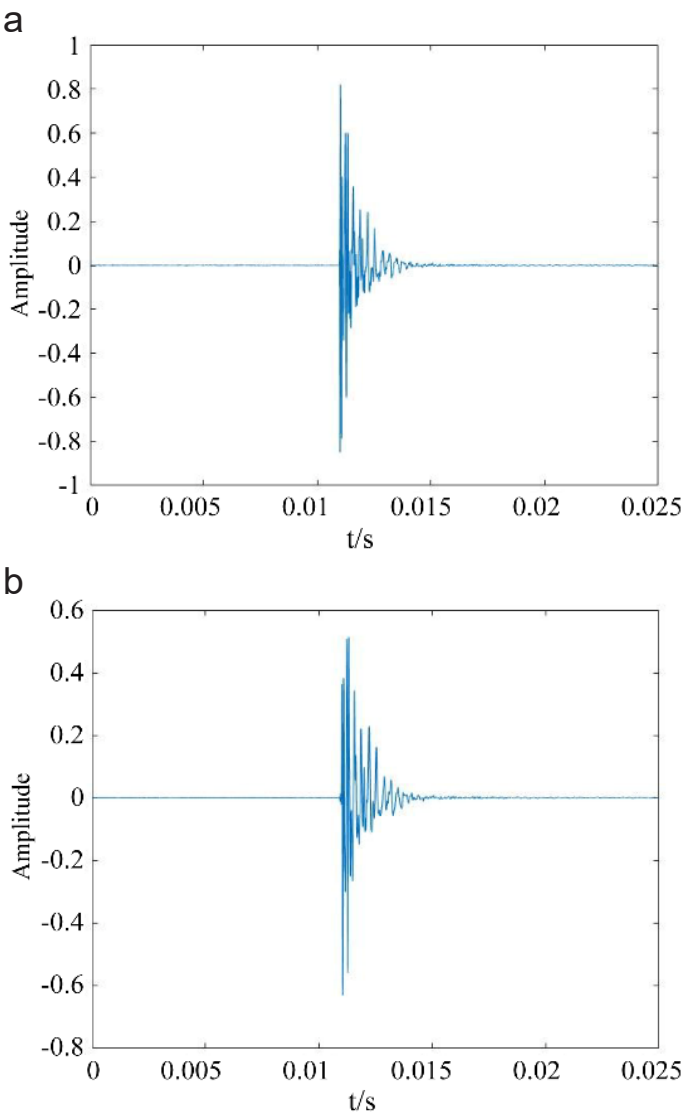

Figure 5. The original signal and denoised signal in grid area 1: (a) Original signal (b) Noise reduction signal.

energy feature vector $[\lambda_1, \lambda_2, \lambda_3, \cdots, \lambda_{512}]$. However, the larger the dimension of the energy feature vector, the more complicated the data calculation when machine learning is performed. This paper utilized the PCA method for dimensionality reduction to obtain the feature vector $[\lambda_1', \lambda_2', \lambda_3', \cdots, \lambda_{244}']$. In this paper, the first 8-dimensional feature vectors with a cumulative contribution rate of more than 99% were selected as the input data for the SVR.

Experimental localization

In order to verify the effectiveness of the SVR method for sound source grid localization on wood boards, localization tests were conducted on thin Chinese fir boards. Forty-nine sample points were used for lead break training on each board, as follows: each sample point on fir board 1 was applied 4 times, for a total of 196 lead breaks to construct the training sample; and each sample point on fir board 2 was applied 1 time, for a total of 49 lead breaks to construct the test sample. This resulted in 245 lead break signals, which constituted the sample matrix $[t_1, t_2, t_3, \cdots, t_{245}]$, where the samples $t_i = [\lambda_1', \lambda_2', \lambda_3', \cdots, \lambda_{244}']_i$. The normalized feature vectors are used to train the SVR model. In the process of SVR modeling, the best penalty coefficient c and kernel function g can be determined by using the cross-validation method, and the final result obtained by the SVR prediction was the localization result. Assuming that the sound source location was l_i, $i = 1, 2 \ldots n$, when using the SVR for sound source localization, the sound source location was expressed as:

$$l = arg \min_{l_i} \frac{2}{\| w \|} \tag{11}$$

Results and discussion

Because of differences in wavelet packet energy amplitude of each sub-band of the acoustic emission signals at different locations, the similarity between the signals at each location differed, and similarity was calculated by the formula (Guo et al. 2017) as:

$$R = \frac{\sum_{i=1}^{n}(x_i - \overline{x})\,(y_i - \overline{y})}{\sqrt{\sum_{i=1}^{n}(x_i - \overline{x})^2 \sum_{i=1}^{n}(y_i - \overline{y})^2}} \tag{12}$$

Where: n is the dimension of the feature vector; $\bar{x}$, and $\bar{y}$ is the mean value of vector x, y. The feature vector of the acoustic emission signal at the coordinates 70 mm, 130 mm in the training set database, i.e., the signal vector of this sample point, was compared with the vector of the acoustic emission signal at each position in the database in terms of similarity. The results (Figure 6) showed that the signal had a high degree of similarity to the feature vector of the nearby signal with a maximum of 1 with this point, and a low degree of similarity to the feature vectors of signals farther away. The signal vector at the coordinates 70 mm, 130 mm was compared with the test signal vectors at each location for similarity (Figure 7) and also showed that the signal had a high degree of similarity with the nearby test signal. The test signal was a maximum of 0.99 at that point, with a low degree of similarity with the more distant test signal. These results suggest that the closer the relative distance between the sound sources, the smaller the difference produced by their signal energy distribution. These results support the premise that the closer the distance

between the locations of the acoustic emission sources, the more similar the frequency domain characteristics of the signal received by the sensor. These results suggest that machine learning methods can be used to train the sound source location using the differences in vectors of wood panels in different grid regions to recognize and evaluate the acoustic emission source location of wood.

The dimension-reduced feature vectors of training samples were used to train an SVR-based sound source localization model that predicted both the coordinates and grid regions of test samples (Figures 8a and 8b). The prediction errors were quantified using the following metrics:

$$S = \sqrt{(x - x_0)^2 + (y - y_0)^2} \tag{13}$$

$$P = \frac{\sqrt{(x - x_0)^2 + (y - y_0)^2}}{140\sqrt{2}} \times 100\% \tag{14}$$

where: s denotes absolute error; p denotes relative error; x, y denotes the position coordinates of the center point of the predicted grid region in x- and y-directions, respectively; x_0, y_0 denotes the position coordinates of the x- and y-directions of the center point of the predetermined grid region, respectively.

Taking the sound source grid size of 20 mm × 20 mm as an example, the sound source localization resolution was 20 mm, and the pencil-lead break test was performed sequentially at 49 positions on the fir board. The average absolute error of the predicted values for all grid areas was 7.51 mm, with an average relative error of 3.79%. Table 1 presents a comparison between the actual and predicted coordinates of the sound source. It is evident that if the x or y values of the predicted sound source location differ from the actual values by more than 10 mm, or if the relative error exceeds 6.5%, it can be determined that the predicted sound source is not in the correct grid area. The incorrectly predicted grids were 2, 4, 14, and 17. Grids 2, 4, and 14 were incorrectly predicted to adjacent grids along the x-direction due to substantial deviation in the x-coordinate, while grid 17 was incorrectly predicted to an adjacent grid along the y-direction due to a large deviation in the y-coordinate (Figure 8 and Table 1). Comparing the incorrect predictions with the locations of the acoustic emission sensors in Figure 1 indicated that the incorrect sound source grids were all located far from the sensors. This indicated that the distance between the sound source and the sensors affected the localization accuracy. Using the SVR-based sound source

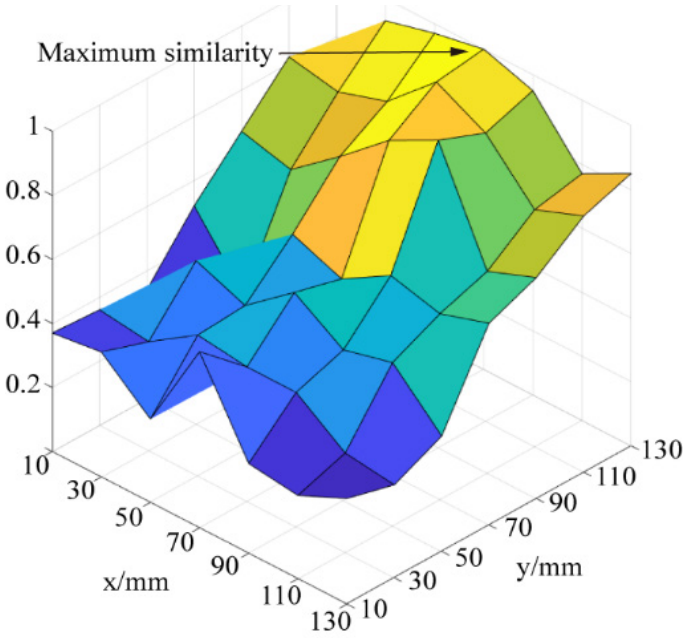

Figure 6. Similarity of feature vectors between the sample point signals and each point signal at coordinates (70mm, 130mm).

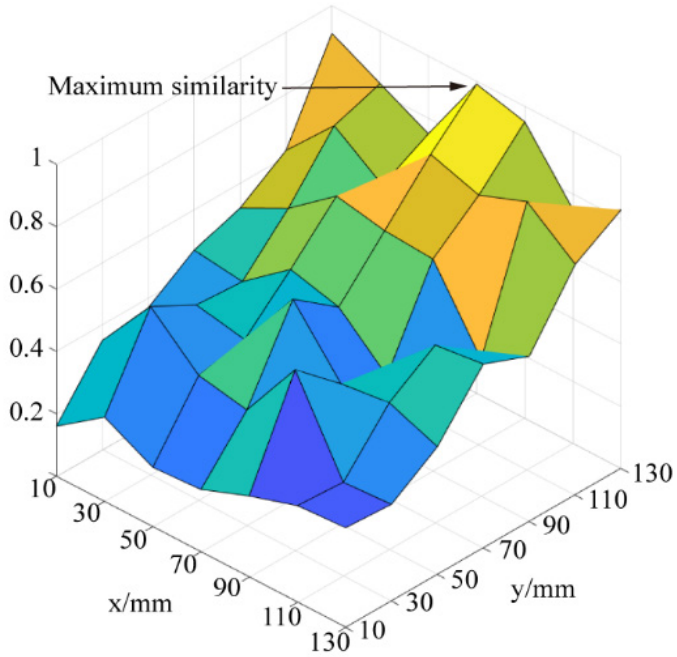

Figure 7. Similarity of feature vectors between the sample point signal and each test point signal at coordinates (70mm, 130mm).

Table 1. Comparison between actual sound source location and predicted values.

Actual Grid	Actual value x_0 /mm	Actual value y_0/ mm	Projected value x/mm	Predicted value y/mm	Absolute error/mm	Relative error/%	Prediction grids
1	10	10	16.3	5.7	7.63	3.85	1
2	30	10	18.5	16.6	13.26	6.70	1
3	50	10	47.2	12.9	4.03	2.04	3
4	70	10	83.8	8.2	13.92	7.03	5
5	90	10	85.0	16.0	7.81	3.94	5
6	110	10	114.2	14.3	6.01	3.04	6
7	130	10	137.3	16.1	9.51	4.80	7
8	10	30	7.0	22.8	7.80	3.94	8
9	30	30	22.8	38.7	11.29	5.70	9
10	50	30	54.7	28.2	5.03	2.54	10
11	70	30	77.8	23.7	10.03	5.06	11
12	90	30	93.3	23.0	7.74	3.91	12
13	110	30	114.1	35.1	6.54	3.31	13
14	130	30	117.6	24.6	13.52	6.83	13
15	10	50	17.8	52.6	8.22	4.15	15
16	30	50	23.4	44.5	8.59	4.34	16
17	50	50	57.9	62.8	15.04	7.60	24
18	70	50	64.1	51.6	6.11	3.09	18
19	90	50	95.8	52.9	6.48	3.28	19
20	110	50	101.7	55.2	9.79	4.95	20
21	130	50	133.5	53.1	4.68	2.36	21
22	10	70	6.2	66.6	5.10	2.58	22
23	30	70	27.3	71.7	3.19	1.61	23
24	50	70	55.6	76.1	8.28	4.18	24
25	70	70	62.1	71.7	8.08	4.08	25
26	90	70	92.6	64.4	6.17	3.12	26
27	110	70	112.6	68.1	3.22	1.63	27
28	130	70	137.7	61.5	11.47	5.79	28
29	10	90	2.0	81.8	11.46	5.79	29
30	30	90	26.7	82.5	8.19	4.14	30
31	50	90	41.9	91.4	8.22	4.15	31
32	70	90	66.8	96.2	6.98	3.52	32
33	90	90	92.9	87.7	3.70	1.87	33
34	110	90	118.4	85.1	9.72	4.91	34
35	130	90	132.9	93.0	4.17	2.11	35
36	10	110	14.4	117.8	8.96	4.52	36
37	30	110	33.5	112.5	4.30	2.17	37
38	50	110	46.8	106.3	4.89	2.47	38
39	70	110	76.5	103.4	9.26	4.68	39
40	90	110	84.0	113.1	6.75	3.41	40
41	110	110	105.7	112.3	4.88	2.46	41
42	130	110	124.6	114.4	6.97	3.52	42
43	10	130	12.9	124.3	6.40	3.23	43
44	30	130	32.5	128.2	3.08	1.56	44
45	50	130	44.9	135.6	7.57	3.83	45
46	70	130	63.6	127.9	6.74	3.40	46
47	90	130	92.9	128.1	3.47	1.75	47
48	110	130	113.3	136.7	7.47	3.77	48
49	130	130	124.0	128.4	6.21	3.14	49

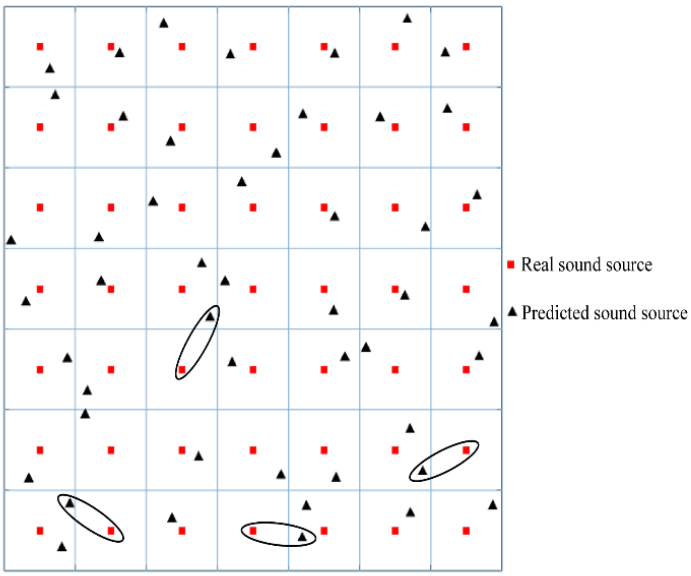

43	44	45	46	47	48	49
36	37	38	39	40	41	42
29	30	31	32	33	34	35
22	23	24	25	26	27	28
15	16	24	18	19	20	21
8	9	10	11	12	13	13
1	1	3	5	5	6	7

Figure 8. Prediction results of sound source location (a) Prediction of sound source location coordinates (b) Prediction of sound source location grid area.

localization method proposed in this study, the localization accuracy was 91.84%, demonstrating that this method achieved high accuracy. Additionally, based on previous research by Kim and Lee (2014), it can be speculated that further increasing the grid resolution, i.e., making the grid divisions finer, will lead to higher localization accuracy.

Conclusion

The acoustic emission acquisition system used to carry out the fir board pencil-lead break test showed that the closer the location of the acoustic emission source, the higher the similarity of the amplitude-frequency characteristics of the signals collected, and the farther the location of the source, the lower the similarity of the amplitude-frequency characteristics of the signals collected. After the signal noise reduction process, the energy feature vector was obtained by 9-layer WPD based on the db5 wavelet, and the first 8-dimensional feature vector was obtained by PCA to do the normalization process. The model of the SVR was constructed, and then the localization calculation was completed according to the SVR model. The average absolute error of the method was 7.51 mm, the average relative error was 3.79%, and the localization accuracy rate was 91.84%, which was obtained through the experiments of lead breakage localization of 140 mm × 140 mm fir boards. The research results show that the grid localization method of acoustic emission source based on SVR is feasible.

Acknowledgements

This work was supported by the “Beijing Natural Science Foundation Project (2182045)”.

References

Aicher S, Hofflin L, Dill-Langer G (2001). Damage evolution and acoustic emission of wood at tension perpendicular to fiber. Holz Roh Werkst 59(1-2):104–116. https://doi.org/10.1007/s001070050482

Ai M, Zhou X, Gao G, Gao S, Du X (2024). Falling damage behavior analysis and degree prediction for wooden pallet based on piezoelectric effect and acoustic emission. Eur J Wood Wood Prod 82(4):1227–1239. https://doi.org/10.1007/s00107-024-02064-4

Boccacci G, Frasca F, Bertolin C, Siani AM (2022). Influencing factors in acoustic emission detection: A literature review focusing on grain angle and high/low tree ring density of Scots pine. Appl Sci 12(2):859. https://doi.org/10.3390/app12020859

Bucur V (2023). A review on acoustics of wood as a tool for quality assessment. Forests 14(8):1545–1567. https://doi.org/10.1007/978-3-662-70209-3_13

Cruz C, Gaju M, Gallego A, Rescalvo F, Suarez E (2022). Non-destructive multi-feature analysis of a historic wooden floor. Buildings 12(12):2193. https://doi.org/10.3390/buildings12122193

Dinçkal C (2011). Analysis of elastic anisotropy of wood material for engineering applications. J Innov Res Eng Sci 2(2):67–80. https://doi.org/10.4314/ijest.v3i4.68553

Ebrahimkhanlou A, Salamone S (2018). Single-sensor acoustic emission source localization in plate-like structures using deep learning. Aerospace 5(2):50. https://doi.org/10.3390/aerospace5020050

Guo F, Zhang P, Zhang D, Han X, Fei Q (2017). Low speed impact localization of fiber Bragg grating based on wavelet packet energy feature vectors. Shock Vib 36:184–189. doi:10.13465/j.cnki.jvs.2017.08.029

Han Y, Chun Q, Wang H (2022). Quantitative safety evaluation of ancient Chinese timber arch lounge bridges. J Wood Sci 68(1):4–18. https://doi.org/10.1186/s10086-022-02011-y

He X, Zhu X (2024). Two-dimensional acoustic emission source localization on layered engineered wood by machine learning: a case study of laminated veneer lumber plate structure. Struct Health Monit 23(4):2423–2442. https://doi.org/10.1177/14759217231202544

Ji M, Zhang W, Diao X, Wang G, Miao H (2023). Intelligent automation manufacturing for Betula solid timber based on machine vision detection and optimization grading system applied to building materials. Forests 14(7):1510–1536. https://doi.org/10.3390/f14071510

Kim K, Lee Y (2014). Acoustic emission source localization in plate-like structures using least-squares support vector machines with delta t feature. J Mech Sci Tech 28:3013–3020. https://doi.org/10.1007/s12206-014-0707-0

Kundu T, Das S, Jata K (2007). Point of impact prediction in isotropic and anisotropic plates from the acoustic emission data. J Acoust Soc Am 122(4):2057–2066. https://doi.org/10.1121/1.2775322

Lamy F, Takarli M, Angellier N, Dubois F, Pop O (2015). Acoustic emission technique for fracture analysis in wood materials. Int J Fract 192:57–70. https://doi.org/10.1007/s10704-014-9985-x

Li X, Deng T, Wang M, Ju S, Li X, Li M (2020). Improvement of linear localization algorithm for wood acoustic emission sources based on wavelet and correlation analysis. J For Eng 5 (3):138–143. doi:10.13360/j.issn.2096-1359.201907045

Li Y, Yu SS, Dai L, Luo TF, Li M (2018). Acoustic emission signal source localization on plywood surface with cross-correlation method. J Wood Sci 64:78–84. https://doi.org/10.1007/s10086-017-1672-x

López G, Vallelado-Cordobes P, Gomez-Royuela J, Basterra L (2023). Diagnosis and assessment of a historic timber structure in La Casa del Corregidor, using non-destructive techniques. Case Stud Constr Mater 19:e02311. https://doi.org/10.1016/j.cscm.2023.e02311

Nocetti M, Mannucci M, Brunetti M (2023). Automatic assessment of insect degradation depth in structural solid wood elements by drilling resistance measurements. Constr Build Mater 366:130273. https://doi.org/10.1016/j.conbuildmat.2022.130273

Park C, Kim J, Jun S, Kim C (2012). Localizations and force reconstruction of low-velocity impact in a composite panel using optical fiber sensors. Adv Compos Mater 21(5-6):357–369. https://doi.org/10.1080/09243046.2012.736346

Pan X, Li M, Hu Q (2024). Study on acoustic emission parameter characteristics of damage in Chinese fir components with T-shaped and L-shaped cracks [J]. J Forest Industry 61(10):17–23. doi:10.19531/j.issn1001-5299.202410004

Qin G, Li M, Fang S, Deng T, Huang C, Mao F, Zhao Y, Xu N (2024). Study of a grid-based regional localization method for damage sources during three-point bending tests of wood. Constr Build Mater 419:135348. https://doi.org/10.1016/j.conbuildmat.2024.135348

Rescalvo FJ, Valverde-Palacios I, Suarez E, Roldan A, Gallego A (2018). Monitoring of carbon fiber-reinforced old timber beams via strain and multiresonant acoustic emission sensors. Sensors 18(4):1224. https://doi.org/10.3390/s18041224

Shrestha P, Kim J, Park Y, Kim C (2015). Impact localization on composite wing using 1D array FBG sensor and RMS/correlation based reference database algorithm. Compos Struct 125:159-169. https://doi.org/10.1016/j.compstruct.2015.01.029

Su H, Ou B, Tong J, Hu J, Wen Z (2012). Pattern recognition method for the source location of acoustic emission generated during the damage of hydraulic concrete. Strain 48(6):482-490.https://doi.org/10.1111/j.1475-1305.2012.00845.x

Xu N, Li M, Fang S, Huang C, Chen C, Zhao Y, Mao F, Deng T, Wang Y (2023). Research on the detection of the hole in wood based on acoustic emission frequency sweeping. Constr Build Mater 400:132761. https://doi.org/10.1016/j.conbuildmat.2023.132761

Xu P, Guan C, Zhang H, Li G, Zhao D, Ross RJ, Shen Y (2021). Application of nondestructive testing technologies in preserving historic trees and ancient timber structures in China. Forests 12(3):318. https://doi.org/10.3390/f12030318

Yin S, Xiao H, Cui Z, Kundu T (2021). Rapid localization of acoustic source using sensor clusters in 3D homogeneous and heterogeneous structures. Struct Health Monit 20(3):1145-1155. https://doi.org/10.1177/1475921720945195

Zhao X, Jiao L, Zhao J, Zhao D (2017). Acoustic emission attenuation characteristics and source localization during bending failure of mortise and tenon structures. J Beijing For Univ 39:107–111. doi:10.13332/j.1000-1522.20160150

Zhou W, Pan ZB, Wang J, Qiao S, Ma LH, Liu J, Ren XY, Liang YZ (2023). Review on acoustic emission source location, damage recognition and lifetime prediction of fiber-reinforced composites. J Mater Sci 58(2):583-607. https://doi.org/10.1007/s10853-022-08063-1